



Very Large Telescope

SPHERE

User Manual

| | |
|---------------|--|
| Reference | PDM-ESO-254263 VLT-MAN-SPH-14690-0430 |
| Issue | P99.0 |
| Status | 6 th public release (P99 Phase 1) |
| Date of Issue | 2016-09-01 |

| | | |
|--|---------------------------|------------------|
| Prepared <i>J. Girard , Z. Wahhaj, A. Vigan, M. van den Ancker, J. Milli, A. Smette, R. Siebenmorgen, D. Mouillet, H. Boffin and the SPHERE consortium</i> | Date 2016-09-15 | Signature |
| Approved <i>S. Mieske</i> | Date | Signature |
| Released <i>A. Kaufer</i> | Date | Signature |

The SPHERE consortium:

Institut de Planétologie et d'Astrophysique de Grenoble, France (PI institute)
Max-Planck-Institut für Astronomie, Heidelberg, Germany (co-PI institute)
Laboratoire d'Astrophysique de Marseille, France
Observatoire de Genève, Switzerland
Laboratoire Lagrange, Nice, France
The Italian National Institute for Astrophysics coordinated by the
Osservatorio Astronomico di Padova, Italy
Laboratoire d'Etudes Spatiales et d'Instrumentation en Astrophysique, Paris, France
Eidgenössische Technische Hochschule (ETH) Zürich, Switzerland
The Astronomical Institute Anton Pannekoek, University of Amsterdam, the
Netherlands
Office National d'Etudes et de Recherches Aérospatiales, Châtillon, France
The Netherlands Research School for Astronomy (NOVA-ASTRON), the Netherlands
The European Southern Observatory (ESO)

Change Record

| Issue | Section | Comments |
|--------------|------------------------|---|
| V95 | All | First public draft |
| V95.1 | Chapter 8, Appendix | Added description of templates in Chapter 8 and associated tables in the Appendix. |
| V96.1 | Many | Science Calibration Plan overview Beta ETC: + links IRDIS Astrometry IFS data reduction Inconsistencies Removed 4Q mask, Added ALC_YH_S mask Large NDIT Warning Added ZIMPOL saturation limits Comment on ND filters Warning about current ETC Clarification about provided flat field in IRDIS/LSS Updated IRDIS filters section Updated IFS dispersive elements information Added information on astrometry in Section 7 Several additions for LSS Corrected execution time calculation and overheads for IRDIFS observations IRDIS DPI mode Quality Assessment Low Wind Effect (LWE) |
| V97.1 | Many | IRDIS_LSS mode offered in service if time critical (section 1.7) More information on the low wind effect (section 5.2) SPARTA files to review image quality now available in ESO archive (section 5.3) IRDIFS mode can now use BB_H filter. IRDIFS_EXT mode can now use BB_Ks filter (section 12.6) Getting calibration files from ESO archive (section 10.1) |

| Issue | Section | Comments |
|-------|---------|--|
| V99.0 | Many | General reformatting Information on astrometric calibration More information on IRDIS DPI & link to the dedicated page |

LIST OF ACRONYMS

| | |
|-------|--|
| ADC | Atmospheric Dispersion Corrector |
| ADI | Angular Differential Imaging |
| AO | Adaptive Optics |
| APLC | Apodized Pupil Lyot Coronagraph |
| BB | Broadband |
| CI | Classical Imaging |
| CLC | Classical Lyot Coronagraph |
| CP | Common Path |
| DBI | Dual Band Imaging |
| DD | Double Difference |
| DIT | Detector Integration Time |
| DM | Deformable Mirror |
| DMS | Detector Motion Stage |
| DPI | Dual Polarization Imaging |
| DRH | Data Reduction and Handling |
| DTTP | Differential Tip Tilt Plate |
| DTTS | Differential Tip Tilt Sensor |
| ESP | Extra-Solar Planet |
| ETC | Exposure Time Calculator |
| FF | Flat-field |
| FLC | Ferro-electric Liquid Crystal |
| FoV | Field of View |
| FP | Focal Plane |
| HA | Hour Angle |
| HAR | High angular resolution |
| HF | High Frequency |
| HODM | High Order Deformable Mirror |
| HW | Hardware |
| HWP | Half Wave Plate |
| IFS | Integral Field Spectrometer |
| INS | Instrument Software |
| IRDIS | IR Differential Imaging Spectrometer |
| ITTM | Image Tip-Tilt Mirror |
| IWA | Inner Working Angle |
| LRS | Low resolution spectroscopy |
| LSS | Long Slit Spectroscopy |
| LWE | Low Wind Effect |
| mas | milli-arcseconds |
| MRS | Medium Resolution Spectroscopy |
| NB | Narrowband |
| NCPA | Non Common-Path Aberrations |
| NDIT | Number of DIT |
| NGC | New Generation Controller |
| NIR | Near Infrared |
| PCA | Principal Component Analysis |
| PDI | Polarimetric Differential Imaging (data reduction technique applied for data obtained in DPI mode) |

| | |
|--------|---|
| PCOM | Polarization Compensator |
| PSF | Point Spread Function |
| PTTM | Pupil Tip-Tilt Mirror |
| QWP | Quarter-Wave Plate |
| RON | Readout Noise |
| RTC | Real-Time Computer |
| RTD | Real-Time Display |
| SAXO | Sphere AO for eXoplanet Observation |
| SC | Science Case |
| SD | Simple Difference |
| SDI | Spectral Differential Imaging |
| SNR | Signal to Noise Ratio |
| SP | Spectral type |
| SPHERE | Spectro-Polarimetric High contrast Exoplanet REsearch |
| SR | Strehl Ratio |
| tbc | to be confirmed |
| tbd | to be defined |
| WFE | WaveFront Error |
| WFS | WaveFront Sensor |
| ZIMPOL | Zurich Imaging POLarimeter |
| ZP | ZeroPoint |

Table of contents

| | |
|--|-----------|
| List of Acronyms | 4 |
| 1. Introduction | 9 |
| 1.1 SPHERE in a nutshell..... | 9 |
| 1.2 High contrast imaging | 11 |
| 1.3 Field and pupil rotation..... | 11 |
| 1.4 Coronagraphy..... | 12 |
| 1.5 Differential Imaging..... | 12 |
| 1.6 Science case examples | 13 |
| 1.7 Mode offering from P98 | 14 |
| 2. Technical description | 15 |
| 2.1 CPI | 15 |
| 2.2 IFS..... | 16 |
| 2.3 IRDIS..... | 17 |
| 2.4 ZIMPOL | 18 |
| 2.4.1 Hardware..... | 21 |
| 2.4.2 Instrumental polarization..... | 21 |
| 2.4.3 Detectors | 22 |
| 2.4.4 Imaging | 23 |
| 2.4.5 Field of view..... | 23 |
| 2.5 Instrument combinations | 23 |
| 3. ADAPTIVE OPTICS Performance | 24 |
| 3.1 SAXO preliminary representative performance | 24 |
| 3.2 IRDIS preliminary representative performance | 25 |
| 3.2.1 IRDIS DBI | 25 |
| 3.2.2 IRDIS LSS | 27 |
| 3.3 IFS preliminary representative performance..... | 28 |
| 3.4 ZIMPOL preliminary representative performance..... | 30 |
| 4. Exposure time calculators | 32 |
| 5. Quality assessment | 33 |
| 5.1 Seeing constraints | 33 |
| 5.2 Low-wind effect (LWE)..... | 33 |
| 5.3 Using SPARTA files to review image quality. | 35 |
| 6. SPHERE observing proposals | 36 |
| 6.1 Observing modes..... | 36 |
| 6.2 Coronagraphs and filters | 39 |
| 6.3 AO limiting magnitudes | 40 |
| 6.4 Telescope time | 40 |
| 7. preparing observations | 42 |
| 7.1 Phase 2..... | 42 |
| 7.2 Observing constraints | 42 |
| 7.3 Target acquisition templates | 43 |
| 7.4 IRDIFS templates | 44 |
| 7.4.1 Observation templates and user-defined parameters..... | 45 |
| 7.4.2 Calibrations..... | 45 |
| 7.5 IRDIS: DBI | 45 |
| 7.5.1 Observation templates and user-defined parameters..... | 45 |
| 7.5.2 Calibrations..... | 46 |
| 7.6 IRDIS alone Classical Imaging (CI)..... | 46 |

| | | |
|-----------------|--|-----------|
| 7.6.1 | Observation templates and user-defined parameters..... | 46 |
| 7.6.2 | Purpose and properties..... | 46 |
| 7.6.3 | Calibrations..... | 46 |
| 7.7 | IRDIS DPI (Dual Polarization Imaging)..... | 46 |
| 7.7.1 | Instrumental polarization..... | 46 |
| 7.7.2 | Observation templates and user-defined parameters..... | 49 |
| 7.7.3 | Calibrations..... | 49 |
| 7.8 | IRDIS alone Long Slit Spectroscopy (LSS)..... | 49 |
| 7.8.1 | Observation templates and user-defined parameters..... | 49 |
| 7.8.2 | Purpose and properties..... | 50 |
| 7.8.3 | Calibrations..... | 51 |
| 7.9 | ZIMPOL polarimetric imaging..... | 51 |
| 7.9.1 | Observation templates and user-defined parameters..... | 51 |
| 7.9.2 | P1 or P2 rotation modes for ZIMPOL polarimetry..... | 53 |
| 7.9.3 | Dithering, mosaicking..... | 53 |
| 7.9.3.1 | Dithering..... | 53 |
| 7.9.3.2 | Off-axis positions..... | 53 |
| 7.9.4 | Observing sequences for ZIMPOL polarimetry..... | 53 |
| 7.9.4.1 | Recommendations for sequences..... | 54 |
| 7.9.4.2 | Recommended sequences for different types of targets..... | 54 |
| 7.9.5 | ZIMPOL polarimetric calibrations..... | 55 |
| 7.10 | ZIMPOL imaging..... | 56 |
| 7.10.1 | Observation templates and user-defined parameters..... | 56 |
| 7.10.2 | Purpose and properties..... | 56 |
| 7.10.3 | Calibrations..... | 57 |
| 8. | Calibration plan SUMMARY..... | 58 |
| 8.1 | Night-time calibrations..... | 58 |
| 8.1.1 | Night-time calibrations provided by the observatory..... | 58 |
| 8.1.2 | Optional night-time calibrations..... | 58 |
| 8.2 | Day-time calibrations..... | 58 |
| 8.3 | Astrometry..... | 61 |
| 8.3.1 | Instrumental distortion and detector orientation in IRDIFS and IRDIFS_EXT..... | 61 |
| 8.3.2 | Plate scale and true north orientation..... | 61 |
| 9. | SPHERE Template parameters..... | 63 |
| 9.1 | SPHERE Acquisition Templates..... | 63 |
| 9.2 | SPHERE Observation Templates..... | 63 |
| 9.3 | SPHERE Night-time Calibration Templates..... | 76 |
| 10. | Data reduction..... | 78 |
| 10.1 | Obtaining calibration files from the ESO archive..... | 78 |
| 10.2 | IFS reduction cascade summary..... | 78 |
| 10.3 | IRDIS reduction cascade summary..... | 78 |
| 10.3.1 | DBI, classical imaging..... | 78 |
| 10.3.2 | Long slit spectroscopy..... | 79 |
| 10.4 | ZIMPOL reduction cascade summary..... | 79 |
| 10.4.1 | Imaging..... | 79 |
| 10.4.2 | Polarimetry..... | 79 |
| 11. | Overheads..... | 81 |
| 11.1 | Target acquisition..... | 81 |
| 11.2 | NIR observation overheads..... | 81 |
| 11.3 | ZIMPOL observation overheads..... | 82 |
| Appendix | | 84 |

| | |
|--|-----------|
| A1. Detector properties..... | 84 |
| A1.1 IRDIS and IFS detectors..... | 84 |
| A1.2 ZIMPOL detectors..... | 85 |
| A2. System throughput..... | 86 |
| A3. Neutral densities | 87 |
| A3.1 CPI..... | 87 |
| A3.2 IFS..... | 88 |
| A3.3 IRDIS..... | 88 |
| A3.4 ZIMPOL..... | 88 |
| A4. IRDIS beam-splitter..... | 89 |
| A5. IRDIS filters | 89 |
| A6. NIR Coronagraphs..... | 93 |
| A6.1 ALC coronagraphs..... | 94 |
| A7. IFS dispersive components | 94 |
| A8. IRDIS dispersive components..... | 95 |
| A8.1 LSS..... | 95 |
| A8.2 Prism..... | 95 |
| A8.3 Grism..... | 95 |
| A9. Visible Coronagraphs..... | 95 |
| A10. ZIMPOL filters..... | 96 |
| A11. Polarimetric calibration components..... | 99 |

1. INTRODUCTION

The aim of the SPHERE User Manual is to provide information on the technical characteristics of the instrument, its performance, observing, calibration and data reduction procedures.

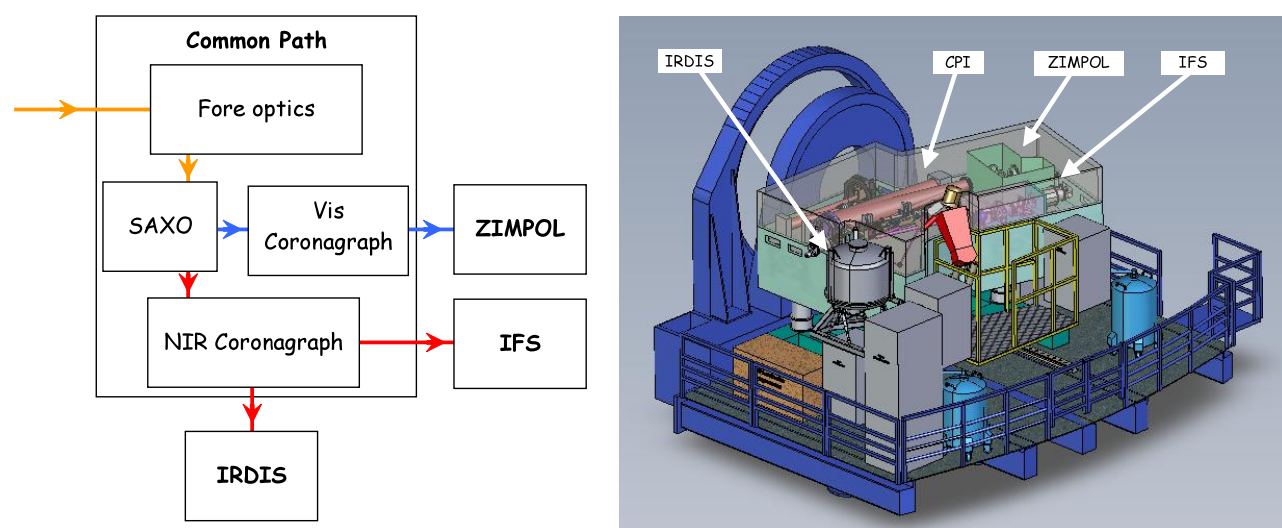


Figure 1: SPHERE sub-systems (left) including the common path (CPI) with adaptive optics system SAXO, coronagraphs, and sub-instruments IRDIS, IFS and ZIMPOL. Left: schematic view of the instrument on the Nasmyth platform.

1.1 SPHERE in a nutshell

The primary science goals of SPHERE are imaging, low-resolution spectroscopic, and polarimetric characterization of exoplanets. The instrument design is driven to provide highest image quality and contrast performance in a narrow field around bright targets observed in the visible or near infrared. SPHERE is installed at one of the UT3 Nasmyth foci of the VLT and consists of four subsystems:

CPI: The common path and infrastructure receives direct light from the telescope, and provides highly stabilized, AO-corrected, and coronagraphic beams to the three sub-instruments, described below.

IFS: The integral field spectrograph provides a data cube of 38 monochromatic images either at spectral resolution of $R \sim 50$ between $0.95 - 1.35 \mu\text{m}$ (Y-J) or at $R \sim 30$ between $0.95 - 1.65 \mu\text{m}$ (Y-H).

IRDIS: The infrared dual-band imager and spectrograph provides classical imaging (CI), dual-band imaging (DBI), dual-polarization imaging (DPI), and long slit spectroscopy (LSS) either between $0.95 - 2.32 \mu\text{m}$, with resolving power of $R \sim 50$ (LRS with $0''.12$ wide slit) or between $0.95 - 1.65 \mu\text{m}$ with $R \sim 350$ (MRS with $0''.09$ wide slit).

ZIMPOL: the Zurich imaging polarimeter provides near diffraction limited classical imaging and dual-polarization imaging (DPI) below 30 mas resolution in the visible.

Dichroic splitters allow simultaneous observations with IRDIS and IFS (IRDIFS modes).

Table 1: IFS

| | | |
|----------------|---|----------------------------------|
| Observing mode | Integral field spectroscopy | |
| Spectral range | 0.95–1.35 μm : R~50 | 0.95 – 1.65 μm : R~30 |
| Sampling | (12.25 mas) ² / spaxel (hexagonal grid), Nyquist at 0.95 μm . Resampled by the pipeline on a square with (7.4 mas) ² / pixel. | |
| FOV | ~ 1.73'' x 1.73'' | |
| Detector type | Hawaii II RG 2048x2048 | |
| Coronagraph | None, or with classical or apodized pupil Lyot coronagraphs. | |
| Stabilization | Pupil- or Field-stabilized | |
| WFS | Visible light | |

Table 2: IRDIS

| | | |
|-----------------|---|---|
| Observing modes | DBI, DPI, CI | LSS |
| Spectral range | 0.95 – 2.32 μm : NB and BB filters | 0.95 - 2.32 μm : R~50 0.95 - 1.65 μm : R~350 |
| Sampling | (12.25 mas) ² / pixel, Nyquist-sampled at 0.95 μm | |
| FOV | 11'' x 11'' | 11'' slit |
| Detector type | Hawaii II RG 2048 x 1024 | |
| Coronagraph | None, or with classical or apodized pupil Lyot coronagraphs. | Central blocking |
| Stabilization | Pupil- or Field-stabilized | Field stabilized |
| WFS | Visible light | |

Table 3: ZIMPOL

| | |
|---------------------|--|
| Observing modes | Imaging (I), differential polarimetric imaging (P1, P2) |
| Spectral range | 500 – 900 nm in broad and narrowband filters |
| Sampling | (7 mas) ² / pixel, diffraction-limited at $\lambda > 600$ nm |
| FOV | 3.5'' x 3.5'' |
| Detectors type | Two 4k × 2k pixel, back-illuminated, frame transfer CCD 220 (e2v CCD 44-82 bi) with 15 μm × 15 μm pixels, equipped with a stripe mask and a micro-lens array.q |
| Linear polarization | Instrumental polarization <1%, polarimetric sensitivity < 0.1% with fast modulation, simultaneously on two CCDs |
| Coronagraph | None, or with classical Lyot coronagraphs |

| | |
|---------------|---|
| Stabilization | <ul style="list-style-type: none"> - Imaging: pupil or field stabilized. - Polarimetry: field stabilized, or fixed derotator with stable and minimized instrumental polarization. |
| WFS | <p>Visible light shared between WFS and ZIMPOL:</p> <ul style="list-style-type: none"> - Dichroic for R-band observation: (100% WFS outside R band / 100% R band to ZIMPOL) - Grey beam splitter: (20% WFS / 80% ZIMPOL), with AO limit lowered by ~ 1.74 mag |

1.2 High contrast imaging

When imaging a star one often aims at discovering companions or other faint structures around it. This requires removing the halo produced by the star. However, close to the star, there are point source structures called speckles that evolve over hour long timescales. Speckles are interference images of (atmospheric or instrumental) wavefront corrugations left uncorrected by the AO system, with a typical size of a resolution element ($\sim \lambda/D$). The sensitivity of an exposure is most often limited by these speckles. Subtracting them is the main goal in high contrast imaging. Speckles are a function of wavelength and change with time as optics and atmosphere change.

SPHERE combines various techniques to provide high contrast imaging, with excellent stellar PSF suppression and stability: a high density high frequency AO system that corrects turbulence and static optical aberrations, coronagraphy, and differential imaging, in which images at different wavelengths or polarization states are observed simultaneously (Figure 2).

The AO corrects the incoming wavefront up to ~ 20 cycles/aperture ($20 =$ half the number of deformable mirror actuators across the pupil), corresponding to a radius = $20 \lambda/D$ in the image plane. Within this correction radius, the coronagraph efficiently suppresses the diffraction pattern down to a much fainter residual halo, which is associated to the uncorrected wavefront errors. Further out ($>20 \lambda/D$), the AO system still corrects the PSF of off-axis sources but does not contribute to the suppression of the stellar halo. Far from the star (beyond an arcsecond), the contrast depends on the filter width, number of detector reads and integration time rather than on AO correction, so that at that location SPHERE performance behaves similar to previous instruments (e.g. NACO). Differential imaging techniques are then used to remove the residual stellar halo and/or speckles (see Section 1.5).

The stability of the PSF becomes critical when combining observations obtained at different times. This is important for angular differential imaging (ADI) or conventional PSF subtraction. The best PSF stability is obtained when observing in pupil-stabilized mode.

1.3 Field and pupil rotation

At the Nasmyth focus, both the pupil and the field rotate when tracking an object. The field rotation is the combination of the parallactic angle and altitude of the object. The pupil rotation is directly related to the altitude of the object being tracked. The SPHERE derotator allows stabilization of either the field or the pupil on the detector.

In *pupil-stabilized* observations the PSF variability is minimized because most of the optical elements do not move. The telescope pupil is also aligned with the Lyot stops of the instrument, which cover the M2 shadow and its spider arms. The pupil-stabilized mode provides the highest PSF stability and is recommended for coronagraphic observations and for high contrast imaging close to the star. The field rotates with the parallactic angle, enabling *angular differential imaging*

(ADI, see Section 1.5). The center of rotation is the central star. One should then be aware of the trade-off between rotation rate and the smearing of off-axis PSF (see Exposure Time Calculator).

In *field-stabilized* mode, light from a specific location in the field of view falls on a particular location on the detector, throughout the observation. For SPHERE observations this is:

- Mandatory in long slit spectroscopy. The slit shall not rotate during the observation and is defined by the observer.
- Mandatory for ZIMPOL P2 polarimetric mode (see Table 8).
- Recommended when smearing of the image within a DIT becomes an issue (e.g. at larger separation). This may be caused by a long DIT, selected to reduce the RON, or by fast field rotation, while observing close to zenith.

Field stabilized mode also ensures that a companion image would fall on the same detector pixels (lenslets for IFS). This reduces concern due to flat-fielding; this might improve stability of photometric time series.

For completeness, we mention that instrumental polarization is best understood when the derotator is static and hence does not move.

1.4 Coronagraphy

A coronagraph suppresses the coherent light coming from on-axis unresolved source (Figure 2). In SPHERE, all coronagraphs consist of a focal plane mask, followed by a pupil stop and sometimes preceded by an entrance pupil apodizer. SPHERE houses several coronagraphs to accommodate different observational needs such as spectral range or inner working angle. Coronagraph choices and trade-offs are detailed in the Appendix.

1.5 Differential Imaging

ADI exploits the fact that the field and the pupil rotate with respect to each other. In pupil-stabilized mode, most speckles are caused by instrumental artifacts and are locked up in the pupil plane, whereas the object of interest, a companion or a disk, will rotate as the field rotates. This allows distinguishing the stellar halo from the object.

Simultaneous observation of several monochromatic images can be used to reduce the impact of speckles (Sparks and Ford, 2002). For a given observation, the location of a companion around a star is constant while the location of speckles from the star increases with wavelength and their intensity decreases. For a wide enough wavelength range this allows subtraction of the speckles. This process is known as *spectral deconvolution* (Thatte et al. 2007). This approach is used in IFS and in IRDIS LSS.

Planets and the host star have different spectral features. This information can be used to suppress speckle noise. For this, one needs simultaneous images at two similar wavelengths at which the brightness of the planet varies, e.g. in and out of a molecular band. This method is called *spectral differential imaging* (SDI). This approach is used in IRDIS DBI. It can also be used with ZIMPOL imaging when different filters are used in ZIMPOL's two arms (e.g., H α and continuum).

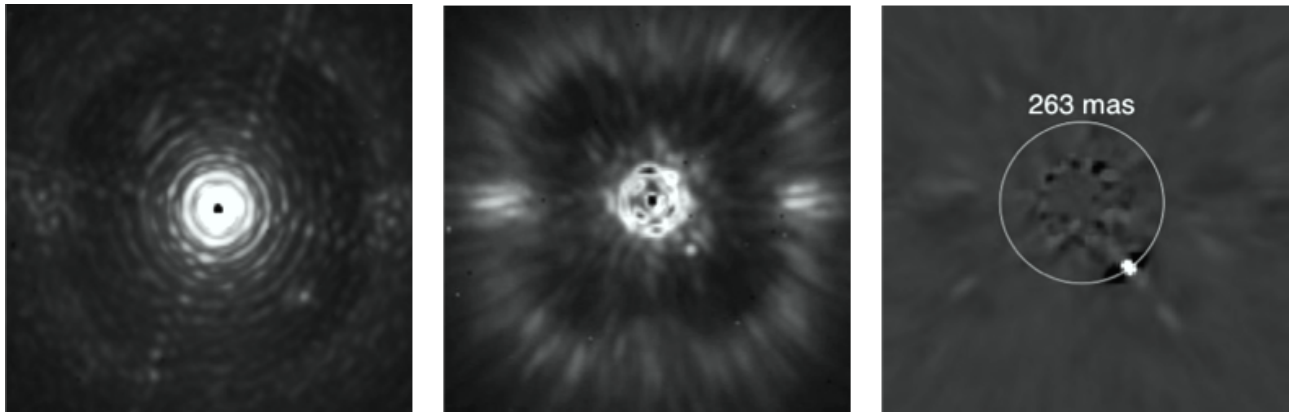


Figure 2: Illustration of the three pillars of high contrast imaging. Left: raw on-sky J-band PSF of SPHERE with IRDIS, showing the diffraction pattern resulting from the almost perfect correction provided by the extreme AO system up to 20 cycles per aperture, and so $20 \lambda/D$ in the image (this is half the number of actuators on the deformable mirror on a side). Middle: raw on-sky J-band coronagraphic image of Iota Sgr, illustrating the efficient removal of diffraction rings and pinned speckles by the coronagraph. Note the very visible AO correction radius. Outside the correction radius ($r > 20 \lambda/D$), the brighter halo results from the uncorrected wings of the seeing halo. Right: result of angular differential imaging (ADI) strategy, and post-processing using principal component analysis, cleaning the remaining speckles in the field after extreme AO and coronagraphy, revealing a faint off-axis companion.

Stars are often unpolarized, whereas circumstellar environments and planets may be highly polarized. This feature is used to increase the image contrast and is called *dual polarization imaging* (DPI). DPI is used in ZIMPOL polarimetric imaging and in IRDIS DPI.

1.6 Science case examples

Besides imaging of exoplanets and companions around stars, there are other science opportunities opened by SPHERE.

1) The close environment around bright stars

Good/median AO performance is obtained for stars up to $R = 11$ mag. For stars with $R > 11$ mag, users should apply for observations in visitor mode. For fainter stars performance is likely to degrade (see Section 3.1 and Section 7.3). With AO, diffraction limited resolution is obtained for IFS within $1.73'' \times 1.73''$, for ZIMPOL up to $3.5'' \times 3.5''$, and IRDIS in an $11'' \times 11''$ FOV, respectively.

2) Circumstellar emission much fainter than the stellar halo

The suppression of the stellar PSF is for SPHERE much improved compared to previous instruments (e.g., NACO). This is in particular true at small separation angles from the star between 1 and $20 \lambda/D$. Beside the high image quality and PSF stability of the instrument, there are dedicated data reduction techniques based on differential imaging to enhance the contrast of circumstellar emission further (ADI, PDI, SDI).

3) High angular resolution observations will support studies of stellar ejecta, binaries at small separations, stellar proper motions, solar system objects, etc.

1.7 Mode offering from P98

Table 4: Modes offered.

| Observing Mode | Comment | Service/ Visitor |
|----------------|--|------------------|
| IRDIFS | - Pupil-stabilized (default) or Field stabilized - Coronagraph: N_ALC_YJH_S | S+V |
| | - Other coronagraphs - NGS R > 11 mag | V |
| IRDIFS_EXT | - Pupil-stabilized (default) or Field stabilized - Coronagraph: N_ALC_YJH_S | S+V |
| | - Other coronagraphs - NGS R > 11 mag | V |
| IRDIS_DBI | - Pupil-stabilized (default) or Field stabilized - Coronagraph: N_ALC_YJH_S, N_ALC_Ks with K-band filters | S+V |
| | - Other coronagraphs - NGS R > 11 mag | V |
| IRDIS_CI | - Pupil-stabilized (default) or Field stabilized - Coronagraph: N_ALC_YJH_S, N_ALC_Ks with K-band filters | S+V |
| | - Other coronagraphs - NGS R > 11 mag | V |
| IRDIS_DPI | - Field stabilized - Coronagraph: N_ALC_YJ_S, N_ALC_YJH_S, N_ALC_Ks - Filters: broad band filters BB_J | S+V |
| | - Field stabilized - Coronagraph: N_ALC_YJ_S, N_ALC_YJH_S, N_ALC_Ks - Filters: broad band filters BB_Y, BB_H, BB_Ks | V |
| IRDIS_LSS | Long Slit Spectroscopy in LRS and MRS | V* |
| ZIMPOL_P1/P2 | - Derotator: P1 (static) or P2 (Field-Stabilized) - Filters: combination of NB and BB filters not allowed - WFS/ZIMPOL splitter: GREY or DIC-HA - No coronagraph (allowing some saturation) or V_CLC_M_WF - Some saturation allowed - Detector/modulator: FastPol, SlowPol - Field-Position: on-axis | S+V |
| | - Other coronagraphs - NGS R > 11 mag - NB and BB filter combination | V |
| ZIMPOL_I | - Same as P1/P2 but with readout mode StdImaging. - Pupil-stabilized | S+V |
| | - Other coronagraphs - NGS R > 11 mag - NB and BB filter combination | V |

* In general, observations using the LSS should be requested in Visitor Mode. However, if very good conditions are critical for the observations, this mode can now also be requested in Service Mode. A clear justification regarding the need for Service Mode should be provided and will be assessed as part of the technical feasibility review: if very good conditions are not required, the programme will be reassigned to Visitor Mode. Observations using the IRDIS_LSS mode in Service Mode should be requested in a separate run from possible other observations.

2. TECHNICAL DESCRIPTION

The SPHERE subsystems CPI, IFS, IRDIS and ZIMPOL are described below.

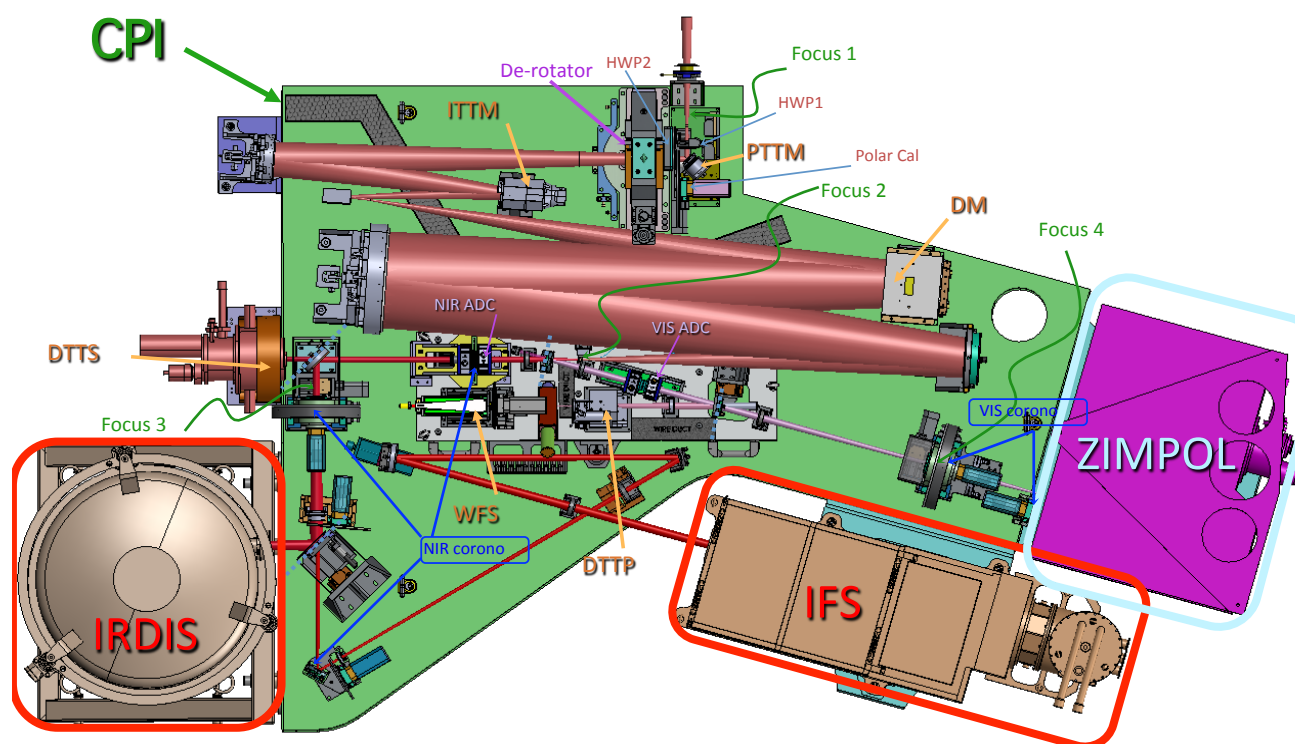


Figure 3: CPI, the common path optical beam on the main optical bench (green) feeding the 3 other sub-systems ZIMPOL (magenta), IRDIS (gray) and IFS (brown).

2.1 CPI

CPI includes the main optical bench, connects the other sub-systems to the light path, and guarantees a static alignment of SPHERE to the VLT focus (Figure 3). It feeds the cryostats and motors with power, includes servo-controlled pods, damping vibrations on the Nasmyth platform. An enclosure protects the SPHERE optics from dust and reduces temperature gradients. From the entrance focal plane up to the second focus (FP2; Focus 2) a reflective design propagates the complete spectral range from 450 to 2320 nm through the instrument. It includes the beam derotator, active optics, with pupil and image tilt mirrors, and the high order deformable mirror DM, which is the heart of the system providing a stable AO-corrected image.

CPI also includes visible and infrared half-wave plates for polarization switching/modulation. After FP2, light is split between visible and NIR. The NIR beam path includes refractive optics: the NIR ADC, coronagraphic components, neutral densities filters and an exchangeable splitter between IRDIS and IFS.

In the optical, atmospheric dispersion correction is applied by the VIS ADC, and then the beam is split between ZIMPOL and AO (WFS). If Zimpol is not used, all the light goes to the WFS. If Zimpol is used, one can chose between the grey beam splitter (sending 80% of the light to Zimpol and the remaining 20% to the WFS) and a dichroic beam splitter (DIC_HA) sending the spectral range around the R band to Zimpol and the rest to the WFS. Before ZIMPOL, the beam goes through a coronagraphic focal plane (FP4; Focus 4) and a pupil plane hosting the corresponding Lyot stops.

The adaptive optics module is called SAXO. It is designed to correct for the turbulence perturbation at high frequency (1.2 kHz). The turbulence is measured by a 40x40 lenslet Shack-Hartmann sensor that is equipped with a red-sensitive sub-electron noise EMCCD. It servo controls the pupil position, and fine-tunes the centering on the coronagraph by means of a dedicated differential tip-tilt sensor (DTTS).

The coronagraphs are set-up by a mask in the focal plane (FP3 for NIR and FP4 for the visible), a Lyot stop in the downstream pupil, and an apodizer in the upstream pupil (before the focal mask). The wheels for the coronagraphs include also field stops and the IRDIS long slit masks. Several set-up combinations are defined for a range of observing conditions and science cases (seeing, inner working angle, wavelength, etc.); they are listed in the Appendix.

2.2 IFS

The SPHERE integral field spectrograph (IFS) is a lenslet-based integral field unit (called BIGRE, Antichi et al. 2009), providing a 1.73'' x 1.73'' FOV that is Nyquist sampled at 0.95 μm (Table 1). The IFS includes a flat calibration source and filters for accurate detector calibrations. The IFS instrument layout is displayed in Figure 4. The raw data 21000 spectra are aligned with the detector columns over a hexagonal grid rotated by $\sim 10.7^\circ$ with respect to the dispersion. Each spectrum from a spaxel is projected on a rectangular area of 5.1x41 pixels on the detector.

During data reduction, the image is translated into a (x,y,λ) data cube, which has for both available spectral resolutions a constant dimension of (291,291,38). Each image is resampled by the pipeline over a square regular grid at $(7.4 \text{ mas})^2 / \text{spaxel}$. Data outside this region are meaningless (see Figure 5).

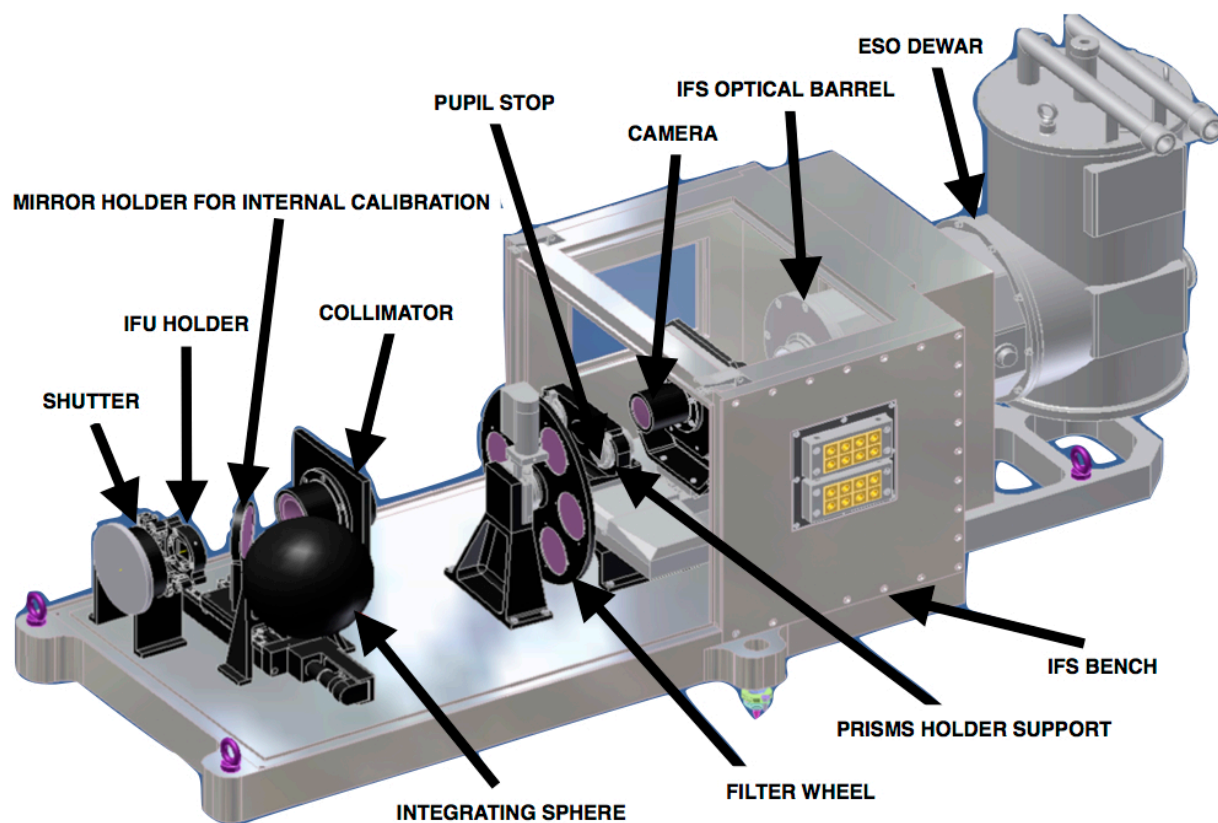


Figure 4: Inside the IFS. Note that the IFS optical bench is not cold, and that it has its own Lyot stop and internal calibration sources.

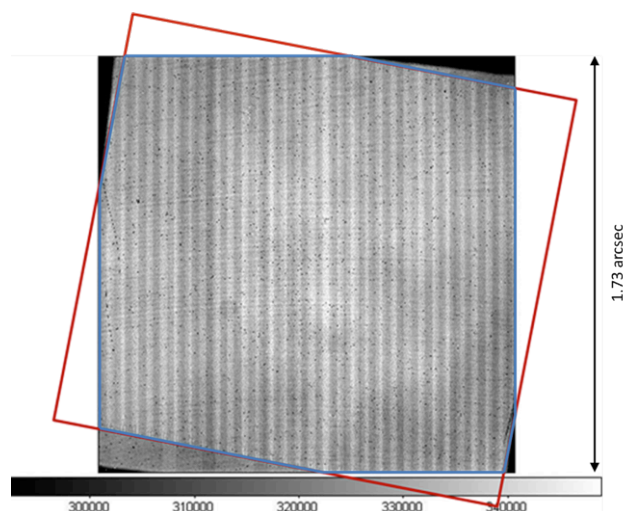


Figure 5: IFS flat-field and projection of the sky on the BIGRE detector (red) and $\sim 1.73'' \times 1.73''$ FOV (blue).

2.3 IRDIS

The FOV is $11'' \times 12.5''$ and the pixel scale is 12.25 mas matching Nyquist sampling at $0.95 \mu\text{m}$. Two parallel beams are projected onto the same $2\text{k} \times 2\text{k}$ detector and each occupies about half of the array. The IRDIS instrument layout is displayed in Figure 6. DBI provides images in two neighbouring filters, simultaneously. Various filter pairs are available for different spectral

features. DPI uses crossed polarizers providing images in the two polarization directions at the same time. For LSS, the coronagraph mask is replaced by a coronagraphic slit.

Three wheels are provided within the cryogenic environment:

- a. **The Lyot stop wheel, with Lyot stops for the coronagraphs of the CPI, LRS prism, and MRS grism.**
- b. **The common filter wheel, with blocking filters, broadband and narrowband filters.**
- c. **The dual filter wheel, with DBI and DPI filter pairs, polarizers, and a pupil-imaging lens.**

The complete list of available filters is summarized in the Appendix. Dual imaging separation is done using a beam-splitter combined with a mirror, producing two parallel beams. IRDIS achieves less than 10 nm differential aberrations between the two channels and, as a consequence, allows high contrast differential imaging.

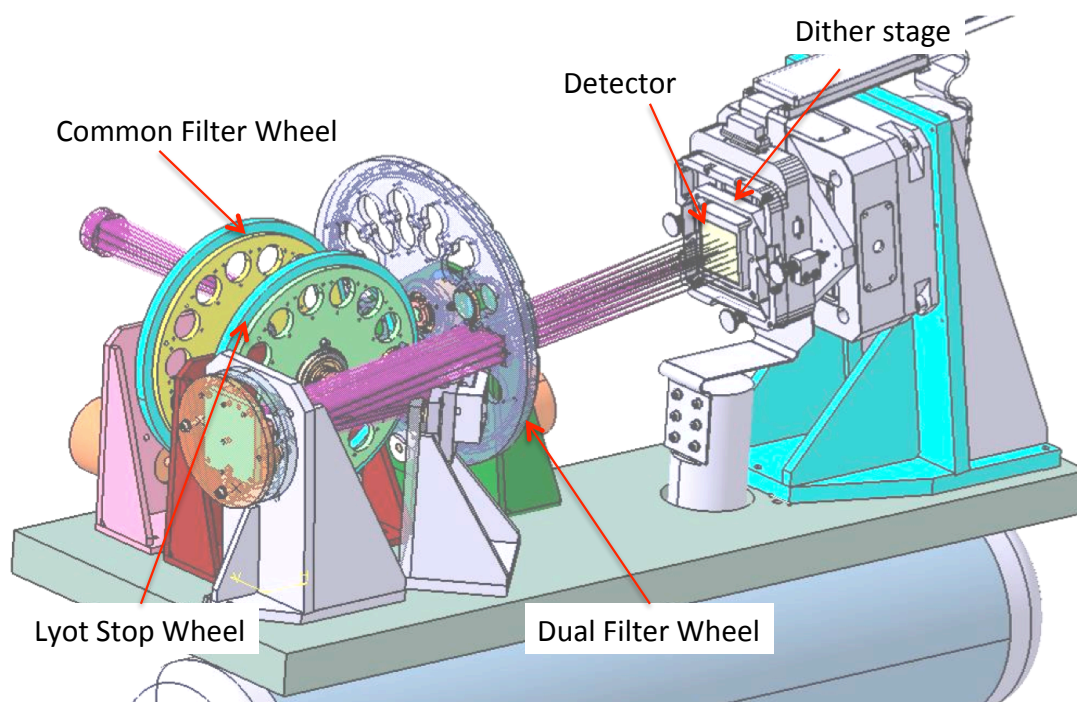


Figure 6: Inside view of the IRDIS cryostat. The CPI beam comes from the left, goes through the common filter and Lyot stop wheels, is split in two, then goes through the dual filter wheel before landing on the infrared detector.

The IRDIS detector is mounted on a detector motion stage (DMS). The DMS enables detector dithering in XY-directions at sub-micron accuracy. Detector dithering is available mainly to improve the flat-field accuracy and to handle cosmetic defects. The recommended pattern is 4x4 pixels (but can be extended up to 10x10).

2.4 ZIMPOL

ZIMPOL is designed as high contrast imaging polarimeter with very high polarimetric sensitivity for the visual range. It also provides at the same time imaging capabilities. Another VLT

instrument, FORS2, provides a polarimetric mode for the visual range which is however complementary to ZIMPOL. FORS2 is a seeing limited Cassegrain imaging and spectrograph polarimeter for accurate absolute polarization measurements (0.1% in the field center). FORS2 has a very high throughput and is therefore suited for faint objects. ZIMPOL is a diffraction limited imaging polarimeter with a very small field of view centered on a bright target. Because ZIMPOL is a Nasmyth instrument, it provides only a limited absolute polarimetric accuracy ($\sim 0.5\%$). The basic observing strategy for ZIMPOL is a relative polarization measurement of the immediate surroundings of a central star, which is used as a (zero)-polarization reference for the correction of the instrument polarization.

Atmospheric seeing variations are a key problem when aiming to achieve high image quality. Differential measurements such as DPI with fast (kHz) polarization modulation can solve this problem. DPI is performed quasi-simultaneously by fast modulation revealing, e.g. faint structures around a bright point source.

The ZIMPOL instrument layout is displayed in Figure 7 and its main capabilities are summarized in Table 3. ZIMPOL includes a new concept for imaging polarimetry, which is based on fast polarimetric modulation and on-chip de-modulation by two CCDs (Figure 7). Thanks to a polarimetric beam-splitter, one polarization is sent to CCD1 and the other perpendicular polarization to CCD2. Further, the polarization modulation is synchronized with an innovative reading scheme of the detectors.

By this technique, the polarization of the incoming light is converted by a polarization modulator and the following polarization beam splitter into an intensity modulation with an amplitude proportional to the polarization signal. The de-modulating CCD has every second row covered by a stripe mask and these covered rows can be used as a buffer storage area. With charge shifting on this masked CCD each “open” pixel can measure the intensity of the two alternating states. Photo-charges created during one half of the modulation cycle are shifted for the second half of the cycle to the next masked row and again back for the subsequent illumination during the next first half of the modulation cycle. In this way two frames are build up in alternating pixel rows, corresponding to opposite polarization states. After many modulations the CCDs can be readout and the raw polarization signal is then the difference between “even” and “odd” rows.

A single arm of ZIMPOL provides a full polarimetric measurement. Because a polarizing beamsplitter is used for the polarization analysis, half of the light goes to the other arm, which can perform polarimetry for the same or another filter.

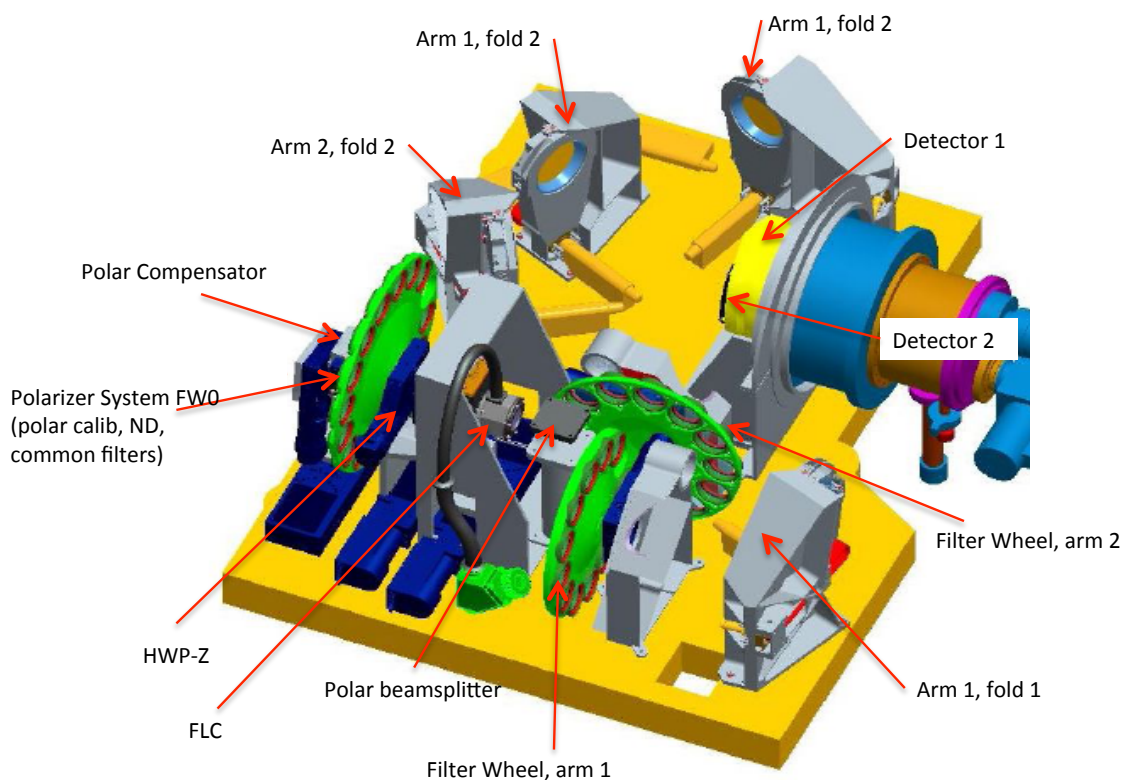


Figure 7: ZIMPOL schematic view showing the main elements of this visible polarimeter, from polarization compensator, common filter wheel, Ferroelectric Liquid Crystal (FLC) modulator to the splitter, filter wheels 1 and 2, and the two detectors.

Advantages of differential polarimetric technique are:

- a. Both images are created *quasi-simultaneously* (the modulation is faster than the seeing variations), and both images are recorded with the *same pixels* reducing significantly flat-fielding issues.
- b. Differential effects due to the storage of two images in different buffer pixels are compensated with a *demodulation phase-switch* between subsequent images.
- c. There are only very small *differential aberrations* between the two images with opposite polarization.
- d. The differential signal does not suffer from *chromatic effects* due to diffraction or speckle chromatism.

The efficiency of the modulation – demodulation process depends on the modulation frequency. The instrument offers a fast modulation mode with a frequency of about 1 kHz and a polarization efficiency of 80% and a slow modulation mode with a frequency of about 30 Hz and an efficiency of 90%. A simple calibration is foreseen to correct for the polarization efficiency taking into account a slight wavelength dependence and possible small temporal variations in the polarization measurement.

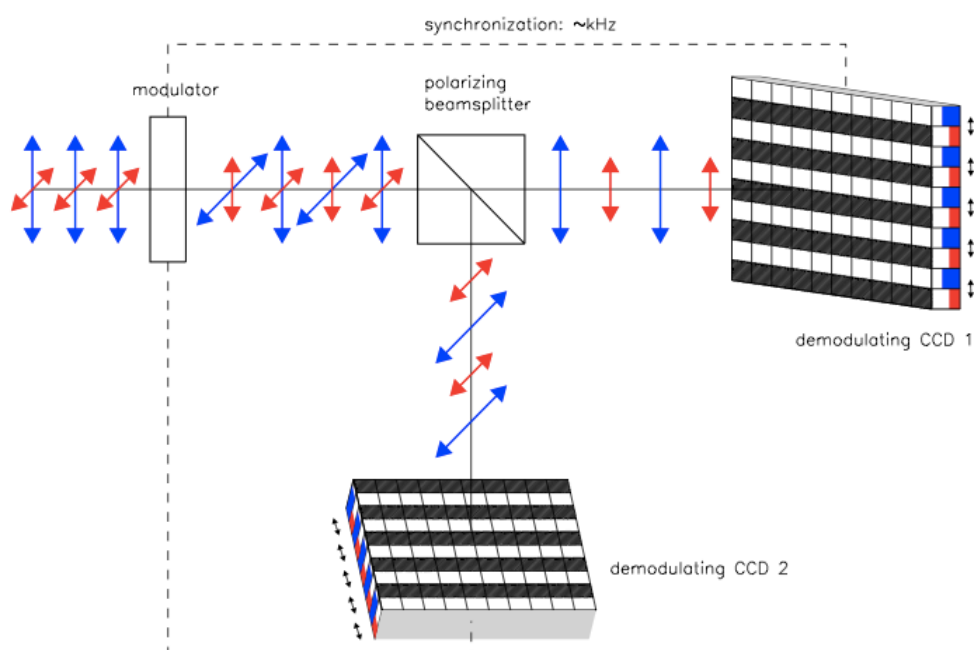


Figure 8: In ZIMPOL the polarized signal is modulated on CCD1 and CCD2. The detectors are read after a charge shifting sequence that is synchronized to the polarization swap.

2.4.1 Hardware

The ZIMPOL sub-system receives the beam from CPI after the visible coronagraph pupil Lyot stop plane. The instrument offers an extended list of broadband (BB) and narrowband (NB) filters that are described in the Appendix. The first filter wheel (FW0) is common to both arms and includes both filters and polarimetric components used to calibrate the intrinsic polarization of ZIMPOL. As a consequence, the filters located in this wheel cannot be calibrated polarimetrically and can therefore be used only for imaging observing mode and not for polarimetric imaging.

Depending on the observing mode, a polarization compensator that can be controlled in orientation and in amplitude, and internal Half-Wave Plates (HWP) are set within the observing template. A Ferro-electric Liquid Cristal polarization modulator (FLC) is inserted in the beam for polarimetric imaging to modulate the polarization direction as selected by the polarization beam-splitter. This splitter then feeds two optical beams of ZIMPOL. Each beam goes through filter wheels FW1 and FW2, the tip-tilt mirror that allows offsetting the FOV, and finally arrives on the detector. Both CCDs are located side by side in the same cryostat. The two filter wheels enable polarimetric observations in two bands. The common filter wheel FW0 contains polarimetric calibration components and additional filters for imaging.

2.4.2 Instrumental polarization

SPHERE includes many optical components that impact the instrumental polarisation. The optical path through the CPI and ZIMPOL is schematized in Figure 9. The polarization signal is measured by ZIMPOL at the position of the modulator and the beam-splitter. The linear polarization intensity is recorded either parallel I_0 or perpendicular I_{90} to the optical bench. Other polarization position angles can be selected by synchronously rotating half-wave plate HWP2 (mounted at the entrance of the CPI) and half-wave plate HWPZ (inside ZIMPOL).

The instrumental polarization is minimized by design. HWP1 and M4 (SPHERE fold mirror) enable reduction of the telescope polarization induced by M3. There is also a tilted, rotatable compensator plate to reduce the instrumental polarization introduced by the derotator.

For a given observation, both orthogonal polarization states are exchanged applying a frequent 45° rotation of HWP2. Thank to this design the introduced instrumental polarization is $< 1\%$. In many science cases, the central bright star can be used as zero-polarization reference allowing for a very accurate correction of the instrument polarization for measurements of circumstellar sources. Cross-talk effects affect the measured fractional polarization signal p (or Q/I and U/I) by $\Delta p/p < 0.05$ providing very good polarization properties for a Nasmyth instrument.

A model of the instrumental polarization of ZIMPOL is currently built for cases where the central star cannot be used as polarization reference and other demanding applications. This should allow even a better correction for the instrumental polarization effects in the data reduction.

2.4.3 Detectors

Schmid et al. (2012) describe the observing method of ZIMPOL, in which a large number of charge states are accumulated and shifted across different detector pixels. The handling of the detector properties and calibration is of particular importance. A *2-phase demodulation scheme is used*: Electrons accumulated on the detector are shifted many times up and down and from one pixel to the next, before the exposure is finally read. Therefore, asymmetries in the charge transfer efficiency in a fraction ($< 1\%$) of detector pixels (charge traps) affect the resulting data. A phase switch between two subsequent DITs calibrates this out for the differential polarization signal I_0-I_{90} . Therefore, all science exposures and calibration frames for ZIMPOL polarimetric observations are taken with an even number of DITs.

It is important to note that the charge traps remain in the intensity frame I_0+I_{90} of polarimetric observations. Their strength is proportional to the number of polarization cycles and affects a substantial fraction ($> 0.1\%$) of pixels for longer integrations (> 10 s) in fast polarimetry or (> 300 s) in slow polarimetry. The impact of this special feature of the ZIMPOL polarimetric mode can be strongly reduced by an appropriate observing strategy, e.g. with dithering, selecting slow polarimetry instead of fast polarimetry mode, or by taking separate frames in ZIMPOL imaging mode where this effect is not present.

Detector bias: The detector readout process includes additional readouts of pre- and over-scan pixels. This ensures a better bias subtraction for all frames. These additional readouts are visible in the raw data and appear at the border and in the middle of the array. In the standard data reduction cascade, average bias values for the overscan pixels are evaluated and subtracted for the two different readout areas of the ZIMPOL detectors. This provides a very good bias correction for imaging and slow polarimetry mode. For fast polarimetry mode two columns originating from the readout process are present which are not corrected by the overscan pixel bias subtraction method. This fixed pattern noise can be removed in a classical way by the subtraction bias frames.

Frame transfer smearing: The ZIMPOL data are taken with frame transfer CCDs. They can simultaneously take images with one half of the detector and readout the other half of the detector where the frame from the previous exposure is stored. At the end of an exposure which must last longer than the readout process (about 1.2s for fast polarimetry and imaging and 10s for slow polarimetry) the newly created frame in the image area is transferred rapidly to the readout area and a new illumination begins.

The detector illumination during the frame transfer introduces a smearing of the image in the direction of the detector columns. The smearing is proportional to the ratio of the frame transfer time, which is constant, and the DIT. For example, a 6s exposure of a point source with 100 000 counts (integrated over 5×5 pixels) and a frame transfer of about 60 ms, will produce a trace parallel to the column directions (~ 1000 pixels) where the illumination is enhanced by about 1 count.

The smearing effect is thus only important for short DITs in particular for non-coronagraphic, high contrast observations of saturated sources.

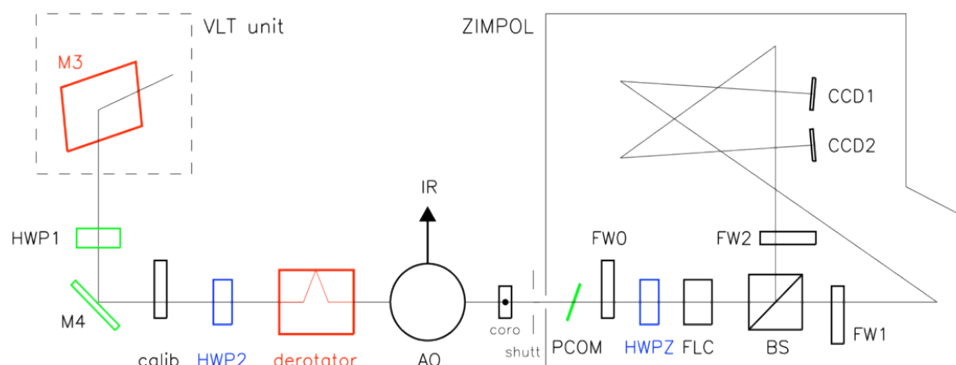


Figure 9: ZIMPOL optical path. Components, which introduce (red) or compensate (green) instrumental polarization, and those, which rotate the Stokes vector into the derotator system (blue), or instrument system (black) are indicated.

2.4.4 Imaging

The ZIMPOL imaging mode provides a higher image quality and is about 10% more efficient than polarimetric observing modes. Moreover, it does not suffer from the charge trap problem created by the charge shifting used for polarimetry.

2.4.5 Field of view

The ZIMPOL instantaneous FoV is $3.5 \times 3.5 \text{ arcsec}^2$. This FoV is roughly centered on the coronagraph position and is identical for both CCDs. On both ZIMPOL optical arms, tip-tilt mirrors can be used to offset the field by small amplitudes. This enables dithering so that light falls onto different pixels. This scheme is commonly used to reduce the impact of bad pixels. The ability to use tip-tilt mirrors for mosaicking up to a radius of $4''$ is not yet validated and not thus offered.

2.5 Instrument combinations

Dichroics allow IFS and IRDIS to take data in parallel. One dichroic setting (used in the IRDIFS_EXT mode) allows IFS observations in the Y-H range, and IRDIS observations in K at somewhat reduced performance (particularly coronagraphic).

Another setting (used in the IRDIFS mode) allows IFS observations in Y-J range, and IRDIS observations in the H band with optimum performance.

For IRDIS-alone observations, a mirror is used ensuring optimal K band performance and access to the complete $0.95 - 2.32 \mu\text{m}$ spectral range.

ZIMPOL can only be used alone.

3. ADAPTIVE OPTICS PERFORMANCE

The performances given in this section are conservative, and still being consolidated (throughout the first year of operations). The following is thus a snapshot of the current performance level as measured during the acceptance tests in Europe, the integration in Paranal, and four commissioning runs on sky (between May and October 2014).

3.1 SAXO preliminary representative performance

The SPHERE Adaptive Optics module SAXO has been verified to perform nominally, and providing H-band Strehl ratio in excess of 90% for median seeing conditions (0.8''-1.2'') and bright NGS ($R < 9$ mag). See Figure 10 and Figure 11 for details.

The AO is not limited by the NGS flux up to $R \sim 9$. In between $R=9$ and 11, the correction remains very good but the lack of photons induces residuals that translates into a brighter residual halo in coronagraphic images. For fainter objects, AO correction can still be applied but at a slower rate, with degraded image quality.

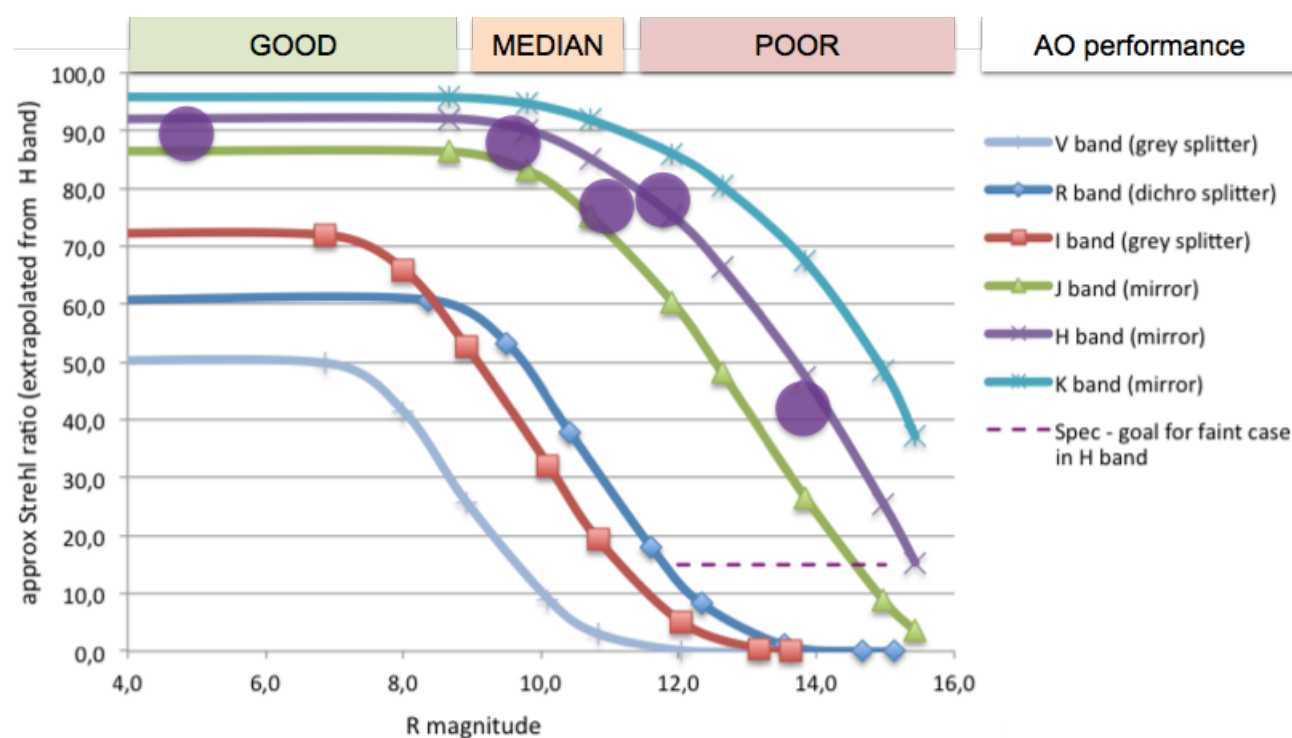


Figure 10: Theoretical and measured (purple circles) SPHERE-SAXO Strehl ratio as a function of R magnitude for good seeing conditions and different wavelength ranges from V to K (see Table 9 and Table 10 for details).

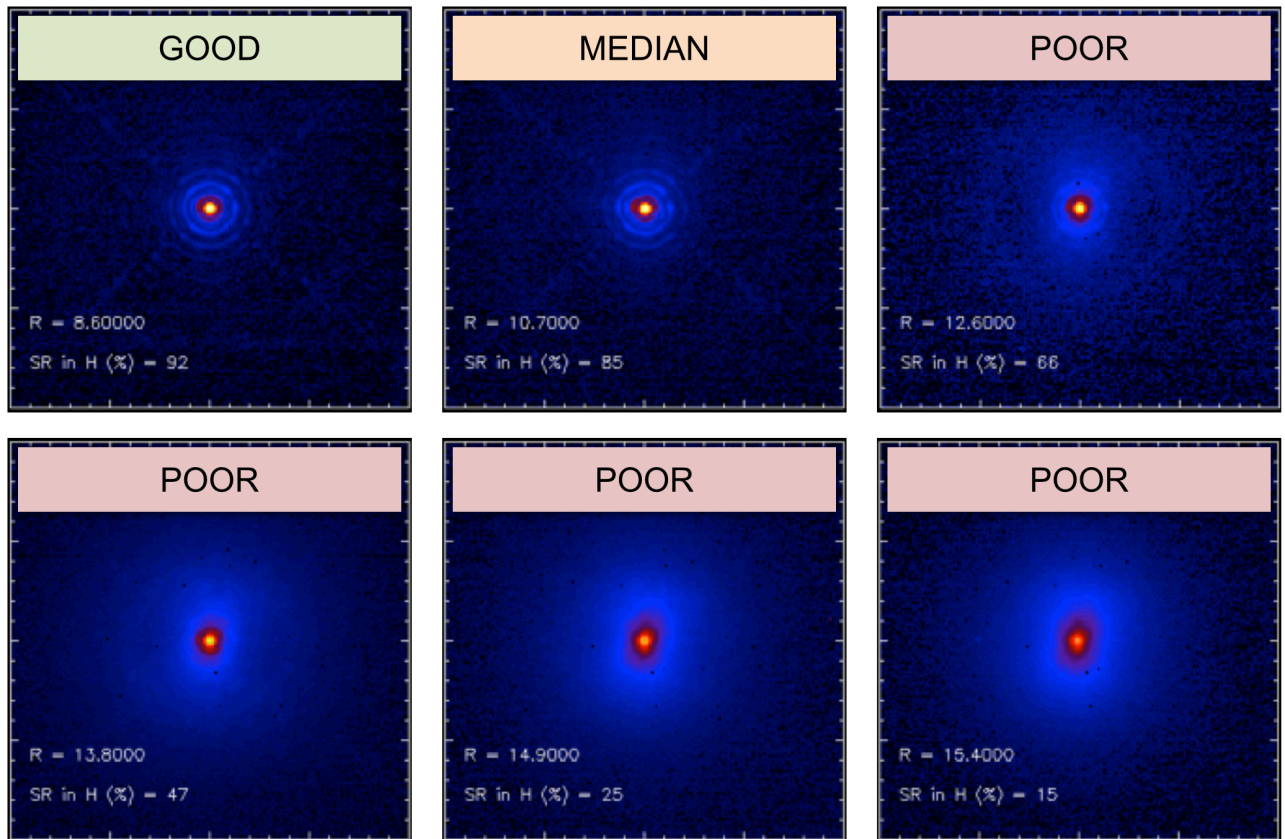


Figure 11: SPHERE PSF morphology and Strehl ratio as a function of R magnitude (see Table 9 and Table 10 for details).

3.2 IRDIS preliminary representative performance

3.2.1 IRDIS DBI

The 1σ -contrast achieved in coronagraphic imaging (IRDIFS_DB I) with filter combination DB_H23 (Figure 12) is shown as a function of angular separation (contrast curves) in Figure 13 for various differential imaging strategy combinations (SDI alone, or combined with ADI).

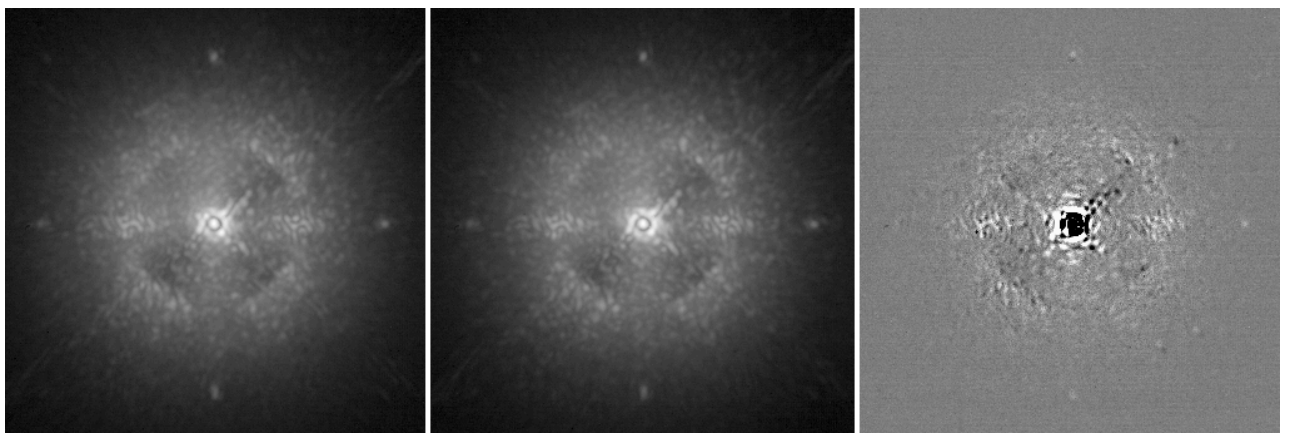


Figure 12: Coronagraphic images obtained in IRDIS H2 (left) and H3 (center) DBI filters, and the result of spectral differential imaging H2-H3 (right).

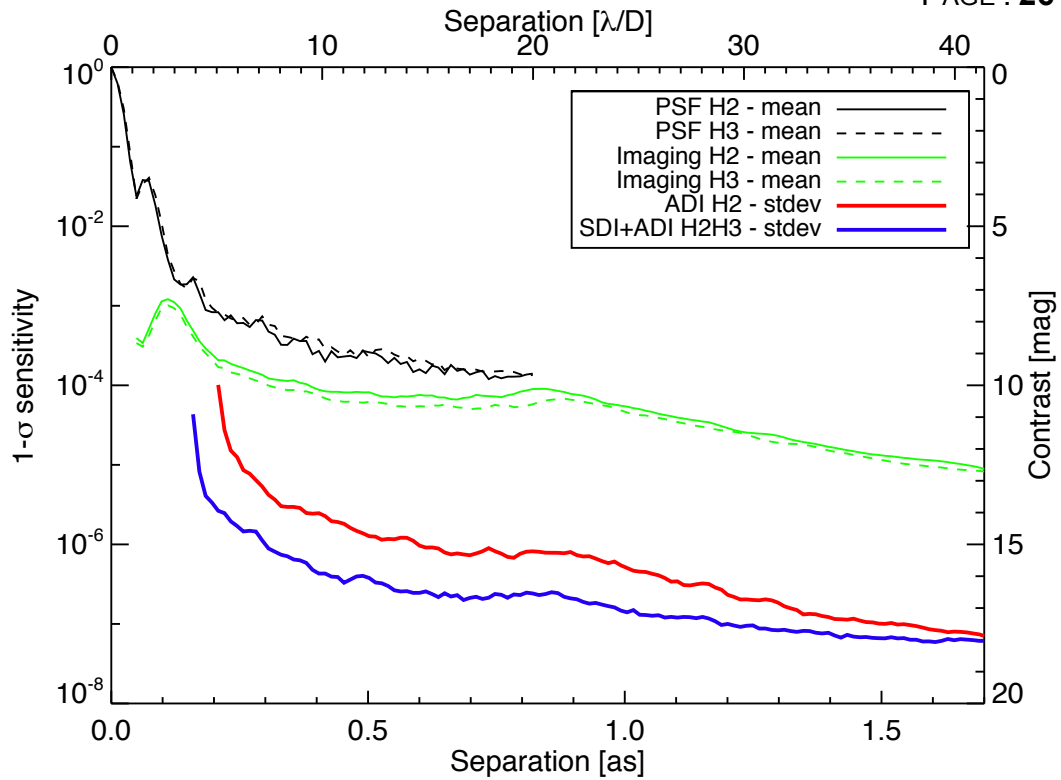


Figure 13: IRDIS DBI H2H3 contrast curves obtained on-sky for a bright target ($H=0.2$), in average conditions (seeing $\sim 1.0''$), with an ADI field rotation of 30 degrees. The plot shows the PSF profiles (black) and coronagraphic profiles (green) in the H2 and H3 filters, the 1σ contrast curve for ADI on the H2 data (red), and the 1σ contrast curve for SDI+ADI on the H2 and H3 data. For the ADI and SDI+ADI analysis, the algorithm throughput is taken into account and compensated, assuming a T8 spectral-type for the planet in SDI.

3.2.2 IRDIS LSS

Representative raw, and processed spectra, and contrast performance for the LSS mode of IRDIS are shown in Figure 14 and Figure 15.

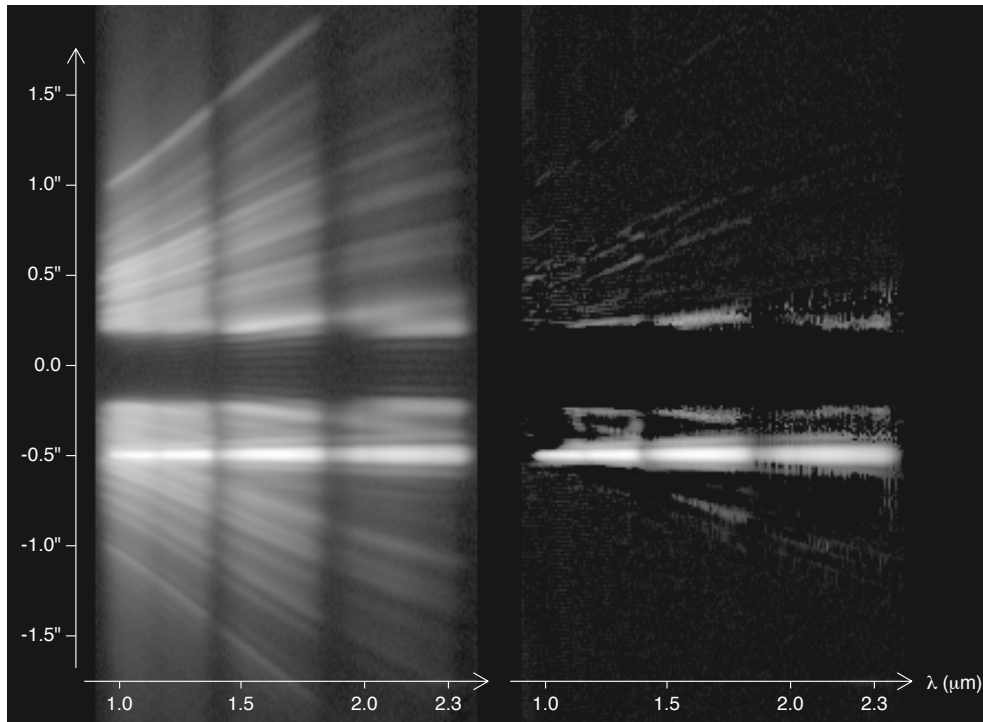


Figure 14: IRDIS LRS data obtained on PZ Tel ($H=6.5$). The left image is the spectrum after preprocessing and cleaning using the data reduction and handling pipeline (DRH). It corresponds to a 20 minutes exposure ($DIT \times NDIT \times NEXP = 20 \times 10 \times 6$) in good conditions (seeing of $0.5''$ - $0.6''$). The spectrum of the companion PZ Tel B is visible as a straight line amidst the speckles at an angular separation of $\sim 0.5''$. The obscured part between $\pm 0.2''$ corresponds to the position of the opaque coronagraphic mask. The contrast of the companion is ~ 5.4 mag in H-band (Biller et al. 2010, ApJ, 720, 82). The right image is the data after stellar halo and speckles subtraction using the spectral difference approach described in Vigan et al. 2008 (A&A, 489, 1345). The spectra are displayed with the same logarithmic color scale.

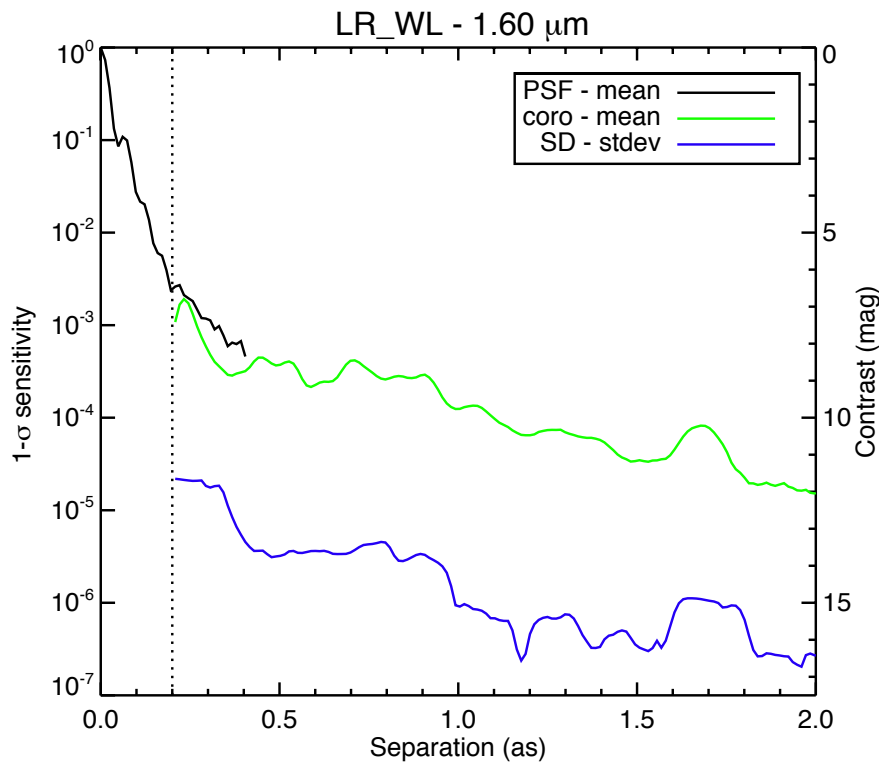


Figure 15: IRDIS LRS 1σ sensitivity curve at $1.6\ \mu\text{m}$ obtained on PZ Tel ($H=6.5$). The plot shows the PSF profile (black), the coronagraphic profile (green) and the noise level after subtraction of the stellar halo and speckles using spectral difference (SD). The dotted vertical line represents the edge of the coronagraphic mask. At a separation of $0.5''$, the raw contrast in LRS data is $2\text{-}5 \times 10^{-4}$, and the speckles can be estimated and subtracted down to a level of a few 10^{-6} . However, this noise level curve does not completely represent the capabilities of IRDIS LRS mode, because one has to consider that the final characterization performance is defined by the overall quality of the spectral subtraction, and not only by the noise level in a single spectral channel, which is always optimistic. A safety margin of a factor 3 to 5 with respect to these limits has to be taken into account when foreseeing LRS observations.

3.3 IFS preliminary representative performance

The IFS contrast floor after speckle subtraction using principal component analysis on Iota Sgr is shown in Figure 16.

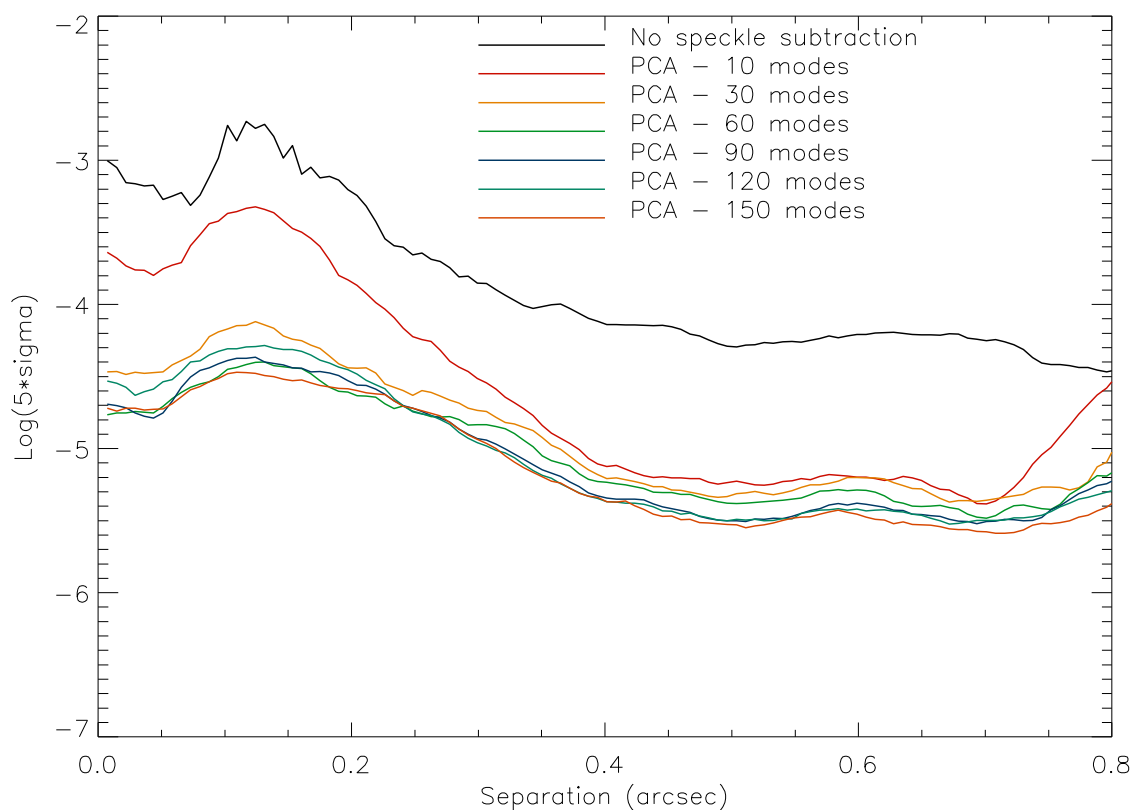


Figure 16: IFS 5σ sensitivity on Iota Sgr as function of angular separation, for different principal components retained in the speckle subtraction using both spectral and temporal diversity (ADI).

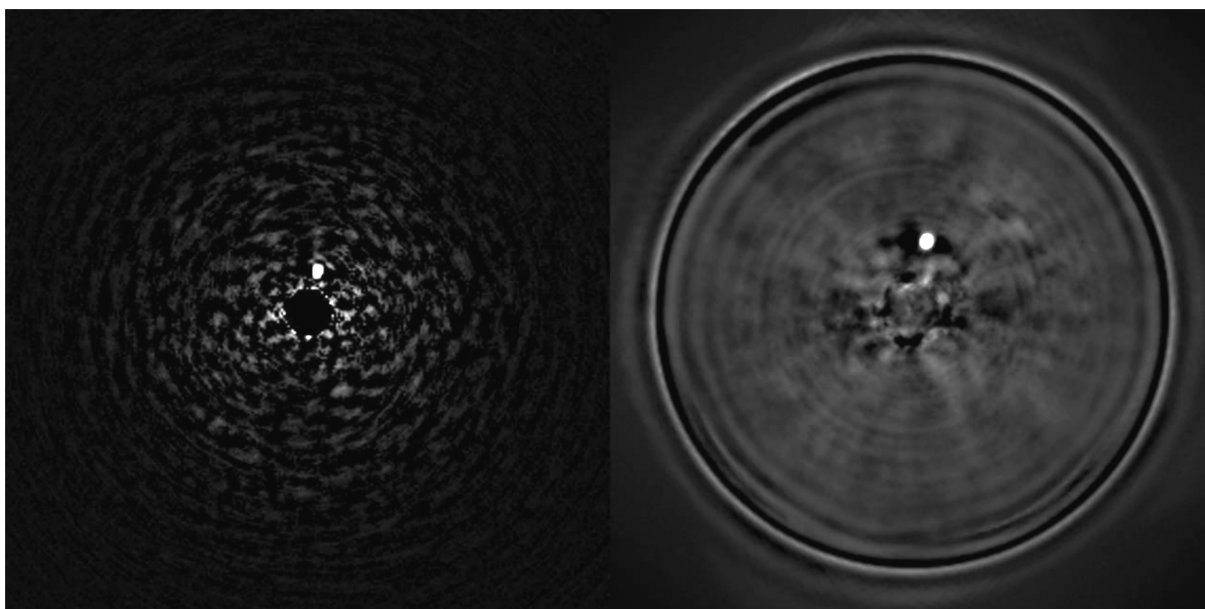


Figure 17: Detection in parallel by IRDIS (left) and IFS (right) of a faint companion at $0.24''$ around the bright star HR7581 (see ESO Press Release 1417, <http://www.eso.org/public/news/eso1417/>).

ZIMPOL preliminary representative performance

ZIMPOL performance as during commissioning is shown in Figure 18 and Figure 19.

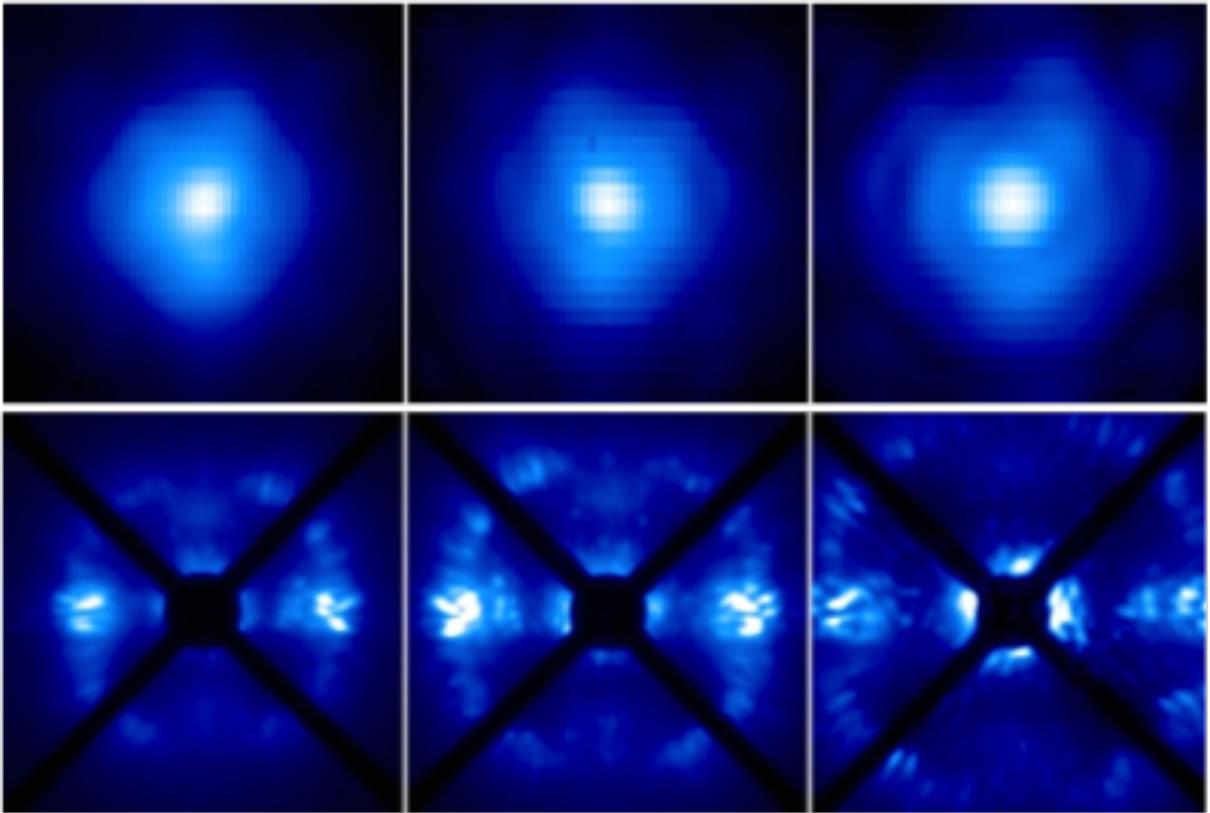


Figure 18: PSF (top) and coronagraphic (bottom) images of ZIMPOL in V, N_R, N_I filters.

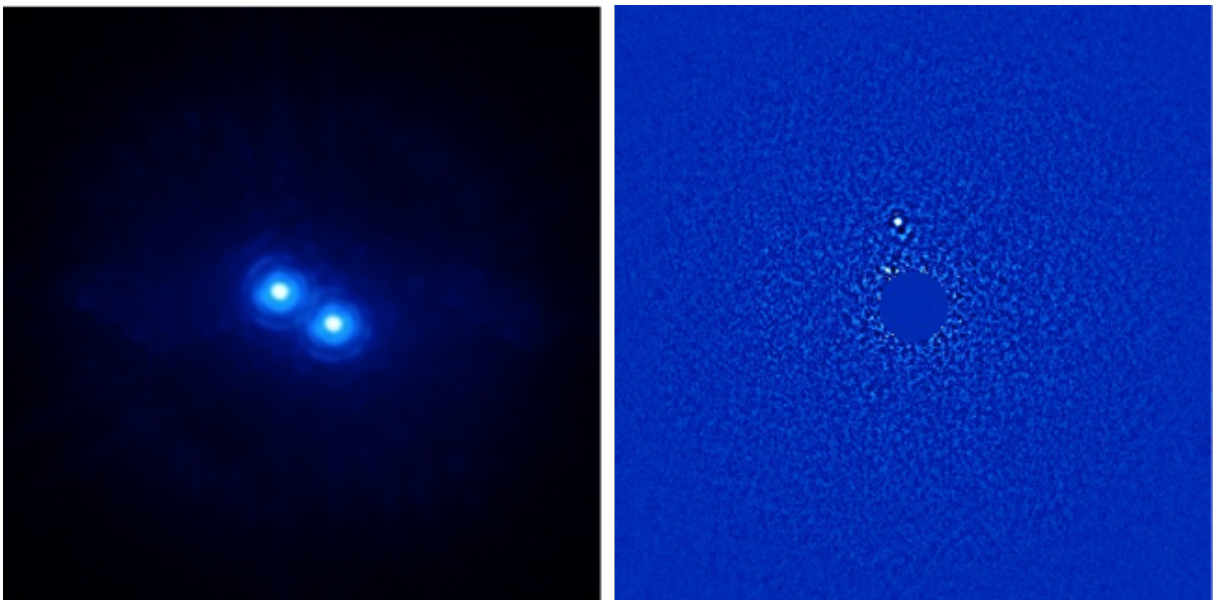


Figure 19: Left: High angular resolution imaging of a binary (150 mas separation) as seen by ZIMPOL in I band. Right: Pupil-stabilized ZIMPOL imaging providing ADI contrast close to 12 mag at 0.2'' (previously unknown companion).

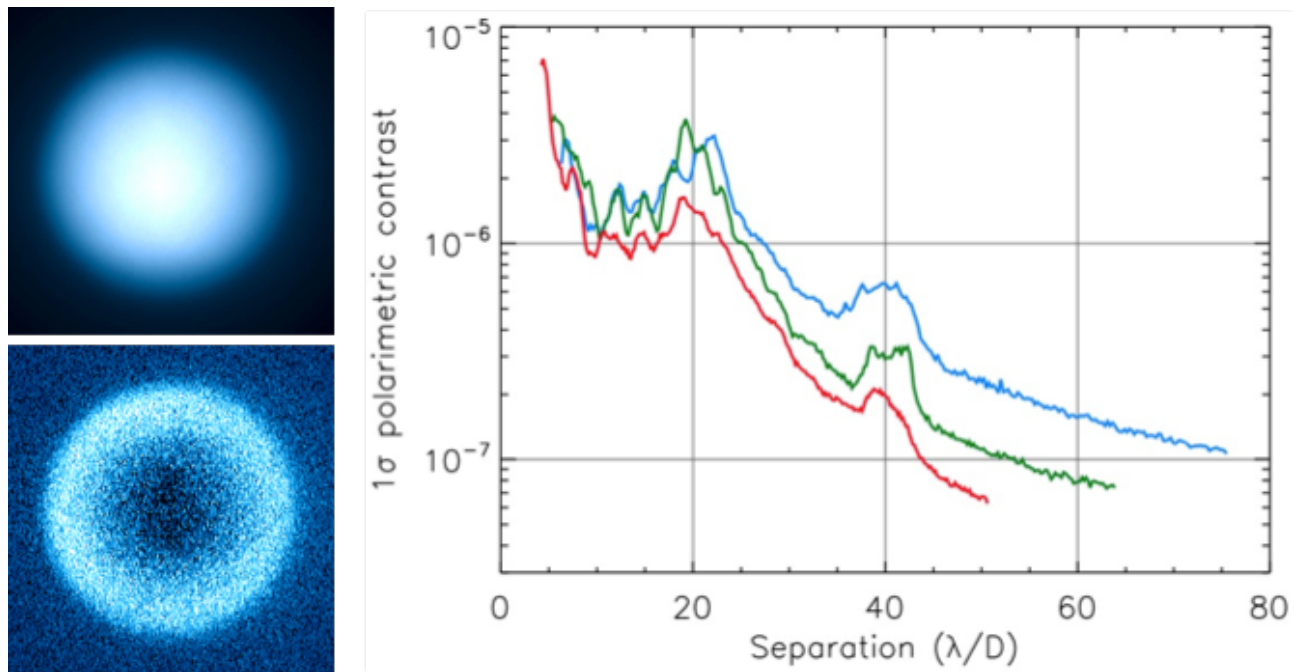


Figure 20: Top left: intensity image of Titan. Bottom Left: polarized intensity. Right: polarimetric contrast (right) on a bright target for the V (blue), N_R (green), N_I (red) filters.

4. EXPOSURE TIME CALCULATORS

The SPHERE ETCs can be found at: <http://www.eso.org/observing/etc>

It returns a realistic estimation of the detection limit. This limit is expressed as the achievable image contrast as a function of separation from the central star. It covers the various observing modes, filters and coronagraph set-ups.

When applying for telescope time, please remember to add the observational overheads as detailed in Section 8.

Currently the SPHERE ETCs comply with the Phase 1 goals mostly, especially in terms of exploring the noise & SNR regimes as well as the contrast (versus angular distance) performances to identify the right mode(s) for the right project and the approximate time needed.

However, the current SPHERE ETCs are not yet suited for accurate DIT prediction, across the suite of instrument modes and filters.

Until the online ETCs are corrected, please refer to the following page for more information:

<https://www.eso.org/sci/facilities/paranal/instruments/sphere/betaETC.html>

On this page you'll find the most up to date Excel DIT calculator for both IRDIS/IFS and ZIMPOL. You can address any question to sphere@eso.org

5. QUALITY ASSESSMENT

5.1 Seeing constraints

Stable adaptive optics performance is only expected for optical seeing $< 1.2''$. However the wind velocity may also affect observations as described below.

5.2 Low-wind effect (LWE)

The service mode quality assessment is not trivial for SPHERE as many parameters affect the achieved contrast at a given angular separation:

**intrinsic calibration of the common-path, AO and the given instrument,
external conditions (seeing, coherence time, wind speed, etc.)
many OB-depend parameters: star brightness, wavelength range and filter bandwidth,
length/field rotation, differential technique(s), post-processing, etc.**

For the time being, we decided to adopt a simple scheme based on the instantaneous image quality as seen by the telescope. For that we use the telescope guide probe FWHM (~ 600 nm) which proves to be rather well correlated to the performance in contrast and to the seeing estimated by the SPARTA real time computer.

When a user request a "seeing" constraint on SPHERE for his/her service mode program, he/she should think in term of guide probe image quality, not DIMM seeing. Hence, a challenging program should request < 0.8 arcsec. It does not make sense to request > 1.4 arcsec. Beyond 1.2 arcsec, SPHERE AO is extremely unstable. Programs requesting 1.2 to 1.4 arcsec seeing will be treated as fillers with possibly a high rate of frame selection to apply and a shallower contrast.

The following table explains the OB classification scheme for SM operations :

Table 5: QC scheme in Service Mode operations:

| OB Grade | Requested seeing constraints met | 6. | Seeing constraints exceeded by |
|-----------------------|----------------------------------|----|--------------------------------|
| A | <i>90% of the time</i> | OR | 5% |
| B | <i>50% of the time</i> | | 10% |
| C (to be repeated) | <i>Less than 50% of the time</i> | | 20% |

The low-wind effect appears when the outdoor wind speed (at 10 or 30m) drops below ~ 3 m/s. This is about 15 to 20% of the time and usually under good seeing conditions. The closer the wind is to 0 m/s, the stronger the effect. It is also referred as the "mickey-mouse" because it affects the PSF which can become double, triple (like "mickey-mouse" ears) or even quadruple. The effect is

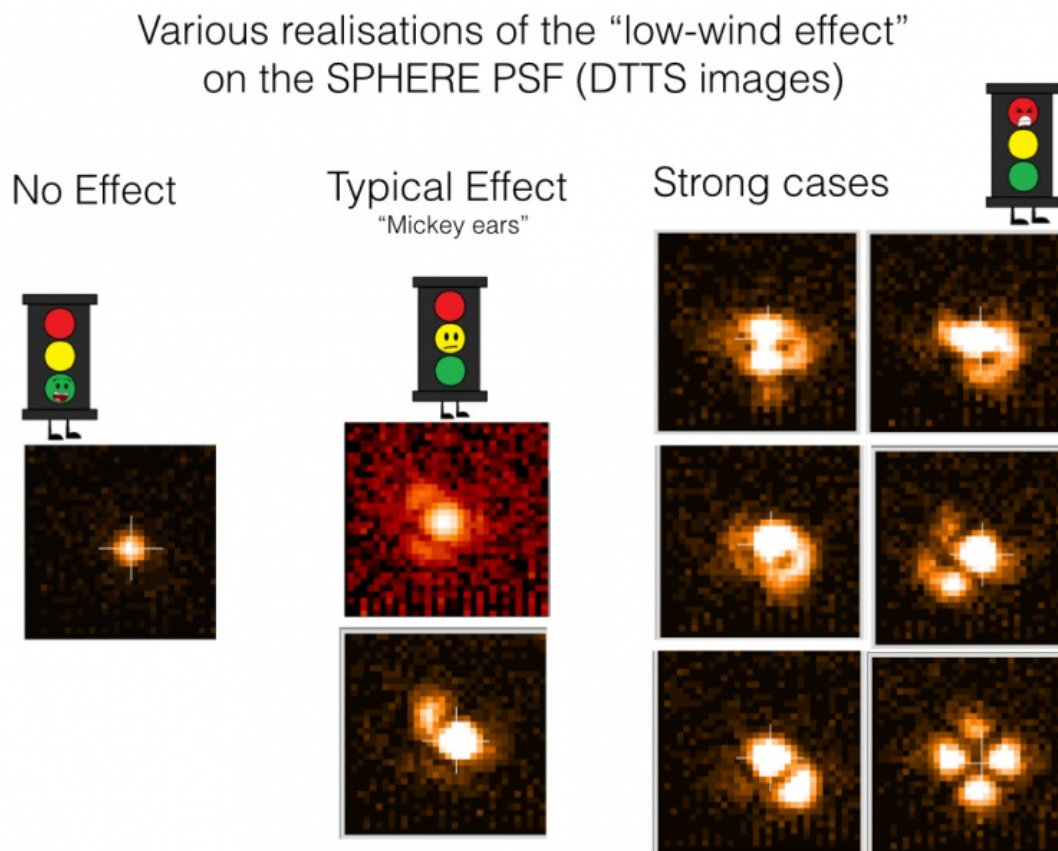
totally unnoticed by the AO system (Shack-Hartmann wavefront sensors are insensitive to differential piston). However, in the image plane, the PSF can be heavily affected by low-order aberrations which change on seconds to minutes time scales.

We are working on a scheme to quantify this effect (how bad is it and what are the percentage of affected frames). Meanwhile, we are recording it when it occurs and applying the scheme reported in Table 6. If it is strong and affects > 50% of the frames, we will classify the OB as "C" (must repeat). Otherwise, if shallow and < 50% of the time, we classify the OB as "B" (if all other constraints are met) and eventually add some frames. Behind the coronagraph, the effect is such that the telescope spiders aren't well suppressed and some time-varying bright speckles appear around the mask. On the F(flux) frames without the mask, **the PSF can appear double or with "mickey-type ears" or even quadruple (when very strong)** as shown on Figure 21.

Table 6: Low-Wind-Effect

| 6.1.1 LWE Strength | Action for support astronomers/operators, influence on the quality assessment |
|-----------------------|---|
| Very strong | Quit operations on SPHERE or wait (i.e VM mode). Eventually try to point in the very direction of the wind. Classify C and comment "Strong low-wind effect degrading the PSF" |
| Strong to mild | Wait and see if the wind increases. Evaluate if it is worth finishing the OB. Classify C and comment "Significant low-wind effect degrading the PSF" OR B if it was < 50% of the time. When possible, try to add some frames to make up for it. |
| Mild/Nominal | Keep observing with SPHERE. Classify B and comment "Mild low-wind effect degrading the PSF on <50% of the frames" if it was present less than 50% of the time |

Figure 21: Low-wind-effect qualitative assessment



6.2 Using SPARTA files to review image quality.

SPARTA files with information on the observing conditions sampled in minute time-scales are saved in the ESO archive (http://archive.eso.org/eso/eso_archive_main.html) along with the science data. To access these files, select “SPHERE/VLT” under *Imaging*, and enter “OBJECT, AO” for *user defined type*, under *Type* in the *Data Product Info* section. From these files one can obtain the SPARTA estimates of the wind and seeing during specific observations. One can also obtain images of the PSF without the coronagraph in the H-band, recorded on the DTTS, a 0.32”x0.32” FoV detector. If the primary target was brighter than 11 mag in the H-band, it should be detected on the DTTS. Hence one can check the PSF-quality, and in particular, whether the low-wind effect was present during a specific observation.

7. SPHERE OBSERVING PROPOSALS

Every semester, a call for proposal is issued by ESO. All relevant information on how to complete the so-called phase 1 proposal submission is available at:

www.eso.org/sci/observing/phase1/proposals.html

Below, we describe SPHERE observing modes and summarize them for IRDIS and IFS observations in Table 7 and for ZIMPOL in Table 8. A recommended choice of observing parameters is shown for some science cases. The feasibility of the project, the expected performance, and required telescope time should to be worked out by the proposer with the help of the ETC, adding the observational overheads listed in Section 8.

7.1 Observing modes

NIR observations of young planetary mass companions around bright stars can be performed using IRDIS and IFS simultaneously. This mode is called IRDIFS. This is the nominal infrared mode of SPHERE, recommended for surveys, with the IFS covering the Y-J wavelength range, and IRDIS offering dual-band filters in and out of the methane spectral features in the H band (around 1.65 μm). The broad-band H filter is also offered in this mode from period 97. IRDIFS offers a limited range of coronagraphs, and allows the user to choose between pupil and field tracking (pupil tracking is recommended for highest contrast performance).

IRDIFS_EXT is similar to IRDIFS but extends IFS coverage to the Y-H range, while enabling (sub-optimal) dual narrow-band observations in the K band with IRDIS. The broad-band K filter is also offered in this mode from period 97. Thanks to a wider spectral range, IRDIFS_EXT improves the IFS detection capability at small inner working angles (inside $\sim 0.2''$). This mode is recommended if additional spectral range is needed (e.g. characterization of known candidate companions).

IRDIS may also be used alone, where it offers a larger range of narrowband and broadband filter choices between 0.95 to 2.32 μm , coronagraphic, polarimetric and long-slit spectroscopic capabilities:

- a. **IRDIS_DBI (dual-band imaging) offers filter pairs in the complete spectral range. This will in particular provide essential spectral information for companions out of the IFS FoV.**
- b. **IRDIS_CI (classical imaging) provides a larger choice of observing parameters such as broadband filters (wider and more sensitive than DBI for faint stars) and narrowband filters.**
- c. **IRDIS_DPI (dual-polarization imaging, offered from P96).**
- d. **IRDIS_LSS (long slit spectroscopy) is a promising experimental mode merging long slit spectroscopy with coronagraphy (the slit is equipped with a blocking mask at its center, see Appendix for details). The IRDIS_LSS mode spectral range starts from Y, either up to H band at resolving power $R\sim 350$ (with $0.09''$ wide slit), or up to the K band at $R\sim 50$ (with $0.12''$ wide slit). The latter is useful for confirmation of a companion that is solely detected by IFS, or to take advantage of IRDIS's larger field of view. However, since speckles scale with wavelength, they move out of the field of view at long wavelengths, such that speckle subtraction is compromised for field of view larger than $5''\times 5''$.**

For other science cases, such as extended sources, DPI or classical imaging is possible in all filters, with or without coronagraph, in pupil or field tracking. Please note that most differential techniques

can cause significant self-subtraction for extended sources (ADI), for sources without spectral features (SDI), or unpolarized sources (PDI).

Table 7: IRDIS and IFS observing modes.

| Mode | Sub-mode | Description | | | Main Science case |
|----------------|------------|---|-------------------------|---|---|
| | | Module/ Spectral range | Derotator | Setup/ options | |
| IRDIFS | IRDIFS | Simultaneous: IFS (Y-J) + IRDIS/DBI (narrow -band) or broad-band H. | Pupil or field stab. | None/ selected coronagraphs | Exoplanet detection and characterization |
| | IRDIFS_EXT | Simultaneous: IFS (Y-H) + IRDIS/DBI (narrow -band) or broad-band K. | Pupil or field stab. | None/ selected coronagraphs | Specific charact. using IFS up to H band |
| IRDIS alone | DBI | Dual Band Imaging, any dual-band filter pair: Y to Ks | Pupil or field stab. | None/ selected coronagraphs | Charact. of companions in outer field, or confirmation of IFS detection |
| | DPI | Dual Polarization Imaging, any BB/NB filter: Y to Ks (BB recommended, especially J) | Field stab. | None/ selected coronagraphs (CPI HWP in) | Polarized circumstellar disks |
| | LSS | Long slit spectroscopy | Field stab. | Low or medium resolution | Characterization of companions |
| | CI | Classical imaging, any BB/NB filter: Y to Ks | Pupil or field stab. | None/ selected coronagraphs | High contrast and high sensitivity (broadband) imaging |

Imaging and polarimetry are available in the optical with ZIMPOL. In imaging mode “I”, polarimetric devices are not used. Both detectors can either observe in the same or in different

filters (e.g. $H\alpha$ on/off for differential imaging). For polarimetric imaging, each arm provides a full polarimetric measurement.

Table 8: ZIMPOL observing modes.

| Mode | Description | | Science case |
|-----------|----------------------|--|---|
| | Derotator | Set-up/options | |
| P1 | Fixed | CPI HWPs in, FLC in <i>Options:</i> focal plane coronagraphic mask or clear field mask, FW1 and FW2 filters, WFS/ZIMPOL beamsplitter | Highest (absolute) precision polarimetry mode |
| P2 | Field stab. | CPI HWPs in, ZIMPOL HWPZ and FLC in <i>Options:</i> focal plane coronagraphic mask or clear field mask, FW1 and FW2 filters, WFS/ZIMPOL beamsplitter | High precision polarimetry suited for fainter targets |
| I | Pupil or field stab. | All polarimetric components out <i>Options:</i> focal plane coronagraphic mask or clear field mask, FW0, FW1 and FW2 filters, FW0 ND-filters, WFS/ZIMPOL beamsplitter | High angular resolution imaging |

The detector has 3 different readout modes (see Appendix for details). The fast polarimetry mode is used for high precision polarimetry of bright targets (with $R \sim 3-7$ mag). The slow polarimetry mode (with lower RON, better efficiency, but also reduced dynamic and longer minimum DIT) is more sensitive to probe the fainter environments (in the outer PSF and/or in narrowband filters). The standard imaging mode is used for non-polarimetric imaging.

7.2 Coronagraphs and filters

The choice of the coronagraph depends on the observing wavelength and inner working angle (see Tables in Sections 10.1 and 10.7). Filter sets are detailed for IRDIS in Section 10.3 and for ZIMPOL in Section 10.8. For ZIMPOL please note the AO limiting magnitudes with the grey beam splitter is ~ 1.74 mag brighter than with the dichroic. Also note that the use of some filters and neutral densities (located in FW0) will result in additional instrumental polarization which cannot be calibrated using the polarization compensator. Therefore the use of filters and neutral densities in the FW0 filter wheel is not recommended for ZIMPOL polarimetric imaging modes.

Coronagraphs set-ups and centering, which are performed in the acquisition template, take ~ 5 minutes. Hence the observer is advised to limit the number of set-up changes of the coronagraph.

7.3 AO limiting magnitudes

The most important feasibility check for SPHERE observations concerns the AO performance, measured by the Strehl ratio (SR). The SR directly impacts raw contrast level C through the rule of thumb $C \propto (1-SR)/N^2$ (Serabyn et al. 2007, ApJ 658, 1386) with N^2 , the number of AO correcting elements (~ 1300 in SAXO).

In Table 9, we define three regimes with good, median, and poor AO corrections as a function of R magnitude and seeing as listed in Table 10. Note that these values are very conservative, and the system will likely deliver better performance, although this is not yet guaranteed (see Section 3, Figure 10).

Table 9: AO performance summary.

| AO performance | H-band Strehl Ratio | R-band Strehl Ratio |
|----------------|---------------------|---------------------|
| Good | > 75% | > 20% |
| Median | 50-75% | 5-20% |
| Poor | < 50% | < 5 % |

Table 10: Three regimes with good, median and poor AO corrections as a function of the R-band magnitude of the target and Seeing.

| NGS mag / Seeing | Seeing < 0.8" | Seeing = 0.8"-1.2" | Seeing > 1.2" |
|----------------------|---------------|--------------------|---------------|
| R = 0-9 mag | Good | Median | Poor |
| R = 9-11 mag | Median | Median | Poor |
| R > 11 mag | Poor | Poor | Poor |

The contrast depends weakly on the seeing in good atmospheric conditions and degrades rapidly for seeing > 1.2", and NGS R mag > 11. For this reason, SPHERE is only offered in service mode for NGS R mag < 11.

7.4 Telescope time

For proposal submission, the astronomer should estimate the total telescope time required for the observing program. The ETC should be used to compute the integration times. When applying for telescope time, please remember to add the overheads described in Section 12. In service mode, observations are executed with observing blocks of at most 1-hour duration. An observing program must therefore take this constraint into account at Phase 1.

For the vast majority of projects, the night-time OBs will contain only one science template and the mandatory target acquisition template. The usual calibration measurements such as darks, flat-field and wavelength calibrations, are taken during the day-time as part of the calibration plan (Section 9). If for some observations, particular calibrations are needed immediately after the science

exposure, these can be obtained by attaching specific calibration templates at the end of the OB or by concatenating a standard-star OB to the science OB.

For phase 2, the ESO Phase 2 Preparation Tool (P2PP) will be able to provide accurate estimates of the execution time, including overheads. It is available at:

<http://www.eso.org/sci/observing/phase2/P2PP3.html>

8. PREPARING OBSERVATIONS

8.1 Phase 2

After proposal submission (phase 1, Section 4), when telescope time has been granted, the observations need to be prepared during phase 2. Please consult the general guidelines on phase 2, service and visitor mode, which are available at:

- **Phase 2 preparation:** <http://www.eso.org/sci/observing/phase2.html>
- **Service mode:** <http://www.eso.org/sci/observing/phase2/SMGuidelines.html>
- **Visitor mode:** http://www.eso.org/paranal/sciops/VA_GeneralInfo.html

The observing blocks (OBs) are created with the aid of the P2PP tool during phase 2. OBs include: one acquisition template, followed by one or more templates for science observations and/or night-time calibrations. Finding charts and readme files need to be created according to the instructions available at:

<http://www.eso.org/sci/observing/phase2/SMGuidelines/FindingCharts.SPHERE>

And,

<http://www.eso.org/sci/observing/phase2/SMGuidelines/ReadmeFile.SPHERE>

Currently, NDITs above 20 are not allowed for any template, since this may cause file readout problems.

8.2 Observing constraints

The SPHERE observing constraints which can be included in Observing Blocks when preparing the observations are:

1. **Seeing:** $1''.2-1''.4$ (depending on τ_0). The optical (V-band) seeing at the position of the sky at which the telescope is pointing,
Transparency: SPHERE's adaptive optics system SAXO has been shown to be tolerant to THIN conditions, so user should only request photometric (PHO) or clear (CLR) conditions only for programmes requiring absolute flux measurements.
2. **Moon illumination and angular distance:** SPHERE's small field of view and pixel scale is such that observations are not sensitive to the moon illumination. The angular distance, however, is recommended to be $> 30^\circ$ because of the VLT active optics.
3. **Airmass:** considering the maximum compensable atmospheric dispersion by ADCs, pointing is restricted to $z < 60^\circ$ (airmass < 2). More generally, observing close to meridian is strongly recommended for ADI performance and PSF stability. Worst pointing directions (with most variable aberrations) are at $|HA| > 3\text{hr}$ for DEC $> -40^\circ$ and $|HA| > 2\text{hr}$ for DEC $> +10^\circ$.

ESO will consider an OB as successfully executed if all the conditions in the constraint set are fulfilled. OBs executed under conditions marginally outside constraints by no more than 10% of the specified value will not be scheduled for re-execution. Unlike other Adaptive Optics-assisted instruments on Paranal, the image quality of observation conducted in service-mode will be

classified according to the seeing constraint only. Once more experience is gained with the instrument performance under a wide range of observing conditions, this situation will change, and Strehl or contrast will be introduced as a formal observing constraint for SPHERE..

SPHERE has been verified to provide optimal performance under stable temperature conditions. Moreover, critical components are sensitive to temperature and humidity. For these reasons, the observatory reserves the right to interrupt observations if conditions put the instrument or the quality of the data in jeopardy. For instance:

1. **Temperature should be between 5°–18°C. Temperatures outside of this range change the DM shape at rest and reduce the tolerance to high seeing values.**
2. **Temperature variations < 1°C/h, and excursions over the night < 4°C. Strong temperature gradients will degrade the PSF stability.**
3. **Humidity should stay below 50%, as it might potentially damage the deformable mirror.**

8.3 Target acquisition templates

Each OB starts with an acquisition template. The selection of the appropriate acquisition template is detailed in

Table 11. It depends on the subsequent observing mode. Target acquisition is nominally performed in a narrow 2''x2'' field of the WFS sub-apertures, and so requires precise target coordinates and proper motion. Requiring a larger FoV by imaging using IRDIS introduces unnecessary overheads times. It is important to note that all observations in a given OB should share the same sub-mode.

For SPHERE, it is typically not necessary to define a specific telescope guide star. Therefore, the telescope guide star selection can be set to “catalogue”, in which case a suitable telescope guide star will automatically be selected from one of the catalogues present at the telescope.

Parameters defined by the observer will be discussed in Section 10.

Table 11: List of SPHERE acquisition templates.

| Acquisition template | Observing mode |
|----------------------|---|
| SPHERE_irdifs_acq | IRDIFS, IRDIFS_EXT |
| SPHERE_irdis_acq | IRDIS alone in DBI or CI. |
| SPHERE_irdis_dpi_acq | IRDIS alone in DPI mode. |
| SPHERE_irdis_lss_acq | IRDIS alone in LSS. |
| SPHERE_zimpol_i_acq | ZIMPOL: Imaging (I). |
| SPHERE_zimpol_p_acq | ZIMPOL: Polarimetric Imaging P1 (derotator fixed) or P2 (field stabilized). |

The acquisition templates include:

- a. **Telescope preset to the target coordinates and acquisition of telescope guide star.**
- b. **Automatic setting of AO parameters, servo loops and checks.**
- c. **Start of tracking components: derotator, ADCs, and polarization components if relevant.**

- d. **Centering on the coronagraphic focal mask, if any. When the user-defined focal mask is different from the previous OB, the new mask is set in and a corresponding calibration can be performed to ensure the best centering and focus accuracy. Note that this coronagraphic device selection cannot be modified in subsequent observation templates: it remains the same in all the templates of the OB.**

8.4 General user defined parameters for IRDIFS and IRDIS templates

IRDIFS and IRDIS observation templates share many common parameters defined by the observer. They include settings of:

- a. **DIT, NDIT, NEXP for IFS and IRDIS. A DIT value of 0 indicates that the smallest possible DIT value (currently 0.83 seconds) is to be used.**
- b. **Number of dithering positions for IRDIS (4x4 recommended). No dithering is offered for IFS.**
- c. **Observation type list. Defines the sequence of Object (O), Sky (S), Flux (F) and Star Center (C) measurements (see below) to be obtained.**
- d. **Detector X and Y offset for flux measurements. Indicates the offset (in mas) which is performed to offset the source from the coronagraphic mask for the flux measurement. The recommended value (and also maximum value) is +500mas or -500mas.**
- e. **Sky RA and Dec offset list. A list of sky offsets (in arcseconds) for the sky background measurement. The number of sky measurements for each "Sky" in the observation type list is equal to the number of offsets defined in the Sky RA and Dec offset list, i.e. for an RA and Dec Sky offset list of "10 -10", "-10 10" will result in two sky background measurements per "S" in the observation type list. An amplitude for the offset greater or equal to 10" is recommended, it should be less than 60".**
- f. **Deformable mirror waffle parameters. These parameters control the amplitude and the pattern of the four symmetric echoes of the PSF core in the Star Center measurement. Details are given in Appendix A 12 concerning the use of the waffle spots for accurate centring. In case of observing an object with a known companion, changing these parameters may be useful to ensure that the position of the echoes do not coincide with the location of the companion. The recommended amplitude is 0.05, corresponding to 5% of the available DM stroke. This makes a ratio between the PSF echoes and the star peak of 1.3% at H band, and scales quadratically with the wavelength.**
- g. **Choice of neutral density filters.**
- h. **Field orientation, for field-stabilized observations.**

Besides the on-axis (coronagraphic or not) observation of the object (observation type O), the observing template sequence should also include these observation types whenever using a coronagraph, or when observing extended objects for the third one:

Star Center - C: in the pupil-stabilized mode, the field rotates. It is thus critical to obtain the exact position of the rotation center. This is also important for accurate measurement of the separation of any potential companion. This allows measuring this position by applying a waffle pattern to the deformable mirror, which creates four replicas of the PSF away from the coronagraphic mask (see Appendix A12). Localizing

the four peaks allows computing the rotation center, at the middle of the square pattern. This measurement is performed with the science template and can be repeated several times during a long science sequence.

Flux - F: a PSF core off-axis measurement can be inserted before and/or after deep coronagraphic observations in order to register the PSF core flux. Contrast curves are derived from this measurement. Off-axis measurements can be performed by moving the star and inserting a neutral density but without moving the coronagraphic focal mask and thus without perturbing the centering accuracy.

Sky – S, optional: observes the sky background. Accurate knowledge of the background is not important for point-like objects. However, it might be important for faint extended emission.

The DIT values for the C and S observations, are not user-defined parameters, but are identical to the DIT used for the O observation. The DIT value for the F observations has to be defined separately within the observing template.

For convenience, especially if the observer is unsure about the saturation level, it is recommended to isolate a Flux F and Star Center C in two independant templates to allow the night astronomer to check the saturation level of these frames before continuing with the rest of the observations (typically observations of type O). This way, the detector integration time can be more easily adjusted, in case of detrimental over- or under-illumination of these critical frames, without aborting the whole sequence of observations.

8.5 IRDIFS templates

8.5.1 Observation templates and user-defined parameters

IRDIFS observation templates are detailed in Table 12. Parameters defined by the observer will be presented in Section 10.

Table 12: IRDIFS observing templates.

| IRDIFS observation templates | Observing modes |
|------------------------------|---|
| SPHERE_irdifs_obs | IRDIFS observations, with IFS observing in Y-J and IRDIS in H-band, DB_H23, or DB_H34 |
| SPHERE_irdifs_ext_obs | IRDIFS_EXT observations, with IFS observing in Y-H and IRDIS in K-band or DB_K12 |

For efficiency reasons it is recommended that the total duration of IFS and IRDIS exposures are similar. The neutral densities inserted in CPI are common to IRDIS and IFS. For minor differential adjustment another ND0.5 (factor $10^{-0.5}$) is available inside IRDIS for the H band dual-band filters.

8.5.2 Calibrations

Calibrating IRDIFS data involves usual day-time internal calibrations (darks/background, flat, spectral calibration of the IFS, see Section 9 for details).

8.6 IRDIS: DBI

8.6.1 Observation templates and user-defined parameters

| IRDIS observation templates | Observing modes |
|-----------------------------|-----------------|
| SPHERE_irdis_dbi_obs | IRDIFS DBI |

For IRDIS-only observations in dual band imaging mode, there is a single template called SPHERE_IRDIS_dbi. Parameters defined by the observer are discussed in Section 9.

The Appendix lists all the available filters. The filter pair DB_ND23 includes a ND0.5 neutral density but is otherwise identical to DB_H23.

8.6.2 Calibrations

Calibrating IRDIS-DBI data involves on-sky and internal (day-time) calibrations similar to the IRDIFS and IRDIFS_EXT modes (see Section 8.5.2). Other night-time and day-time calibrations provided as part of the SPHERE calibration plan are detailed in Section 9.

8.7 IRDIS alone Classical Imaging (CI)

8.7.1 Observation templates and user-defined parameters

| IRDIS observation template | Observing mode |
|----------------------------|----------------|
| SPHERE_irdis_ci_obs | IRDIS CI |

A complete list of user-defined parameters is presented in Section 10.

8.7.2 Purpose and properties

This mode is a general-purpose mode, which can be used in pupil, or field stabilized regime. In this mode any filters from the common filter wheel can be used. The recommended derotator rotation law to be used for observation of extended objects should be the field stabilized to avoid image smearing. Coronagraphs can also be used with any filter in classical imaging mode (see Appendix for details).

8.7.3 Calibrations

The calibrations for IRDIS CI observations are the same as for DBI observations.

8.8 IRDIS DPI (Dual Polarization Imaging)

Dual polarimetry (via DPI) is a proxy to achieve greater contrasts at small inner-working-angles. This is provided that the object of interest features polarized scattered light in the near IR (i.e debris and proto-planetary disks, etc.). If the latter condition is satisfied, DPI offers an enormous advantage over other high contrast differential techniques : images at orthogonal linear polarizations are taken simultaneously. If both beams have the same optical aberrations, DPI allows very efficient speckle suppression in the control radius of the AO/coronagraph.

This mode has been used in Science Verification time and by the GTO in “shared risks” because its characterization was incomplete. It is now offered starting in P96.

8.8.1 Instrumental polarization

Thanks to the SVT and P95/P94 experience, we were able to better characterize the IRDIS DPI mode. We found out that the control law of the HWP was not ideal and changed it in late April 2015.

In addition, we measured the effect of polarization cross-talks inside the instrument for four BB filters during P94 & P95.

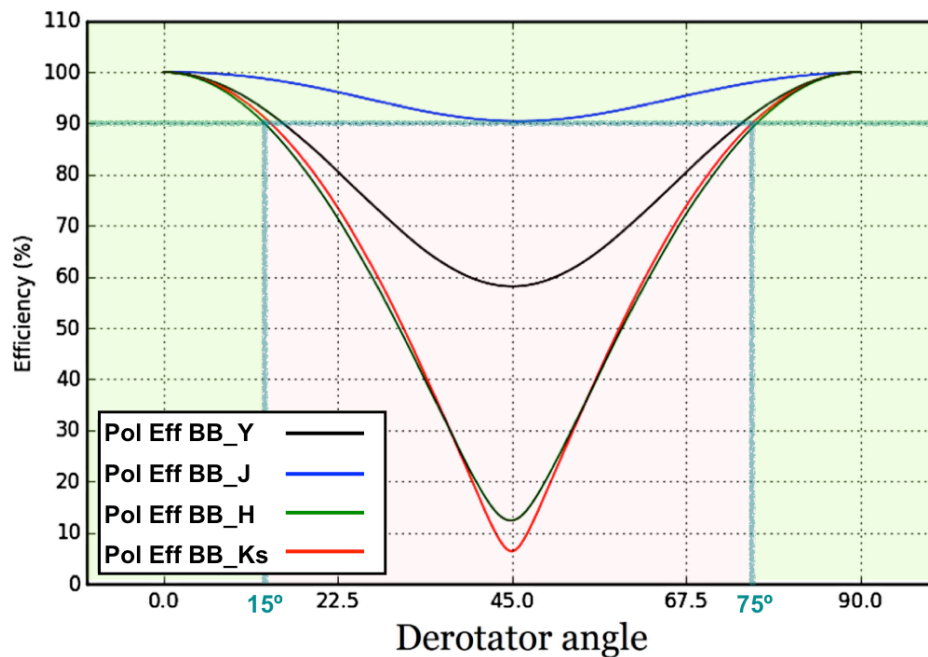


Figure 22: Measurements of the instrumental polarization efficiency (not accounting the telescope) for four broad band filters. For best use of the DPI mode, one should avoid the pink zone where the efficiency drops below 90° (> 10° loss due to cross-talks). For that, one should make sure the derotator angle stays < 15° or > 75°. J-band is the least affected and therefore the most recommended filter, especially for long observations featuring a large parallactic angle variation. At J-band the efficiency is always > 90%.

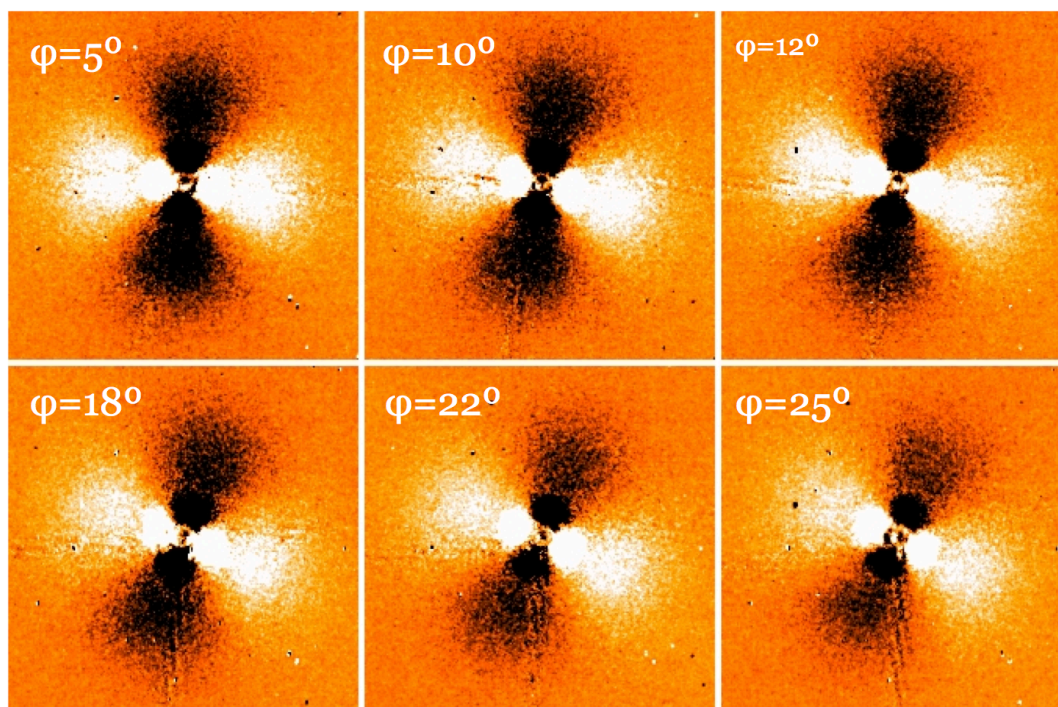


Figure 23: Effect of the instrumental polarization (efficiency loss due to increased cross-talks at a varying derotator angle). The « butterfly pattern » rotates with time and its signal to noise ratio decreases significantly. This is the polarimetric signature of a bright face-on disk (H-band observations).

Figure 23 shows the « butterfly » pattern of a bright face-on polarized disk. Its SNR and orientation varies in time. This is because of the departure, during the observation from the ideal ($< 15^\circ$ or $> 75^\circ$) derotator position as it tracks the field, in H-band (as shown in Figure 22). This effect was even stronger before the end of April 2015 when we changed the half-wave-plate control law.

We recommend the following when using the DPI mode:

- Use the BB filters as much as possible
- J-band is the least affected filter (efficiency always $> 90\%$)
- For Y, H and K-band DPI, try to keep the derotator angle $< 15^\circ$ or $> 75^\circ$. This can be done by entering a derotator position angle in the science template (bottom parameter). You can use this formula:

$$\text{Derotator position angle} = \langle \text{parang} - \text{alt} \rangle \text{ or } = 180 + \langle \text{parang} - \text{alt} \rangle$$

Where $\langle \text{parang} - \text{alt} \rangle$ is the mean value of the difference between the parallactic angle and altitude of the target during the template. If the amplitude of that difference is greater than 15° during the template, split the template in 2 shorter ones, and repeat the calculation.

To help you check whether your observation, at a given time will be affected by efficiency problem, an Excel table is now available here:

It calculates for a given declination and position angle (as entered in p2pp), in which regime of Figure 22 the derotator is and hence, which is the implication on the polarimetric efficiency. Time is given in Local HA (how far away one is before and after the meridian) and the efficiency regimes are “green” when $< 20^\circ$ from the ideal derotator angle, yellow when $> 20^\circ$ and $< 30^\circ$, red otherwise:

http://www.eso.org/sci/facilities/paranal/instruments/sphere/doc/IRDIS_DPI.html

8.8.2 Observation templates and user-defined parameters

| IRDIS observation templates | Observing modes |
|-----------------------------|-----------------|
| SPHERE_irdis_dpi_obs | IRDIS DPI |

For IRDIS only observations in dual polarized imaging mode, there is a single template called SPHERE_IRDIS_dpi. Parameters defined by the observer are discussed in Section 9. They include setting:

- a. **DIT, NDIT, NEXP.** A DIT value of 0 indicates that the smallest possible DIT value (currently 0.83 seconds) is to be used.
- b. **IRDIS Filter Combination and Neutral density filters.**
- c. **Stokes parameters to be measured (Q or Q and U).**
- d. **Number of polarimetric cycles**
- e. **The polarization gamma parameter.** This parameter reflects the on-sky orientation (measured clockwise from North) of the measured polarization in the first image of a Q cycle.

8.8.3 Calibrations

Differential polarimetry is a proxy to achieve greater contrasts at small inner-working-angles. This is provided that the object of interest features polarized scattered light in the near IR (i.e debris and proto-planetary disks, etc.).

Calibrating IRDIS-DPI data involves on-sky and internal calibrations similar to the IRDIS CI and IRDIFS_DBI modes (see Section 8.5.2). Other night-time and day-time calibrations provided as part of the SPHERE calibration plan are detailed in Section 9.

8.9 IRDIS alone Long Slit Spectroscopy (LSS)

8.9.1 Observation templates and user-defined parameters

| IRDIS observation template | Observing mode |
|----------------------------|----------------|
| SPHERE_irdis_lss_obs | IRDIS LSS |

User-defined parameters are:

- a. **DIT, NDIR, NEXP. A DIT value of 0 indicates that the smallest possible DIT value (currently 0.83 seconds) is to be used.**
- b. **Spectral resolution and range: LRS (R~350) / MRS (R~50).**

The slit selection (for width and size of the central blocking mask) is made in the acquisition template that also ensures the appropriate on-slit target centering.

The complete list of user-defined parameters is presented in Section 10.

8.9.2 Purpose and properties

Scope of LSS:

IRDIS long slit spectroscopy mode (LSS) is designed for the spectral characterization of already detected objects either at low resolution (LRS, $R \sim 50$) over Y to Ks, or medium resolution (MRS, $R \sim 350$) over Y to H. It offers the unique combination of a classical Lyot coronagraph with long slit spectroscopy.

Configurations:

In practice, the slits and opaque coronagraphic masks have been merged into a single device that is placed in the coronagraph wheel of the CPI. The specifications of the three slits that are available for LSS are listed in Table 13. In addition to the slit+coronagraphic masks, two dispersive elements are placed in the IRDIS cryostat in the Lyot stop wheel: a prism for the LRS mode and a grism for the MRS mode (the dispersion curves for these two components are available in the Appendix). The combination of the three slits and the two dispersive elements provides 4 different configurations listed in Table 14.

As a consequence of using a slit, the observations in this mode are necessarily done in field-stabilized mode to maintain the object of interest inside the slit during the observations.

Target size and spectral resolution:

Positioning of the object with respect to the slit is of significant importance in IRDIS LSS because the diffraction limit is reached inside the slit. The actual spectral resolution for point-like sources is thus set by the diffraction limit rather than the slit width. The central star halo (the star PSF core is hidden behind the coronagraphic mask) can be considered as an extended object in the sense that the speckle field of the star will fully cover the slit, decreasing the effective resolution of its spectrum.

Because the object is unresolved inside the slit, the wavelength calibration can be impacted by the position of the object. Indeed, the wavelength calibration is performed by observing an extended source through the slit, which means that it is only fully valid for the star, or if the object is perfectly centered in the slit. If the object is not well centered, this will induce a systematic shift of the wavelength for the object with respect to that of the star. Also, note that the inaccurate positioning of the object inside the slit can induce differential flux losses (see e.g. Goto et al. 2003, SPIE, 4839) that might affect the spectral slope of the continuum of the object.

Table 13: Specifications of the LSS slits+coronagraphic focal masks available in the coronagraphic wheel to use in IRDIS LSS mode.

| <i>Slit name</i> | <i>Width</i> | <i>Coronagraphic mask radius</i> |
|------------------|--------------|----------------------------------|
| SLIT_WL | 0.12'' | 0.2'' |

| | | |
|---------|--------|-------|
| SLIT_WS | 0.12'' | 0.1'' |
| SLIT_NL | 0.09'' | 0.2'' |

Table 14: Configurations available in IRDIS LSS mode.

| <i>Configuration</i> | <i>Slit</i> | <i>Dispersive element</i> |
|----------------------|-------------|---------------------------|
| S_LR_WL | SLIT_WL | PRISM |
| S_LR_WS | SLIT_WS | PRISM |
| S_MR_WL | SLIT_WL | GRISM |
| S_MR_NL | SLIT_NL | GRISM |

8.9.3 Calibrations

The calibration frames acquired automatically by the observatory include:

- **Internal background, Internal flat-field sequences:** a series of flat-field images is produced in all setups used during the night. In the LSS mode, a flat-field in the spectroscopic wide-band filters YJKs (in LRS) or YJH (in MRS) are provided. It is also possible to calibrate the detector flat field using a flat acquired in the H broad-band filter if no wide-band flat field is available.
- **Wavelength calibration:** the SPHERE calibration unit provides the user with six laser emission lines covering the spectral range 988 to 2015 nm in LRS. In MRS, five emission lines are available for calibration, from 988 to 1730. This calibration is automatically obtained during day-time, after a spectroscopic observation has been done. It is however recommended that observers attach the wavelength calibration to their OB for improved accuracy. For this, the SPHERE_irdis_iss_cal_wave template should be used. The time needed to execute this template will be charged to the user.

The following additional calibrations can also be requested, but will be charged to the observer:

- **Sky background:** the acquisition of sky background frames during the night may be necessary, especially in the LRS mode covering the K band where the sky background may be bright and variable. Such background file provides an efficient correction of the thermal background of the sky + instrument, the dark features and the static bad pixels. The SPHERE_irdis_iss_obs_sky template should be used.
- **Telluric standard observation:** allows calibrating the telluric absorption on a featureless stellar spectrum. This calibration is done on request and prepared by the user with the template SPHERE_irdis_iss_obs_telluric. If the chosen star is a spectro-photometric standard, use of the widest slit is recommended to avoid the slit losses.

8.10 ZIMPOL polarimetric imaging

8.10.1 Observation templates and user-defined parameters

| | |
|----------------------|----------------|
| observation template | Observing mode |
|----------------------|----------------|

| | |
|----------------------|--------------------------------|
| SPHERE zimpol p1 obs | ZIMPOL polarimetric imaging P1 |
| SPHERE zimpol p2 obs | ZIMPOL polarimetric imaging P2 |

User-defined parameters are:

- a. **Detector readout mode and exposures: DIT, NDIT, NEXP.** As the polarized signal is modulated between two CCDs (cf. Fig. 8), NDIT must be an even number.
- b. **Polarization orientation and switching scheme.** See section 8.10.4
- c. **Derotator: fixed (P1) or field-stabilized (P2).** In case of field-stabilized observations, the field orientation. See details in Section 8.10.2.
- d. **Beam Splitter:** This is selected in the acquisition template. Note that the grey beam splitter gives worse AO performance, since the light reaching the WFS decreases by 1.4 mag.
- e. **Filter: ZIMPOL filters, excluding the filters located in the common FW0, which are not currently supported for polarimetry.** The selected filters may or may not be the same for both arms (in FW1 and FW2). Note that if the dichroic beam splitter (between AO WFS and ZIMPOL) is set in the acquisition template, then the choice of ZIMPOL filters is restricted to the R band, narrowband R, H-alpha broad, H-alpha continuum or (for arm 2 only) H-alpha narrow. See Section 4.1.
- f. **Stokes parameters to be measured (Q or Q and U).**
- g. **Number of polarimetric cycles.**
- h. **Polarization gamma parameter:** Selects the on-sky orientation (measured in degrees clockwise from North) of the measured polarization in the first image of a Q cycle.
- i. **ZIMPOL polarization compensator selector:** Determines whether the derotator polarization compensator is in the beam (COMP) or not (OPEN).
- j. **ZIMPOL polarization compensator tilt angle.** Tilt of the compensator plate in degrees. It is recommended to leave this at the default value of 25 degrees.
- k. **Observation type list.** Defines the sequence of Object (O), Flux (F) and Star Center (C) measurements to be obtained.
- l. **Detector X and Y offset for flux measurements.** Indicates the offset (in mas) which is performed to offset the source from the coronagraphic mask for the flux measurement.
- m. **Deformable mirror waffle parameters.** These parameters control the amplitude and the pattern of the four symmetric echoes of the PSF core in the Star Center measurement. In case of observing an object with a known companion, changing these parameters may be useful to ensure that the position of the echoes do not coincide with the location of the companion.
- n. **Field position:** see Section 8.10.3.

A complete list of user-defined parameters is presented in Section 10.

Table 15: ZIMPOL P1/P2 modes in a nutshell.

| | |
|---------|---|
| P1 mode | <p>Highest precision polarimetry mode without derotation:</p> <ul style="list-style-type: none"> • best suited for absolute polarimetric calibration • arbitrary Q/U orientation selection with HWP2 • derotator and compensator always in the same fixed position |
|---------|---|

| | |
|---------|--|
| P2 mode | Polarimetry mode with derotation: <ul style="list-style-type: none"> • arbitrary Q/U orientation selection with HWP2 • stable field on detector with user-defined orientation • derotator, compensator and HWP-Z move during observations |
|---------|--|

8.10.2 P1 or P2 rotation modes for ZIMPOL polarimetry

Two field rotation modes are offered for ZIMPOL polarimetry. They provide two different observing strategies:

- **P1: No field derotation. This mode is only intended for experts as special algorithms will be required to reduce the data.** For bright targets the integration times can be short enough for observations without image derotation because the rotational smearing of the signal on the detector can be neglected. The rotator is fixed in vertical position. This has the advantage that all components are fixed except for HWP1, which needs to correct for the altitude dependence of the M3 polarization, and HWP2, which rotates the polarization position angle correctly into the orientation of the derotator and the ZIMPOL system. This mode will provide the highest polarimetric sensitivity and polarimetric calibration accuracy and is best suited for the search of planets around bright stars because nothing moves after HWP2.
- **P2: Active field derotation.** This mode is suited for long integration of fainter targets. Field derotation is activated and the polarization vector is rotated by HWP2 into the rotating derotator system and rotated back by HWPZ into the ZIMPOL system. Therefore, the field is fixed but the remaining instrument polarization of about $p=0.5\%$ can have some complex, hard to calibrate drifts due to the rotating components.

8.10.3 Dithering, mosaicking

8.10.3.1 Dithering

Dithering with the tip-tilt folding mirrors in front of the detector is possible. Dithering moves the image by several pixels on the detector so that effects of individual pixels can be averaged-out or corrected. The user can select a dithering pattern which is applied to both arms. A recommended pattern is a 9 point dithering pattern with shifts of 50 mas or 14 pixels (3.5 mas each) on the detector:

The dithering positions (in pixels) are setup in the observing template as follows, for instance:

$[x,y] = [-14,-14], [-14,0], [-14,+14], [0,-14], [0,0], [0,+14], [+14,-14], [+14,0], [+14,+14]$

This pattern can be restricted to a 3 point or 5 point dithering pattern or additional dithering positions can be added.

8.10.3.2 Off-axis positions

Using the tip-tilt mirrors to explore the full 8 arcsec diameter is currently not offered.

8.10.4 Observing sequences for ZIMPOL polarimetry

An individual exposure with ZIMPOL polarimetry includes at least two frames taken with opposite charge shifting phasing (double phase mode). This corrects for the charge shifting effects. This minimum unit can be called within several levels of sequences. The recommended sequences for ZIMPOL polarimetry are from low level to high level:

NDIT: number of frames taken (MUST BE an even number) per exposure or data cube.

NEXPO: Number of data cubes taken per higher order sequence.

STOKES sequence: Q or QU for a HWP2 cycle (Q switch), at 0 and 45 degrees, or double cycle (QU switch) with 0, 45, 22.5 and 67.5 degrees. The QU switch sequence should be used by default. Other settings are for experts.

NPOL: Number of STOKES cycles taken within a higher order sequence.

DITH.PATTERN.LIST: List of dithering positions.

FIELD.ETA: List of image rotation angles (only for P2 mode).

Example: one can have a sequence with:

- a. 3 field orientation (list given with eta = 0, 30, 60)
- b. For each field orientation 3 dithering positions (e.g. list [-14, 0], [0, 0], [+14, 0])
- c. For each dithering position 2 (=NPOL) STOKES QU cycles
- d. For each HWP position 1 exposure (NEXPO=1)
- e. Each exposure with 50 frames of 1.2s integration time

This yields: 50 x 1 x 4 x 2 x 3 x 3 frames or 3600 frames with a net integration time of 3960s.

8.10.4.1 Recommendations for sequences

Large NDIT (>10) reduces the observing overhead. NDIT=20 should be preferred to, e.g., NEXPO=4, NDIT=5. NDIT is limited to 20 because too large fits files can also generate errors when written to disk.

STOKES Q or STOKES QU cycles should not be too long (less than a few minutes), because the HWP2 switch corrects well for many instrumental polarization effects if the 0 – 45 degree or 22.5 – 67.5 degree switch cycle is shorter than drifts in the instrument polarization. We recommend a HWP2 switch should be made every few minutes.

DITHERINGS can correct for detector effects. A reasonable number of dithering is 3 or 5. One should also consider that ZIMPOL has a second arm where the same data can be taken simultaneously with another detector.

8.10.4.2 Recommended sequences for different types of targets

ZIMPOL polarimetry in P2 mode for faint sources:

One STOKES QU cycle with NDIT=2, DIT=100s (total = 800s in 4 exposures including 8 frames). This mode is appropriate for faint sources observed in slow polarimetry and yields photon noise limited or readout ZIMPOL polarization accuracy including the correction for instrumental polarization. Second arm (with the same or another filter) can be used for the identification of bad pixels and other instrumental effects.

ZIMPOL polarimetry in P1 mode of very bright star with high sensitivity:

Short exposure DIT=1.2 sec with many frames (NDIT=50) per exposure, NEXPO=2 for a total of 100 frames between each HWP2 switch. A STOKES QU cycle, where one full polarization cycle has 400 frames, has an integration time of 8 minutes. 10 such cycles (NPOL=10) form then one observing block, which may be repeated several times during the night with slight offsets of the dithering position.

8.10.5 ZIMPOL polarimetric calibrations

For ZIMPOL polarimetry the same principles for CCD detector calibrations apply. Therefore the ZIMPOL polarimetry calibration plan includes bias, dark and flat-field calibrations. One also needs a calibration of the polarimetric modulation-demodulation efficiency of ZIMPOL. The polarimetric calibration of the telescope and instrument is not required for most application because the ZIMPOL/SPHERE design has well-defined polarimetric properties. The telescope polarization is compensated to less than 1%, and the instrument polarization is self-calibrated with the half-wave plate (HWP2) switch. The zero-point of the polarization position angle will be available after commissioning to an accuracy of better than 5 degrees. Polarization cross-talks affect the measured fractional polarization p (or Q/I and U/I) by less than $\Delta p/p = 0.1$. These polarimetric properties are monitored by the observatory with the measurement and analysis of high polarization standard stars and zero polarization standard stars on a regular basis. The user should consider additional standard star measurements for science cases requiring a better accuracy in the polarimetric calibration. One can expect that the instrument will be characterized with higher precision, once more measurements become available.

Modulation-demodulation efficiency calibration: the standard polarimetric calibration to be carried out for each polarimetric observation is the modulation-demodulation efficiency calibration. These frames can be obtained during day-time with a flat-field illumination of the detectors using a linear polarizer in the beam producing a fully (100%) polarized illumination of ZIMPOL. The polarization signal measured by ZIMPOL provides then polarization efficiency (e.g. about $\varepsilon \sim 0.8$ for fast polarimetry or $\varepsilon \sim 0.9$ for slow polarimetry) and the polarization signal in the science data must be corrected by the obtained frame ($Q_{cal} = Q_{measured} / \varepsilon$). The modulation-demodulation efficiency calibration depends on various parameters, most importantly on the modulation frequency, the used filter, and the location on the detector. Therefore one must obtain for each polarimetric science frame a calibration taken in the same modulation mode (fast or slow) and with a similar broadband color filter. It is recommended to use for narrowband or line filter polarimetry a corresponding broadband filter calibration because they can be obtained with short exposures reducing the charge trap problem while the color dependence is sufficiently taken into account (see Section 9). The calibration frames for the modulation-demodulation efficiency are also affected by the charge trap problem. Therefore it is recommended to take these frames only with short integrations (limited number of charge shifts). For narrowband and line filter data one can use broadband filter calibrations.

Bias calibrations for polarimetry: bias subtraction for ZIMPOL is mainly based on the overscan pixel bias level. Fast polarimetry produces a fixed pattern along two columns originating from the read-out process. To remove them it is important to have a set of bias calibration (e.g. 50 frames) available. It is useful to take similar calibrations for slow polarimetry as a detector quality check.

Dark calibrations: can be useful for subtracting the dark current from long integrations. For most cases this calibration is not needed.

Intensity flat-fields for polarimetry (polarization flats): well illuminated intensity flats are required to calibrate pixel to pixel sensitivity variations. Intensity flats should be taken with the same filters as the science observations. If a coronagraph on a substrate is selected then sensitivity features due to dust and inhomogeneities of the plate can be corrected with a flat-field with the same focal plane plate inserted. The charge traps are an issue for the flat-fielding in polarimetric mode and therefore one should use

short integration times. Detector fringing is an issue for the flat-fielding of frames taken with the line filters.

8.11 ZIMPOL imaging

8.11.1 Observation templates and user-defined parameters

| observation template | Observing mode |
|----------------------|---------------------------------|
| SPHERE zimpol i_obs | ZIMPOL non-polarimetric imaging |

User-defined parameters are:

- a. **Detector readout mode and exposures: DIT, NDIT, NEXP**
- b. **Derotator: field-stabilized or pupil-stabilized. In case of field-stabilized observations, the field orientation.**
- c. **Filter: ZIMPOL filters. The selected filters may or may not be the same for both arms (in FW1 and FW2). Note that if the dichroic beam splitter (between AO WFS and ZIMPOL) is selected in the acquisition template, then the choice of ZIMPOL filters is restricted within the R band: narrowband R, H-alpha broad, H-alpha continuum or (for arm 2 only) H-alpha narrow.**
- d. **Observation type list. Defines the sequence of Object (O), Flux (F) and Star Center (C) measurements to be obtained.**
- e. **Detector X and Y offset for flux measurements. Indicates the offset (in mas) which is performed to offset the source from the coronagraphic mask for the flux measurement.**
- f. **Deformable mirror waffle parameters. These parameters control the amplitude and the pattern of the four symmetric echoes of the PSF core in the Star Center measurement. In case of observing an object with a known companion, changing these parameters may be useful to ensure that the position of the echoes do not coincide with the location of the companion.**
- g. **Field position: see before.**

The exhaustive list of user-defined parameters, as extracted from the Template Reference Manual, is presented in Section 10.

8.11.2 Purpose and properties

ZIMPOL provides an instrument mode for imaging without polarimetry. In principle, the polarimetric mode of ZIMPOL provides differential polarization signal and intensity images. But having a dedicated imaging mode ensures optimal imaging performance. The resulting data are less affected by instrumental effects (e.g. the HWP are out of the beam). Thus, if one seeks high quality imaging for targets where the polarimetric signal is not relevant then one should consider the imaging mode. Imaging provides in particular a pupil-stabilized observing mode and also features which are not available in polarimetric imaging.

The following list highlights the main advantages of the imaging mode:

- All polarimetric components are out of the beam. This enhances the throughput and reduces ghost effects and the scattered light level. Components which are not in the beam when compared to polarimetric imaging are: HWP1, HWP2, FLC modulator and eventually the polarization compensator and HWPZ.
- A pupil stabilized observing mode is offered for imaging which enables angular differential imaging (ADI).
- No charge shifting is required on the CCD. Therefore, one has no problems with the charge traps which appear in polarimetric imaging.
- The Filters in the common filter wheel are also available for imaging.
- The format of the resulting data is simpler.

Only minor drawbacks are related to the imaging mode when compared with the polarimetric imaging mode:

- Currently only the fast readout mode with a high readout noise of 20 e-/pix is offered.
- The two channels of ZIMPOL are strongly polarization sensitive. The total efficiency of one arm depends more strongly on the telescope pointing direction and the instrument configuration than in polarimetric mode.

8.11.3 Calibrations

Typical day-time (bias, flats, distortion maps) and night-time (photometric standard stars and astrometric fields/stars) calibrations are provided by the observatory (see Section 9).

9. CALIBRATION PLAN SUMMARY

9.1 *Night-time calibrations*

Some observing modes require attached calibration to be taken during the night. Here we detail which ones are mandatory and will be charged to the user observing time, and which ones are part of the calibrations provided by the observatory.

Whenever a coronagraph is used, the SPHERE calibration plan recommends including Flux (F) and Star Center (C) observation types in observing templates both before and after the science observing template. The purpose of the first calibration (Flux - F) is to measure the unsaturated peak flux of the star by offsetting it from the coronagraph spot, in order to ensure accurate relative photometry, and thus contrast calibration. The second calibration (Star Center - C) applies a waffle pattern on the deformable mirror to produce echoes of the PSF hidden behind the coronagraphic mask at very specific locations. The goal of (Star Center - C) is to accurately measure the position of the star behind the coronagraph, which is critical for astrometric measurements of off-axis sources.

9.1.1 **Night-time calibrations provided by the observatory**

The SPHERE calibration plan foresees taking photometric standard stars for all imaging modes using broadband filters, and polarimetric standard stars for all polarimetric modes (polarized and zero-polarization standard stars). The calibration plan also foresees observing reference astrometric fields (binary systems or star clusters with high precision astrometry available) without coronagraph (including ND filters if needed to avoid detector saturation) on a regular basis (frequency ~1 week).

9.1.2 **Optional night-time calibrations**

Photometric standard stars in narrow band filters, or wavelength calibration for IRDIS_LSS, must be requested by the user and is charged to the observer. No spectro-photometric standards or telluric standard will be taken unless explicitly requested as special night-time calibrations. The time required to do so will be charged to the observer.

9.2 *Day-time calibrations*

In addition, all necessary day-time calibrations will be acquired by the observatory staff during the day following the night of the observations (or within the validity period indicated in the tables below). In the following tables, "Modes" refers to the instrument mode among IRDIFS, IRDIFS_EXT, IRDIS_DBI, IRDIS_CI, IRDIS_LSS, and ZIMPOL_I, ZIMPOL_P1, ZIMPOL_P2, when applicable. "Matching parameters" describes the most critical parameter for generating the automatic calibration. For instance, darks/backgrounds will have the same DIT as the science, flats will be taken in the same filter as the science, etc. On the other hand, ZIMPOL polarimetric calibrations will be done in corresponding broadband filters (see filter correspondence table below).

Table 16: Day-time calibrations for IRDIS.

| Calibration | Modes | Matching parameter(s) | Validity |
|------------------------|-----------------------|---------------------------------|----------|
| Background | all | DIT | 1 day |
| Lamp Flat | all | Filter | 1 day |
| Distortion map | All, except IRDIS_LSS | Filter, Coronagraph combination | 1 week |
| Wavelength calibration | IRDIS_LSS | Slit/Grism combination | 1 day |

Table 17: Day-time calibrations for IFS.

| Calibration | Modes | Matching parameter(s) | Validity |
|------------------------|-------|---|----------|
| Dark | all | DIT | 1 day |
| Lamp Flat | all | Prism | 1 week |
| Wavelength calibration | all | Prism | 1 week |
| Spectra registration | all | Prism | 1 day |
| Distortion map | all | Filter (+dichroic), Coronagraph combination | 1 week |

Table 18: Day-time calibrations for ZIMPOL.

| Calibration | Modes | Matching parameter(s) | Validity |
|-----------------------|-------------------------|---|------------|
| Bias | all | mode | 1 day |
| Dark | all | DIT, readout mode | on request |
| Imaging flat | all | Filter (+dichroic), readout mode, focal plane mask on substrate (if used) | 1 day |
| Polarimetric flat | ZIMPOL_P1, ZIMPOL_P2 | Filter (+dichroic), readout mode, focal plane mask on substrate (if used) | 1 day |
| Modulation efficiency | ZIMPOL_P1, ZIMPOL_P2 | Filter (+dichroic), readout mode | 1 day |

NOTE: ZIMPOL distortion maps are taken weekly in V, N_R, N_I for monitoring purposes.

Table 19: Filter correspondence table for ZIMPOL calibrations.

| Filter of Science | Filter for imaging and polarimetric flat | Filter for modulation efficiency |
|-------------------|--|----------------------------------|
| Ha_NB | Ha_NB | N_R |
| OI_630 | OI_630 | N_R |
| HeI | HeI | V |
| V_S | V_S | V |
| V_L | V_L | V |
| 730_NB | 730_NB | N_R |
| I_L | I_L | N_R |
| RI | RI | RI |
| I_PRIM | I_PRIM | I_PRIM |
| R_PRIM | R_PRIM | R_PRIM |
| N_I | N_I | N_I |
| N_R | N_R | N_R |
| B_Ha | B_Ha | N_R |
| CntHa | CntHa | N_R |
| V | V | V |
| Cnt820 | Cnt820 | N_I |
| TiO_717 | TiO_717 | N_I |
| CH4_727 | CH4_727 | N_I |
| KI | KI | N_I |
| N_Ha | N_Ha | N_R |
| Cnt748 | Cnt748 | N_I |

9.3 Astrometry

9.3.1 Instrumental distortion and detector orientation in IRDIFS and IRDIFS_EXT

Observations of the globular cluster 47 Tuc have been used to calibrate the distortion, plate scale and true north orientation at the level of the IRDIS and IFS detectors. The cylindrical mirrors in the SPHERE common path are the main source for the optical distortion, hence these distortion effects are common to IRDIS and IFS, and they dominate the telescope distortion effects (Maire et al. 2016). The SPHERE distortion at first order is an anamorphism of $0.60 \pm 0.02\%$ between the horizontal and vertical pixel scales. This effect if uncorrected translates into an astrometric error of 6 mas at $1''$, which is larger than the astrometric specifications for SPHERE (5 mas).

The following steps are required for accurately calibrating IRDIFS data :

IRDIS: there a very small anamorphic distortion between the x and y axes. It can be corrected by multiplying the Y coordinate by 1.0062 ± 0.0002 . This value has been calibrated during commissioning and was measured to be stable within the provided error bar;

IFS: similarly to IRDIS, the IFS is affected by the same anamorphic distortion, but because the IFS field is rotated by $+100.56$ (counter-clockwise), the corrections to be applied are 1.0059 in x and 1.0011 in y.

Field orientation: once the anamorphism is corrected, the position angle on sky of any object can be determined using the following formulas:

| Stabilization | Sub-system | Formula |
|---------------|------------|--|
| Field | IRDIS | $PA_{\text{sky}} = PA_{\text{detector}} + \text{POSANGLE} + \text{TN}$ |
| | IFS | $PA_{\text{sky}} = PA_{\text{detector}} + \text{POSANGLE} + \text{TN} + \text{IFS}_{\text{offset}}$ |
| Pupil | IRDIS | $PA_{\text{sky}} = PA_{\text{detector}} + \text{PARANGLE} + \text{TN} + \text{PUPIL}_{\text{offset}}$ |
| | IFS | $PA_{\text{sky}} = PA_{\text{detector}} + \text{PARANGLE} + \text{TN} + \text{PUPIL}_{\text{offset}} + \text{IFS}_{\text{offset}}$ |

With:

PUPIL_{offset}: 135.99 ± 0.11 deg

IFS_{offset}: -100.48 ± 0.13 deg

TN: true North correction (see below)

POSANG: position angle offset (input in the observing template)

PARANGLE: parallactic angle

9.3.2 Plate scale and true north orientation

Basic astrometry, i.e. plate scale and true north orientation is provided by the observatory on a regular basis using a few reference calibrators. We selected as main reference fields 47 Tucanae, the Orion Trapezium B1–B4, NGC 3603, and NGC 6380 (Tab. 1 and Fig. 1), as well as a handful of long-period binaries (HIP 67745, HIP 68725, HIP 102979) with Hipparcos data and separations larger than the IFS field of view (separations $\sim 2\text{--}5''$). The catalogs of the stellar positions for these fields come from various sources: Washington Double Star (WDS) catalog for the binaries, literature for the Orion Trapezium B1–B429, and private requests for 47 Tucanae (A.

Bellini/STScI), NGC 6380 (E. Noyola/Univ. Texas Austin), and NGC 360330 (Z. Khorrami/OCA). Additional details are given in Maire et al. (2016).

For all runs before mid-December 2015, the true north TN is $-1.700^\circ \pm 0.076^\circ$. For the runs between mid-December 2015 and February 2016 a value of $-2.10^\circ \pm 0.38^\circ$ is to be used.

The IRDIS plate scale was evaluated in the H2 filter with the N_ALC_YJH_S coronagraph. The value is 12.255 ± 0.021 mas/pix. The plate scale can be adjusted for different filters using the following relations :

plate_scale(H3)=plate_scale(H2)-0.005

the plate_scale for J2/J3 is 0.004 mas/pix larger than for H2/H3

the plate_scale for Y2/Y3 is 0.024 mas/pix larger than for H2/H3

the plate_scale for non-coronagraphic observations is 0.019+/-0.001 mas/pixel smaller than that for coronagraphic observations

The plate scale of the IFS is 7.46 ± 0.02 mas/pix.

A web page with updated information about astrometric calibrations with SPHERE will be posted here (please visit often when performing your True North calculations):

www.eso.org/sci/facilities/paranal/instruments/sphere/doc/Astrometry.html

10. SPHERE TEMPLATE PARAMETERS

The instrument, detector and telescope are controlled by OBs, which are made up of templates. Templates are divided into three categories: acquisition, observation and calibration.

Usually, OBs consist of an acquisition template and one or more observation templates for nighttime observations and, in some limited cases, an additional nighttime calibration template.

Only one acquisition template is allowed in an OB, and therefore only one preset on sky. It is not possible e.g. to group in the same OB observation templates on the science object and calibration template on a standard star. The next sections provide a short summary of the templates offered from P95. These templates should cover most needs. If this is not the case, users must contact the User Support Department (usd-help@eso.org) well before the start of observations.

10.1 SPHERE Acquisition Templates

Telescope presets can only be done via acquisition templates and all observing blocks must start with one. There are six acquisition templates and they are to be used with nine different observation templates with the following associations:

| | |
|------------------------------|-----------------------------|
| SPHERE_irdifs_acq : | |
| SPHERE_irdifs_obs | |
| SPHERE_irdifs_ext_obs | |
| SPHERE_irdis_acq: | |
| SPHERE_irdis_ci_obs | |
| SPHERE_irdis_dbi_obs | |
| SPHERE_irdis_dpi_acq: | |
| SPHERE_irdis_dpi_obs | |
| SPHERE_irdis_lss_acq: | SPHERE_irdis_lss_obs |
| SPHERE_zimpol_i_acq: | |
| SPHERE_zimpol_i_obs | |
| SPHERE_zimpol_p_acq: | |
| SPHERE_zimpol_p1_obs | |
| SPHERE_zimpol_p2_obs | |

The setups allowed by each template are shown in Tables 21–26 in terms of the parameters which may be set. For example, the SPHERE_irdifs_acq (see Table 20) allows the setting of IRDIS and IFS coronagraphs, derotator mode (field or pupil tracking), adaptive optics (AO or no AO) and position angle offset.

The parameter SEQ.AO.ST specifies with the AO loop should be closed (T) or opened (F). Unless specific calibration purposes, the state will therefore be T (loop closed).

10.2 SPHERE Observation Templates

The templates SPHERE_irdifs_obs and SPHERE_irdifs_ext_obs both use IRDIS and IFS together. They should be used for modes IRDIFS (Y-J range with IFS and H-band range with IRDIS) and IRDIFS_EXT (Y-H range with IFS, K-band range with IRDIS) as described in section 1.7. Please

Table 21: SPHERE_irdis_acq

| SPHERE_irdis_acq.tsf | | |
|-------------------------|---|--|
| Parameter | Range (Default) | Label |
| INS.COMB.ICOR | N_4Q_YJH N_4Q_Ks N_ALC_Y N_ALC_YJ_S N_ALC_YJ_L N_ALC_YJH_S N_ALC_YJH_L N_ALC_Ks N_CLC_SW_S N_CLC_LW_S N_CLC_SW_L N_CLC_LW_L N_BAR N_S_LR_WL N_S_LR_WS N_S_MR_WL N_S_MR_NL N_S_LR_OPEN N_S_MR_OPEN N_NC_4QPM N_NC_ALC_1 N_NC_ALC_2 N_NC_CLC_1 N_NC_CLC_2 N_NS_VLT N_NS_CLEAR N_NS_APO_1 N_NS_APO_2 N_NS_OPAQUE (NODEFAULT) | Infrared IRDIS coronagraph combination |
| INS.COMB.ROT | FIELD PUPIL (NODEFAULT) | Derotator and ADC modes combination |
| INS.CPRT.POSANG | 0.0..360.0 (0.0) | Derotator position angle (deg) |
| SEQ.AO.ST | T F (T) | SAXO state |
| SEQ.TARGET.HMAG | 0..18 (0) | Target H magnitude |
| SEQ.TARGET.RMAG | 0..18 (0) | Target R magnitude |
| TEL.AG.GUIDESTAR | NONE SETUPFILE CATALOGUE (CATALOGUE) | Telescope guide star selection |
| TEL.GS1.ALPHA | ra (0.) | RA of guide star |
| TEL.GS1.DELTA | dec (0.) | DEC of guide star |
| TEL.TARG.ALPHA | ra () | RA |
| TEL.TARG.DELTA | dec () | DEC |
| TEL.TARG.EPOCH | -2000..3000 (2000) | Epoch |
| TEL.TARG.EQUINOX | QUERY-TARG getEquinoxList (2000) | Equinox |
| TEL.TARG.PMA | -500..500 (0) | Proper motion in RA |
| TEL.TARG.PMD | -500..500 (0) | Proper motion in DEC |

Table 22: SPHERE_irdis_dpi_acq

| SPHERE_irdis_dpi_acq.tsf | | |
|--------------------------|---|--|
| Parameter | Range (Default) | Label |
| INS.COMB.ICOR | N_4Q_YJH N_4Q_Ks N_ALC_Y N_ALC_YJ_S N_ALC_YJ_L N_ALC_YJH_S N_ALC_YJH_L N_ALC_Ks N_CLC_SW_S N_CLC_LW_S N_CLC_SW_L N_CLC_LW_L N_BAR N_S_LR_WL N_S_LR_WS N_S_MR_WL N_S_MR_NL N_S_LR_OPEN N_S_MR_OPEN N_NC_4QPM N_NC_ALC_1 N_NC_ALC_2 N_NC_CLC_1 N_NC_CLC_2 N_NS_VLT N_NS_CLEAR N_NS_APO_1 N_NS_APO_2 N_NS_OPAQUE (N_ALC_YJH_S) | Infrared IRDIS coronagraph combination |
| INS.CPRT.POSANG | 0.0..360.0 (0.0) | Derotator position angle (deg) |
| SEQ.AO.ST | T F (T) | SAXO state |
| SEQ.TARGET.HMAG | 0..18 (0) | Target H magnitude |
| SEQ.TARGET.RMAG | 0..18 (0) | Target R magnitude |
| TEL.AG.GUIDESTAR | NONE SETUPFILE CATA- LOGUE (CATALOGUE) | Telescope guide star selection |
| TEL.GS1.ALPHA | ra (0.) | RA of guide star |
| TEL.GS1.DELTA | dec (0.) | DEC of guide star |
| TEL.TARG.ALPHA | ra () | RA |
| TEL.TARG.DELTA | dec () | DEC |
| TEL.TARG.EPOCH | -2000..3000 (2000) | Epoch |
| TEL.TARG.EQUINOX | QUERY-TARG getEquinoxList (2000) | Equinox |
| TEL.TARG.PMA | -500..500 (0) | Proper motion in RA |
| TEL.TARG.PMD | -500..500 (0) | Proper motion in DEC |

Table 23: SPHERE_irdis_iss_acq

| SPHERE_irdis_iss_acq.tsf | | |
|--------------------------|---|--|
| Parameter | Range (Default) | Label |
| INS.COMB.ICOR | N_S_LR_WL N_S_LR_WS N_S_MR_WL N_S_MR_NL (NODEFAULT) | Infrared IRDIS coronagraph combination |
| INS.CPRT.POSANG | 0.0..360.0 (0.0) | Derotator position angle (deg) |
| SEQ.AO.ST | T F (T) | SAXO state |
| SEQ.TARGET.HMAG | 0..18 (0) | Target H magnitude |
| SEQ.TARGET.RMAG | 0..18 (0) | Target R magnitude |
| TEL.AG.GUIDESTAR | NONE SETUPFILE CATA- LOGUE (CATALOGUE) | Telescope guide star selection |
| TEL.GS1.ALPHA | ra (0.) | RA of guide star |
| TEL.GS1.DELTA | dec (0.) | DEC of guide star |
| TEL.TARG.ALPHA | ra () | RA |
| TEL.TARG.DELTA | dec () | DEC |
| TEL.TARG.EPOCH | -2000..3000 (2000) | Epoch |
| TEL.TARG.EQUINOX | QUERY-TARG getEquinoxList (2000) | Equinox |
| TEL.TARG.PMA | -500..500 (0) | Proper motion in RA |
| TEL.TARG.PMD | -500..500 (0) | Proper motion in DEC |

Table 24: SPHERE_zimpol_i_acq

| SPHERE_zimpol_i_acq.tsf | | |
|-------------------------|---|-------------------------------------|
| Parameter | Range (<i>Default</i>) | Label |
| INS.COMB.VCOR | V_CLC_S_WF V_CLC_S_NF V_CLC_MT_WF V_CLC_M_WF V_CLC_M_NF V_CLC_L_WF V_CLC_XL_WF V_BAR V_4Q_SW V_4Q_LW V_NC_WF V_NC_NF V_CLC_M_WF_B V_CLC_L_WF_B (<i>NODEFAULT</i>) | Visible coronagraph combination |
| INS.CPRT.MODE | FIELD PUPIL (<i>FIELD</i>) | Pupil derotator mode |
| INS.CPRT.POSANG | 0.0..360.0 (<i>0.0</i>) | Derotator position angle (deg) |
| INS.ZISL.NAME | BS_GREY DIC_HA (<i>BS_GREY</i>) | Position of the ZIMPOL/WFS selector |
| SEQ.AO.ST | T F (<i>T</i>) | SAXO state |
| SEQ.TARGET.RMAG | 0..18 (<i>0</i>) | Target R magnitude |
| TEL.AG.GUIDESTAR | NONE SETUPFILE CATALOGUE (<i>CATALOGUE</i>) | Telescope guide star selection |
| TEL.GS1.ALPHA | ra (<i>0.</i>) | RA of guide star |
| TEL.GS1.DELTA | dec (<i>0.</i>) | DEC of guide star |
| TEL.TARG.ALPHA | ra (<i>0.</i>) | RA |
| TEL.TARG.DELTA | dec (<i>0.</i>) | DEC |
| TEL.TARG.EPOCH | -2000..3000 (<i>2000</i>) | Epoch |
| TEL.TARG.EQUINOX | QUERY-TARG getEquinoxList (<i>2000</i>) | Equinox |
| TEL.TARG.PMA | -500..500 (<i>0</i>) | Proper motion in RA |
| TEL.TARG.PMD | -500..500 (<i>0</i>) | Proper motion in DEC |

Table 25: SPHERE_zimpol_p_acq

| SPHERE_zimpol_p_acq.tsf | | |
|-------------------------|---|-------------------------------------|
| Parameter | Range (<i>Default</i>) | Label |
| INS.COMB.VCOR | V_CLC_S_WF V_CLC_S_NF V_CLC_MT_WF V_CLC_M_WF V_CLC_M_NF V_CLC_L_WF V_CLC_XL_WF V_BAR V_4Q_SW V_4Q_LW V_NC_WF V_NC_NF V_CLC_M_WF_B V_CLC_L_WF_B (<i>NODEFAULT</i>) | Visible coronagraph combination |
| INS.CPRT.MODE | FIELD FIXED (<i>FIELD</i>) | Pupil derotator mode |
| INS.CPRT.POSANG | 0.0..360.0 (<i>0.0</i>) | Derotator position angle (deg) |
| INS.ZISL.NAME | BS_GREY DIC_HA (<i>BS_GREY</i>) | Position of the ZIMPOL/WFS selector |
| SEQ.AO.ST | T F (<i>T</i>) | SAXO state |
| SEQ.TARGET.RMAG | 0..18 (<i>0</i>) | Target R magnitude |
| TEL.AG.GUIDESTAR | NONE SETUPFILE CATALOGUE (<i>CATALOGUE</i>) | Telescope guide star selection |
| TEL.GS1.ALPHA | ra (<i>0.</i>) | RA of guide star |
| TEL.GS1.DELTA | dec (<i>0.</i>) | DEC of guide star |
| TEL.TARG.ALPHA | ra (<i></i>) | RA |
| TEL.TARG.DELTA | dec (<i></i>) | DEC |
| TEL.TARG.EPOCH | -2000..3000 (<i>2000</i>) | Epoch |
| TEL.TARG.EQUINOX | QUERY-TARG getEquinoxList (<i>2000</i>) | Equinox |
| TEL.TARG.PMA | -500..500 (<i>0</i>) | Proper motion in RA |
| TEL.TARG.PMD | -500..500 (<i>0</i>) | Proper motion in DEC |

Table 26: SPHERE_obs

| SPHERE_irdifs_obs.tsf | | |
|----------------------------------|--|---|
| Parameter | Range (Default) | Label |
| DET.IFS.DIT | 0 2 4 8 16 32 64 (0) | IFS Detector Integration Time |
| DET.IFS.NDIT | 1..1000 (1) | IFS Number of DIT |
| DET.IRDIS.DIT | 0 2 4 8 16 32 64 (0) | IRDIS Detector Integration Time |
| DET.IRDIS.NDIT | 1..1000 (1) | IRDIS Number of DIT |
| INS.COMB.IFLT | DB_H23 DB_H34 DB_NDH23 BB_H (NO DEFAULT) | IRDIS filter combination |
| INS.COMB.IND.FLUX | ND_N_0.0 ND_N_1.0 ND_N_2.0 ND_N_3.5 (NODEFAULT) | Infrared neutral density filters combination (flux) |
| INS.COMB.IND | ND_N_0.0 ND_N_1.0 ND_N_2.0 ND_N_3.5 (NODEFAULT) | Infrared neutral density filters combination |
| INS.COMB.ROT | PUPIL FIELD (NODEFAULT) | Derotator and ADC modes combination |
| INS.CPRT.POSANG | 0.0..360.0 (0.0) | Derotator position angle (deg) |
| SEQ.IFS.DIT.FLUX | 0 2 4 8 16 32 64 (0) | IFS Integration Time (flux) |
| SEQ.IFS.NDIT.FLUX | 1..1000 (1) | IFS Number of integrations (flux) |
| SEQ.IFS.NDIT.SKY | 1..1000 (1) | IFS Number of integrations (sky) |
| SEQ.IFS.NDIT.STARCENTER | 1..1000 (1) | IFS Number of integrations (star center) |
| SEQ.IFS.NEXPO | 1..100 (1) | IFS exposures per dithering position |
| SEQ.IRDIS.DIT.FLUX | 0 2 4 8 16 32 64 (0) | IRDIS Integration Time (flux) |
| SEQ.IRDIS.DITH.NPATTERN | 1..100 (1) | IRDIS dithering pattern repetitions |
| SEQ.IRDIS.DITH.PATTERN | 1x1 2x2 4x4 6x6 8x8 10x10 (4x4) | IRDIS dithering pattern sequence |
| SEQ.IRDIS.NDIT.FLUX | 1..1000 (1) | IRDIS Number of integrations (flux) |
| SEQ.IRDIS.NDIT.SKY | 1..1000 (1) | IRDIS Number of integrations (sky) |
| SEQ.IRDIS.NDIT.STARCENTER | 1..1000 (1) | IRDIS Number of integrations (star center) |
| SEQ.IRDIS.NEXPO | 1..100 (1) | IRDIS exposures per dithering position |
| SEQ.OBSTYPE.LIST | F C O S (NODEFAULT) | Observation type (F, C, O, S) |
| SEQ.TARG.OFFSETALPHA | 0..60 (NODEFAULT) | Sky RA offset list (arcsec) |
| SEQ.TARG.OFFSETDELTA | 0..60 (NODEFAULT) | Sky DEC offset list (arcsec) |
| SEQ.TARG.OFFSETX | 0..400 (400) | Detector X offset (mas) |
| SEQ.TARG.OFFSETY | 0..400 (400) | Detector Y offset (mas) |
| SEQ.WAFFLE.AMPLITUDE | 0..0.05 (0.02) | DM waffle pattern amplitude |
| SEQ.WAFFLE.ORIENTATION | x + (x) | DM waffle pattern orientation |
| <i>Fixed values:</i> | | |
| SEQ.IFS.DITH.NPATTERN | 1 | IFS dithering pattern repetitions |
| SEQ.IFS.DITH.PATTERN | 1x1 | IFS dithering pattern sequence |

Table 27: SPHERE_irdifs_ext_obs

| SPHERE_irdifs_ext_obs.tsf | | |
|----------------------------------|---|---|
| Parameter | Range (<i>Default</i>) | Label |
| DET.IFS.DIT | 0 2 4 8 16 32 64 (<i>0</i>) | IFS Detector Integration Time |
| DET.IFS.NDIT | 1..1000 (<i>1</i>) | IFS Number of DIT |
| DET.IRDIS.DIT | 0 2 4 8 16 32 64 (<i>0</i>) | IRDIS Detector Integration Time |
| DET.IRDIS.NDIT | 1..1000 (<i>1</i>) | IRDIS Number of DIT |
| INS.COMB.IND.FLUX | ND_N_0.0 ND_N_1.0 ND_N_2.0 ND_N_3.5 (<i>NODEFAULT</i>) | Infrared neutral density filters combination (flux) |
| INS.COMB.IND | ND_N_0.0 ND_N_1.0 ND_N_2.0 ND_N_3.5 (<i>NODEFAULT</i>) | Infrared neutral density filters combination |
| INS.COMB.ROT | PUPIL FIELD (<i>NODEFAULT</i>) | Derotator and ADC modes combination |
| INS.CPRT.POSANG | 0.0..360.0 (<i>0.0</i>) | Derotator position angle (deg) |
| SEQ.IFS.DIT.FLUX | 0 2 4 8 16 32 64 (<i>0</i>) | IFS Integration Time (flux) |
| SEQ.IFS.NDIT.FLUX | 1..1000 (<i>1</i>) | IFS Number of integrations (flux) |
| SEQ.IFS.NDIT.SKY | 1..1000 (<i>1</i>) | IFS Number of integrations (sky) |
| SEQ.IFS.NDIT.STARCENTER | 1..1000 (<i>1</i>) | IFS Number of integrations (star center) |
| SEQ.IFS.NEXPO | 1..100 (<i>1</i>) | IFS exposures per dithering position |
| SEQ.IRDIS.DIT.FLUX | 0 2 4 8 16 32 64 (<i>0</i>) | IRDIS Integration Time (flux) |
| SEQ.IRDIS.DITH.NPATTERN | 1..100 (<i>1</i>) | IRDIS dithering pattern repetitions |
| SEQ.IRDIS.DITH.PATTERN | 1x1 2x2 4x4 6x6 8x8 10x10 (<i>4x4</i>) | IRDIS dithering pattern sequence |
| SEQ.IRDIS.NDIT.FLUX | 1..1000 (<i>1</i>) | IRDIS Number of integrations (flux) |
| SEQ.IRDIS.NDIT.SKY | 1..1000 (<i>1</i>) | IRDIS Number of integrations (sky) |
| SEQ.IRDIS.NDIT.STARCENTER | 1..1000 (<i>1</i>) | IRDIS Number of integrations (star center) |
| SEQ.IRDIS.NEXPO | 1..100 (<i>1</i>) | IRDIS exposures per dithering position |
| SEQ.OBSTYPE.LIST | F C O S (<i>NODEFAULT</i>) | Observation type (F, C, O, S) |
| SEQ.TARG.OFFSETALPHA | 0..60 (<i>NODEFAULT</i>) | Sky RA offset list (arcsec) |
| SEQ.TARG.OFFSETDELTA | 0..60 (<i>NODEFAULT</i>) | Sky DEC offset list (arcsec) |
| SEQ.TARG.OFFSETX | 0..400 (<i>400</i>) | Detector X offset (mas) |
| SEQ.TARG.OFFSETY | 0..400 (<i>400</i>) | Detector Y offset (mas) |
| SEQ.WAFFLE.AMPLITUDE | 0..0.2 (<i>0.05</i>) | DM waffle pattern amplitude |
| SEQ.WAFFLE.ORIENTATION | x + (<i>x</i>) | DM waffle pattern orientation |
| <i>Fixed values:</i> | | |
| Parameter | Value | Label |
| INS.COMB.IFLT | DB_K12 BB_K (<i>NODEFAULT</i>) | IRDIS filter combination |
| SEQ.IFS.DITH.NPATTERN | 1 | IFS dithering pattern repetitions |
| SEQ.IFS.DITH.PATTERN | 1x1 | IFS dithering pattern sequence |

Table 28: SPHERE_irdis_dbi_obs

| SPHERE_irdis_dbi_obs.tsf | | |
|----------------------------------|---|---|
| Parameter | Range (<i>Default</i>) | Label |
| DET.IRDIS.DIT | 0 2 4 8 16 32 64 (<i>0</i>) | IRDIS Detector Integration Time |
| DET.IRDIS.NDIT | 1..1000 (<i>1</i>) | IRDIS Number of DIT |
| INS.COMB.IFLT | DB_Y23 DB_J23 DB_H23 DB_H32 DB_H34 DB_K12 DB_NDH23 DB_NDH32 (<i>DB_H23</i>) | IRDIS filter combination |
| INS.COMB.IND.FLUX | ND_N_0.0 ND_N_1.0 ND_N_2.0 ND_N_3.5 (<i>NODEFAULT</i>) | Infrared neutral density filters combination (flux) |
| INS.COMB.IND | ND_N_0.0 ND_N_1.0 ND_N_2.0 ND_N_3.5 (<i>NODEFAULT</i>) | Infrared neutral density filters combination |
| INS.COMB.ROT | FIELD PUPIL (<i>NODEFAULT</i>) | Derotator and ADC modes combination |
| INS.CPRT.POSANG | 0.0..360.0 (<i>0.0</i>) | Derotator position angle (deg) |
| SEQ.IRDIS.DIT.FLUX | 0 2 4 8 16 32 64 (<i>0</i>) | IRDIS Integration Time (flux) |
| SEQ.IRDIS.DITH.NPATTERN | 1..100 (<i>1</i>) | IRDIS dithering pattern repetitions |
| SEQ.IRDIS.DITH.PATTERN | 1x1 2x2 4x4 6x6 8x8 10x10 (<i>4x4</i>) | IRDIS dithering pattern sequence |
| SEQ.IRDIS.NDIT.FLUX | 1..1000 (<i>1</i>) | IRDIS Number of integrations (flux) |
| SEQ.IRDIS.NDIT.SKY | 1..1000 (<i>1</i>) | IRDIS Number of integrations (sky) |
| SEQ.IRDIS.NDIT.STARCENTER | 1..1000 (<i>1</i>) | IRDIS Number of integrations (star center) |
| SEQ.IRDIS.NEXPO | 1..100 (<i>1</i>) | Number of exposures |
| SEQ.OBSTYPE.LIST | F C O S (<i>NODEFAULT</i>) | Observation type (F, C, O, S) |
| SEQ.TARG.OFFSETALPHA | 0..60 (<i>NODEFAULT</i>) | Sky RA offset list (arcsec) |
| SEQ.TARG.OFFSETDELTA | 0..60 (<i>NODEFAULT</i>) | Sky DEC offset list (arcsec) |
| SEQ.TARG.OFFSETX | 0..400 (<i>400</i>) | Detector X offset (mas) |
| SEQ.TARG.OFFSETY | 0..400 (<i>400</i>) | Detector Y offset (mas) |
| SEQ.WAFFLE.AMPLITUDE | 0..0.2 (<i>0.05</i>) | DM waffle pattern amplitude |
| SEQ.WAFFLE.ORIENTATION | x + (<i>x</i>) | DM waffle pattern orientation |

Table 29: SPHERE_irdis_ci_obs

| SPHERE_irdis_ci_obs.tsf | | |
|----------------------------------|---|---|
| <i>To be specified:</i> | | |
| Parameter | Range (Default) | Label |
| DET.IRDIS.DIT | 0 2 4 8 16 32 64 (0) | IRDIS Detector Integration Time |
| DET.IRDIS.NDIT | 1..1000 (1) | IRDIS Number of DIT |
| INS.COMB.IFLT | BB_Y BB_J BB_H BB_Ks NB_HeI NB_CntJ NB_PaB NB_CntH NB_FeII NB_CntK1 NB_H2 NB_BrG NB_CO NB_CntK2 (NODEFAULT) | IRDIS filter combination |
| INS.COMB.IND.FLUX | ND_N_0.0 ND_N_1.0 ND_N_2.0 ND_N_3.5 (NODEFAULT) | Infrared neutral density filters combination (flux) |
| INS.COMB.IND | ND_N_0.0 ND_N_1.0 ND_N_2.0 ND_N_3.5 (NODEFAULT) | Infrared neutral density filters combination |
| INS.COMB.ROT | FIELD PUPIL (NODEFAULT) | Derotator and ADC modes combination |
| INS.CPRT.POSANG | 0.0..360.0 (0.0) | Derotator position angle (deg) |
| SEQ.IRDIS.DIT.FLUX | 0 2 4 8 16 32 64 (0) | IRDIS Integration Time (flux) |
| SEQ.IRDIS.DITH.NPATTERN | 1..100 (1) | IRDIS dithering pattern repetitions |
| SEQ.IRDIS.DITH.PATTERN | 1x1 2x2 4x4 6x6 8x8 10x10 (4x4) | IRDIS dithering pattern sequence |
| SEQ.IRDIS.NDIT.FLUX | 1..1000 (1) | IRDIS Number of integrations (flux) |
| SEQ.IRDIS.NDIT.SKY | 1..1000 (1) | IRDIS Number of integrations (sky) |
| SEQ.IRDIS.NDIT.STARCENTER | 1..1000 (1) | IRDIS Number of integrations (star center) |
| SEQ.IRDIS.NEXPO | 1..100 (1) | Number of exposures |
| SEQ.OBSTYPE.LIST | F C O S (NODEFAULT) | Observation type (F, C, O, S) |
| SEQ.TARG.OFFSETALPHA | 0..60 (NODEFAULT) | Sky RA offset list (arcsec) |
| .LIST | | |
| SEQ.TARG.OFFSETDELTA | 0..60 (NODEFAULT) | Sky DEC offset list (arcsec) |
| .LIST | | |
| SEQ.TARG.OFFSETX | 0..400 (400) | Detector X offset (mas) |
| SEQ.TARG.OFFSETY | 0..400 (400) | Detector Y offset (mas) |
| SEQ.WAFFLE.AMPLITUDE | 0..0.2 (0.05) | DM waffle pattern amplitude |
| SEQ.WAFFLE.ORIENTATION | x + (x) | DM waffle pattern orientation |

Table 30: SPHERE_irdis_dpi_obs

| SPHERE_irdis_dpi_obs.tsf | | |
|-----------------------------|--|--|
| Parameter | Range (Default) | Label |
| DET.IRDIS.DIT | 0 2 4 8 16 32 64 (0) | IRDIS Detector Integration Time |
| DET.IRDIS.NDIT | 1..1000 (1) | IRDIS Number of DIT |
| INS.COMB.IFLT | DP_0_BB_Y DP_0_BB_J DP_0_BB_H DP_0_BB_Ks DP_0_NB_HeI DP_0_NB_CntJ DP_0_NB_PaB DP_0_NB_CntH DP_0_NB_FeII DP_0_NB_CntK1 DP_0_NB_H2 DP_0_NB_BrG DP_0_NB_CO DP_0_NB_CntK2 DP_45_BB_Y DP_45_BB_J DP_45_BB_H DP_45_BB_Ks DP_45_NB_HeI DP_45_NB_CntJ DP_45_NB_PaB DP_45_NB_CntH DP_45_NB_FeII DP_45_NB_CntK1 DP_45_NB_H2 DP_45_NB_BrG DP_45_NB_CO DP_45_NB_CntK2 | IRDIS filter combination |
| INS.COMB.IND | (NODEFAULT) ND_N_0.0 ND_N_1.0 ND_N_2.0 ND_N_3.5 (NODEFAULT) | Infrared neutral density filters combination |
| INS.CPRT.POSANG | 0.0..360.0 (0.0) | Derotator position angle (deg) |
| SEQ.IRDIS.NEXPO | 1..100 (1) | Number of exposures |
| SEQ.IRDIS.POL.STOKES | Q QU (QU) | Stoke parameter measure |
| SEQ.POL.NCYCLE | 1..100 (1) | Number of polarimetric cycles |
| SEQ.POL.OFFSET.GAMMA | -360..360 (0) | Polarization: gamma parameter (degrees) |
| <i>Fixed values:</i> | | |
| Parameter | Value | Label |
| INS.COMB.ROT | FIELD | Derotator and ADC modes combination |

Table 31: SPHERE_irdis_iss_obs

| SPHERE_irdis_iss_obs.tsf | | |
|--------------------------|--|--|
| Parameter | Range (Default) | Label |
| DET.IRDIS.DIT | 0 2 4 8 16 32 64 (0) | IRDIS Detector Integration Time |
| DET.IRDIS.NDIT | 1..1000 (1) | IRDIS Number of DIT |
| INS.COMB.IND | ND_N_0.0 ND_N_1.0 ND_N_2.0 ND_N_3.5 (NODEFAULT) | Infrared neutral density filters combination |
| INS.CPRT.POSANG | 0.0..360.0 (0.0) | Derotator position angle (deg) |
| SEQ.IRDIS.NEXPO | 1..100 (1) | Number of exposures |

Table 32: SPHERE_zimpol_p1_obs

| SPHERE_zimpol_p1_obs.tsf | | |
|--|--|--|
| Parameter | Range (<i>Default</i>) | Label |
| DET.ZIMPOL.DIT | 0..1200 (<i>1.3</i>) | Integration time |
| DET.ZIMPOL.NDIT | 1..1000 (<i>2</i>) | Number of integrations |
| DET.ZIMPOL.READOUT | FastPolarimetry SlowPolarimetry (<i>FastPolarimetry</i>) | ZIMPOL read-out mode |
| DET.ZIMPOL.SHUTTER | Enabled Disabled (<i>Disabled</i>) | ZIMPOL detector shutter |
| INS.ZCSL.NAME | OPEN COMP (<i>COMP</i>) | ZIMPOL polarization compensator selector |
| INS.ZCTT.POS | -90.0..90.0 (<i>25.0</i>) | ZIMPOL polarization compensator, tilt angle |
| INS.ZIFW0.NAME | OPEN P_VIS PQ_VIS Q_VIS ND_1.0 ND_2.0 ND_4.0 Ha_NB OI_630 HeI V_S V_L 730_NB LL (<i>OPEN</i>) | ZIMPOL common filter wheel |
| INS.ZIFW1.NAME | OPEN VBB I_PRIM R_PRIM N_I N_R B_Ha CntHa V Cnt820 TiO_717 CH4_727 KI (<i>N_R</i>) | Arm 1 filter |
| INS.ZIFW2.NAME | OPEN VBB I_PRIM R_PRIM N_I N_R B_Ha CntHa V Cnt820 N_Ha Cnt748 PUPIM (<i>N_R</i>) | Arm 2 filter |
| SEQ.ZIMPOL.DITH.PATTERN .LIST | -14..14 (<i>-14 -14 0 0 +14 +14</i>) | List of pixel coordinates for dithering |
| SEQ.ZIMPOL.FIELD.POS | 0 1 2 3 4 5 6 7 8 9 (<i>0</i>) | Field position on ZIMPOL detector |
| SEQ.ZIMPOL.NEXPO | 1..100 (<i>1</i>) | Number of exposures per dithering position |
| SEQ.ZIMPOL.NPOL | 1..100 (<i>1</i>) | ZIMPOL - Number of polarimetric cycles |
| SEQ.ZIMPOL.POL.GAMMA | 0..360 (<i>0</i>) | ZIMPOL - Polarization: gamma parameter. |
| SEQ.ZIMPOL.POL.PCOMLOOP | T F (<i>F</i>) | Initial computation of PCOM tilt angle |
| SEQ.ZIMPOL.POL.STOKES | Q QU QnoSwitch (<i>QU</i>) | Defines if we measure (+Q,-Q) or (+Q,-Q,+U,-U) |

Table 33: SPHERE_zimpol_p2_obs

| SPHERE_zimpol_p2_obs.tsf | | |
|--|--|--|
| Parameter | Range (Default) | Label |
| DET.ZIMPOL.DIT | 0..1200 (1.3) | Integration time |
| DET.ZIMPOL.NDIT | 1..1000 (2) | Number of integrations |
| DET.ZIMPOL.READOUT | FastPolarimetry SlowPolarimetry (FastPolarimetry) | ZIMPOL read-out mode |
| DET.ZIMPOL.SHUTTER | Enabled Disabled (Disabled) | ZIMPOL detector shutter |
| INS.ZCSL.NAME | OPEN COMP (COMP) | ZIMPOL polarization compensator selector |
| INS.ZCTT.POS | -90.0..90.0 (25.0) | ZIMPOL polarization compensator, tilt angle |
| INS.ZIFW0.NAME | OPEN P_VIS PQ_VIS Q_VIS ND_1.0 ND_2.0 ND_4.0 Ha_NB OI.630 HeI V_S V_L 730_NB I_L (OPEN) | ZIMPOL common filter wheel |
| INS.ZIFW1.NAME | OPEN VBB I_PRIM R_PRIM N_I N_R B_Ha CntHa V Cnt820 TiO_717 CH4_727 KI (N_R) | Arm 1 filter |
| INS.ZIFW2.NAME | OPEN VBB I_PRIM R_PRIM N_I N_R B_Ha CntHa V Cnt820 N_Ha Cnt748 PUPIM (N_R) | Arm 2 filter |
| SEQ.ZIMPOL.DITH.PATTERN .LIST | -14..14 (-14 -14 0 0 +14 +14) | List of pixel coordinates for dithering |
| SEQ.ZIMPOL.FIELD.POS | 0 1 2 3 4 5 6 7 8 9 (0) | Field position on ZIMPOL detector |
| SEQ.ZIMPOL.FIELD.POSANG | 0..360 (0.0) | Field orientation on detector |
| SEQ.ZIMPOL.NEXPO | 1..100 (1) | Number of exposures per dithering position |
| SEQ.ZIMPOL.NPOL | 1..100 (1) | ZIMPOL - Number of polarimetric cycles |
| SEQ.ZIMPOL.POL.GAMMA | 0..360 (0) | ZIMPOL - Polarization: gamma parameter. |
| SEQ.ZIMPOL.POL.STOKES | Q QU QnoSwitch (QU) | Defines if we measure (+Q,-Q) or (+Q,-Q,+U,-U) |

Table 34: SPHERE_zimpol_i_obs

| SPHERE_zimpol_i_obs.tsf | | |
|--|--|---|
| Parameter | Range (Default) | Label |
| DET.ZIMPOL.DIT | 0..1200 (1.3) | Integration time |
| DET.ZIMPOL.NDIT | 1..1000 (1) | Number of integrations |
| DET.ZIMPOL.READOUT | StandardImaging SnapShotImag- ing (StandardImaging) | ZIMPOL read-out mode |
| DET.ZIMPOL.SHUTTER | Enabled Disabled (Disabled) | ZIMPOL detector shutter |
| INS.CPRT.MODE | FIELD PUPIL (FIELD) | Pupil derotator mode |
| INS.ZIFW0.NAME | OPEN P_VIS PQ_VIS Q_VIS ND_1.0 ND_2.0 ND_4.0 Ha_NB OI.630 HeI V_S V_L 730_NB I.L (OPEN) | ZIMPOL common filter wheel |
| INS.ZIFW1.NAME | OPEN VBB I_PRIM R_PRIM N_I N_R B_Ha CntHa V Cnt820 TiO_717 CH4_727 KI (N_R) | Arm 1 filter |
| INS.ZIFW2.NAME | OPEN VBB I_PRIM R_PRIM N_I N_R B_Ha CntHa V Cnt820 N_Ha Cnt748 PUPIM (N_R) | Arm 2 filter |
| SEQ.ZIMPOL.DITH.PATTERN .LIST | -14..14 (-14 -14 0 0 +14 +14) | List of pixel coordinates for dither- ing |
| SEQ.ZIMPOL.FIELD.POS | 0 1 2 3 4 5 6 7 8 9 (0) | Field position on ZIMPOL detector |
| SEQ.ZIMPOL.FIELD.POSANG | 0..360 (0.0) | Field orientation on detector |
| SEQ.ZIMPOL.NEXPO | 1..100 (1) | Number of exposures per dithering position |

10.3 SPHERE Night-time Calibration Templates

There are three calibration templates that can be useful for night time observations to support science. SPHERE_irdis_iss_obs_sky SPHERE_irdis_iss_obs_sky allow to get additional sky backgrounds and a telluric standard star respectively, in LSS mode, and SPHERE_zimpol_i_cal_star_center estimates the stellar position just as with the IRDIS star_center observations. The parameters which may be modified for these templates are shown in Tables 36-38.

Table 35: SPHERE_irdis_iss_obs_sky

| SPHERE_irdis_iss_obs_sky.tsf | | |
|---|--|---|
| <i>To be specified:</i> | | |
| Parameter | Range (Default) | Label |
| DET.IRDIS.DIT | 0 2 4 8 16 32 64 (0) | IRDIS Detector Integration Time |
| DET.IRDIS.NDIT | 1..1000 (1) | IRDIS Number of DIT |
| INS.COMB.IFLT | S_LR S_MR (NODEFAULT) | IRDIS filter combination |
| INS.COMB.IND | ND_N_0.0 ND_N_1.0 ND_N_2.0 ND_N_3.5 (NODEFAULT) | Infrared neutral density filters com- bination |
| INS.CPRT.POSANG | 0.0..360.0 (0.0) | Derotator position angle (deg) |
| SEQ.SKY.TARG.OFFSETALPHA .LIST | 0..60 (NODEFAULT) | Sky RA offset list (arcsec) |
| SEQ.SKY.TARG.OFFSETDELTA .LIST | 0..60 (NODEFAULT) | Sky DEC offset list (arcsec) |

Table 36: SPHERE_irdis_iss_obs_telluric

| SPHERE_irdis_iss_obs_telluric.tsf | | |
|--|--|--|
| <i>To be specified:</i> | | |
| Parameter | Range (Default) | Label |
| DET.IRDIS.DIT | 0 2 4 8 16 32 64 (0) | IRDIS Detector Integration Time |
| DET.IRDIS.NDIT | 1..1000 (1) | IRDIS Number of DIT |
| INS.COMB.IND | ND_N_0.0 ND_N_1.0 ND_N_2.0 ND_N_3.5 (NODEFAULT) | Infrared neutral density filters combination |
| INS.CPRT.POSANG | 0.0..360.0 (0.0) | Derotator position angle (deg) |
| SEQ.TARG.OFFSETX | 0..500 (500) | Detector X offset (mas) |

Table 37: SPHERE_zimpol_i_obs_star_center

| SPHERE_zimpol_i_obs_star_center.tsf | | |
|--|-----------------|-------------------------------|
| <i>To be specified:</i> | | |
| Parameter | Range (Default) | Label |
| DET.ZIMPOL.DIT | 0..1200 (1.1) | Integration time |
| DET.ZIMPOL.NDIT | 1..1000 (1) | Number of integrations |
| SEQ.WAFFLE.AMPLITUDE | 0..0.2 (0.05) | DM waffle pattern amplitude |
| SEQ.WAFFLE.ORIENTATION | x + (x) | DM waffle pattern orientation |

11. DATA REDUCTION

11.1 Obtaining calibration files from the ESO archive

Darks and flats are taken every morning after SPHERE observations, in the appropriate filters and with the appropriate exposure times for the science data. Moreover, to check the health of the instrument, calibrations are also taken on a weekly basis using standard setups (see chapter on the calibration plan). One can download necessary calibration files from the ESO Data Archive (archive.eso.org/eso/eso_archive_main.html). For example, to download IRDIS calibrations from the archive page, one can enter the *Start* and *End* UT dates for the data they want. Furthermore, one can select *SPHERE/VLT* under *Imaging*, *CALIB* under *Category*, *Dark* under *Data Product Info:Type*. If desired one can also choose the exposure time under *Instrumental Setup: Exptime*. Pressing the *Search* button displays the calibrations available for download. **To pin point calibrations more rapidly and avoid downloading unnecessary files, one can use the SPHERE specific form which allows to narrow down the searches with help of header keywords:**

archive.eso.org/wdb/wdb/eso/sphere/form

The data reduction procedures are described in the SPHERE pipeline manual. For a short summary we outline the principal steps for each instrument:

11.2 IFS reduction cascade summary

1. **Correction using a dark frame taken with the IFS shutter closed and all internal lamps off. In this step hot pixels and cosmic ray hits are removed and the background subtracted. The IFS background is dominated by thermal emission, which depends on the temperature of the instrument.**
2. **Correction for the wavelength-dependent detector flat-field (pixel-to-pixel response variations). This needs at least three detector flats taken at different wavelengths, possibly another one taken in white light. These are taken with IFS shutter closed and one of its internal calibration sources switched on.**
3. **Wavelength calibration using a pixel description table that holds the wavelengths assigned to each pixel, its illumination fraction, and spectrum ID. This table is made in two steps: First, spectra are detected on an external flat-field frame with IFS shutter open and the external white light calibration source switched on. Then, a wavelength solution is found on a frame where again IFS shutter is open and 3 or 4 of the monochromatic external calibration sources are switched on. Wavelength calibration is obtained using an integrating sphere and laser lines at 0.9877, 1.1237, 1.3094, and 1.5451 (μm).**
4. **Application of an IFU flat. This corrects for throughput variations between individual lens-lets (spaxels). It is derived from the same flat-field as used in the first step 3.**
5. **Construction of a cube of evenly spaced monochromatic planes. This is actually the endpoint of the automated pipeline. Note that it does not combine several cubes. The results can be fed to (manually operated) data analysis recipes or dedicated software packages.**

11.3 IRDIS reduction cascade summary

11.3.1 DBI, classical imaging

Data reduction of DBI and classical imaging mode data is as follows:

1. **Correction using a dark frame.**
2. **Application of the internal flat-field.**
3. **Determination of the position of the optical axis in each of the two simultaneous images. To do this, a dedicated calibration is used where a waffle pattern is applied to SPHERE's high-order deformable mirror. This causes four off-axis peaks to appear (even in coronagraphic images), the positions of which are detected and measured. Their centers of illumination are then used as center of rotation and to align the two frames.**
4. **The combination of all input frames. This includes optionally de-rotation, spectral differencing, and angular differencing.**

11.3.2 Long slit spectroscopy

Data reduction of LSS mode data is as follows:

1. **Correction using dark.**
2. **Application of internal flat.**
3. **Wavelength calibration, taken the same way as for IFS.**
4. **Combination of all input frames. Output is a frame that has wavelengths assigned to each pixel. The extraction of a spectrum, e.g. a correction for telluric absorption that is measured in the same way on a calibration star, is left to the user.**

The DPI mode of IRDIS works essentially the same way as the other imaging modes. The pipeline does not currently provide any (polarimetric) analysis recipes.

11.4 ZIMPOL reduction cascade summary

Because of the stripe mask on the ZIMPOL detector, all recipes include a pre-processing step that re-orders the image rows into logical and viewable images. All recipes provide these pre-processed data as optional output.

11.4.1 Imaging

The principal calibration steps for imaging are:

1. **Subtraction of the bias level. The default method is a subtraction of the mean value for the overscan pixels. A bias frame subtraction can be used if a fixed read-out noise pattern is present.**
2. **Possibly a subtraction of a dark frame of matching exposure time or interpolated to a matching exposure time. For short integration times (e.g. <30 s) this is not needed. Noise in the dark frame may add noise to the science image.**
3. **Flat-fielding with flat field calibration frames taken with the same filter (and the same focal plane coronagraph plate if a coronagraph on a substrate is used).**
4. **Combination of all frames using optionally some filtering of outliers. The combination includes back-shifting of dithered images and optionally also the derotation of the frames.**

The ZIMPOL QuickLook RTD (real time display) shows the pre-processed, overscan bias subtracted image of the first frame in an exposure.

11.4.2 Polarimetry

The principle calibration steps for polarimetry are:

1. **Subtraction of the bias level. For slow polarimetry a subtraction of the mean value for the overscan pixels provides good results. For fast polarimetry, a bias frame subtraction should be used to remove the fixed read-out column feature.**
2. **Dark current correction as for imaging**
3. **Correction for the modulation-demodulation efficiency. This is derived from frames illuminated evenly by the 100% polarized flat field calibration source and corrects for the pixel-dependent efficiency to in shifting charges back and forth during integration, thus measuring polarization. The modulation-demodulation efficiency calibration is only applied to the polarization frame.**
4. **Flatfielding as for imaging. The flatfielding is only applied to the intensity frame.**
5. **Combination of all frames as for imaging (with dithering and rotation corrections) and derivation of the intensity image and Q, or U polarization state.**

The ZIMPOL QuickLook RTD shows the pre-processed, overscan bias subtracted intensity frame (top) and the polarimetrically combined fractional polarization frame (bottom) for the two first frames of an exposure.

12. OVERHEADS

The most important contributors to overheads are:

- a. **Target acquisition: this strongly dominates the overheads when staying on the same target less than 1hr.**
- b. **Detector: overheads associated to the detector operations.**

Additionally, the HW setup changes (including dithering, filter or HWP swapping) also contribute, depending on the observing sequence.

12.1 Target acquisition

Target acquisition (whenever a new target is pointed at) includes the telescope preset (= 6 min, see, e.g. <http://www.eso.org/sci/facilities/paranal/cfp/cfp95/overheads.html>), AO loop closing (including the measurement of flux, performance, and the check of the selected setup). Given the small fields of view of the 3 instruments accurate coordinates and proper motions of all targets are mandatory. In case the initial pointing is not accurate enough to guarantee that the AO sensors detect the star within its ~2'' FoV, larger FoV images should be obtained by the operator. This could easily cost an additional 2 minutes.

If the coronagraph set-up has been changed (or if the previous check is older than typically one hour), it is recommended to repeat the coronagraph centering.

Observing Blocks (OBs) typically last 1 hour. Hence, in Service Mode, single OBs or the first OB in a concatenation must take into account the overhead for centering given in Table 38. In Visitor Mode, the overhead mentioned in Table 38 should be taken into account every hour.

Table 38: Target acquisition execution times for all acquisition templates, including the 6 min of telescope preset, along with typical execution times for star center (C), and flux (F).

| Action | Approximate duration |
|-----------------------|---|
| Acquisition | 10 min (including 6 min of telescope preset) |
| Coronagraph centering | + 5 min |
| Star Center – C | + 3.5 min |
| Flux – F | + 3.5 min |

12.2 NIR observation overheads

The formula to compute execution time for IRDIS and IFS, including overheads, are:

$$\begin{aligned} \text{time_IFS} &= (\text{O_START_IFS} + \text{NDIT_IFS} * (\text{DIT_DELAY_IFS} + \text{DIT_IFS} + \\ &\text{ROT_IFS}) + \text{O_EXP_IFS}) * \text{NEXP_IFS} \\ \text{time_IRD} &= ((\text{T_START_IRD} + \text{NDIT_IRD} * (\text{DIT_DELAY_IRD} + \text{DIT_IRD} + \\ &\text{ROT_IRD}) + \text{O_EXP_IRD}) * \text{NEXPO_IRD} + \text{O_DITH_IRD}) * \text{NDITHER} * \\ &\text{NPATTERN} \end{aligned}$$

The total execution for an IRDIFS sequence is :

$$\text{time_obs} = \text{MAX}(\text{time_IFS}, \text{time_IRD})$$

In these formulas, DIT_IFS and DIT_IRD are the detector integration times for IFS and IRDIS, NDIT_IFS and NDIT_IRD the number of DITs, NEXP_IFS the number of IFS exposures, NDITHER the number of dithering positions for IRDIS, NEXPO_IRD the number of exposures per dithering position, ROT_IFS and ROT_IRD the readout times, DIT_DELAY_IFS and DIT_DELAY_IRD an additional readout delay, and O_* various detector and mechanical overheads for IFS and IRDIS. The value of these overheads are given in the table below.

Note that the minimum DIT for IRDIS is 0.838 s for IRDIS, while it is 1.65 s for IFS. You have to take this different into account when trying to match the execution time of IRDIFS observations.

Table 39: Overheads for IFS and IRDIS observations

| Operation | IFS | IRDIS |
|------------|------|-------|
| O_START | 0.3 | 0.3 |
| DIT_DELAY | 0.2 | 0.1 |
| ROT | 1.65 | 0.838 |
| O_EXP | 1.1 | 1.1 |
| O_DITH_IRD | | 1.77 |

12.3 ZIMPOL observation overheads

The formula to compute typical ZIMPOL execution times, including overheads is:

$$(DIT + O_DIT) * NDIT * NEXPO * CYCLE * NPOL * NDITH * NETA + O_EXPO * NEXPO * CYCLE * NPOL * NDITH * NETA + O_NPOL * CYCLE * NPOL * NDITH * NETA + O_DITH * NDITH * NETA + O_ETA * NETA$$

Where DIT is the detector integration time, O_DIT, the DIT overhead, NDIT, the number of DITs, NEXPO, the number of exposures per position, O_EXPO, the exposure overhead, NPOL, the number of polarimetric cycles (CYCLE = 1 for QnoSwitch, 2 for Q, 4 for QU), NDITH, the number of dithering positions, O_DITH the overhead associated with dithering, NETA, the number of field angles, O_NETA, the overhead associated with derotator setting.

Table 40: ZIMPOL approximate overheads.

| Mode | FastPol | SlowPol | StdI |
|--------|---------|---------|------|
| O_DIT | 0.1 | 0.1 | 0.1 |
| O_EXPO | 3 | 13 | 3 |

Table 41: HW setup overheads in ZIMPOL observations.

| Operation | Overhead |
|-----------|----------|
| O_NPOL | 5 |
| O_DITH | 5 |
| O_ETA | 5 |

Typical examples (CYCLE = 2, Q):

| | DIT | NDIT | NEXPO | NPOL | NDITH | NETA | OST | Duration | | Effic. |
|----------------|-----|------|-------|------|-------|------|------|----------|-------|--------|
| | | | | | | | | (s) | (min) | |
| SlowPol | 50 | 2 | 2 | 2 | 1 | 3 | 2400 | 2852 | 47 | 0.84 |
| FastPol | 1.2 | 50 | 1 | 2 | 3 | 3 | 2160 | 2688 | 45 | 0.8 |
| StdI | 5 | 6 | 2 | N/A | 40 | N/A | 2400 | 2888 | 48 | 0.83 |

APPENDIX

A1. Detector properties

A1.1 IRDIS and IFS detectors

IRDIS and IFS are equipped with a 2Kx2K Hawaii-2RG arrays manufactured by Teledyne Imaging Sensors. The detectors are operated with cryogenic preamplifiers located next to the focal plane and operating at temperatures of ~ 80 K. The data acquisition system is the ESO New Generation Controller (NGC). The controller reads all the 32 video channels of each of the two Hawaii-2RG detectors in parallel.

Table 42: IRDIS and IFS detector properties.

| | IRDIS | IFS |
|---------------------------------|--|---|
| Detector arrays | 2k x 2k (2k x 1k read) Hawaii-2RG | 2k x 2k Hawaii-2RG |
| Readout mode | Non destructive sampling (NonDest) | Non destructive sampling (NonDest) |
| Readout noise | 4 (long DIT) - 10 (short DIT) e^- rms/pix/readout | 4 (long DIT) - 10 (short DIT) e^- rms/pix/readout |
| Dark current | Negligible | Negligible |
| Gain | 1.75 e^- /ADU | 1.8 e^- /ADU |
| Quantum efficiency | >95% from Y to K | >95% from Y to H |
| MINDIT/readout time | 0.83s | 1.66s |
| Linearity and saturation | 0.1% up to $10^5 e^-$ 15000 ADU for DIT=0.83s 25000 ADU for DIT=4s 30000 ADU for DIT>8s | 0.1% up to $10^5 e^-$ 15000 ADU for DIT=1.66s 25000 ADU for DIT=8s 30000 ADU for DIT>16s |

A1.2 ZIMPOL detectors

The ZIMPOL detectors CCD1 and CCD2 consist of 4k x 2k pixel, back-illuminated, frame transfer CCDs (e2v CCD 44-82 bi) with 15 μm x 15 μm pixels. They have two read-out registers which work in parallel, each reading out half a line. The 2k x 2k CCD is in all modes operated like a 1k x 1k pixel CCD with 2 x 2 pixel binning allowing faster read-out and providing an effective pixel size of 30 μm x 30 μm . The saturation limit is at 65000 while linearity is at 63000 ADUs.

Table 43: ZIMPOL detector and readout mode properties.

| | Fast polarimetry | Slow polarimetry | Standard Imaging |
|------------------------------------|--|---|---|
| Science application | high precision polarimetry of targets with intermediate brightness ($R \sim 3-7$ mag) in broad band filters | photon noise limited polarimetry of faint targets, or bright star observations of the outer PSF or in narrow band filters | Standard imaging, when polarization information is not needed |
| Modulation: frequency, time | 967 Hz, 1.03 ms | 27 Hz, 37ms | N/A |
| Row shift time (binned row) | 54.7 μs | 72.3 μs | N/A |
| Detector field of view* | 3.5"×3.5", 1024 × 512 pix | 3.5"× 3.5", 1024 × 512 pix | 3.5"×3.5", 1024 × 512 pix |
| Integration times: min-max | 1.2 – 100 s | 10 – 1000 s | 1.2 – 1000 s |
| Frame transfer time | 56 ms | 74 ms | 66 ms |
| Max. frame rate | 0.86 Hz | 0.1 Hz | 0.86 Hz |
| Shutter use | Not offered | Not offered | Not offered |
| Readout: noise, frequency | 20 e^- , 625 kHz | 3 e^- , 100 kHz | 20 e^- , 625 kHz |
| Gain, well depth | 10.5 e^- /ADU, 670 ke^- | 1.5 e^- /ADU, 100 ke^- | 10.5 e^- /ADU, 670 ke^- |
| Dark current | 0.2 e^- /(s pix) | 0.015 e^- /(s pix) | 0.2 e^- /(s pix) |

* Effective field of view for one polarization mode I_0 or I_{90} .

A2. System throughput

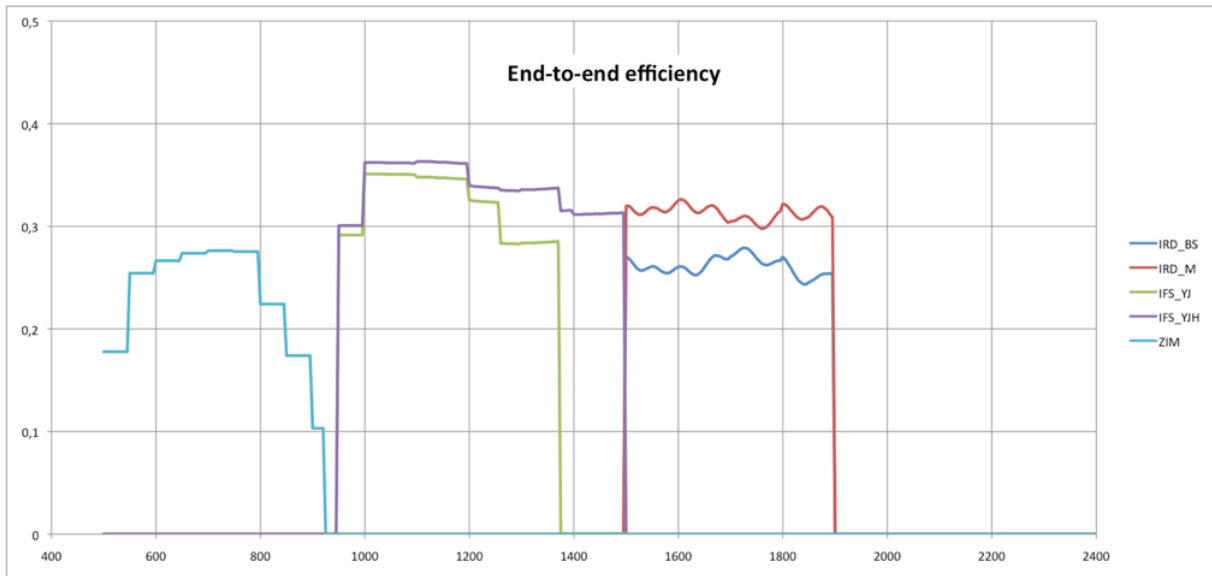


Figure 24: Transmission from SPHERE entrance to the science detectors, including the detector efficiency, assuming i) no coronagraph, ii) ZIMPOL path goes through the GREY beamsplitter (80% to ZIMPOL), and iii) the H dichroic separating the flux between IFS (up to 1450 nm) and IRDIS. Note that IRDIS cannot observe in K band in this setup.

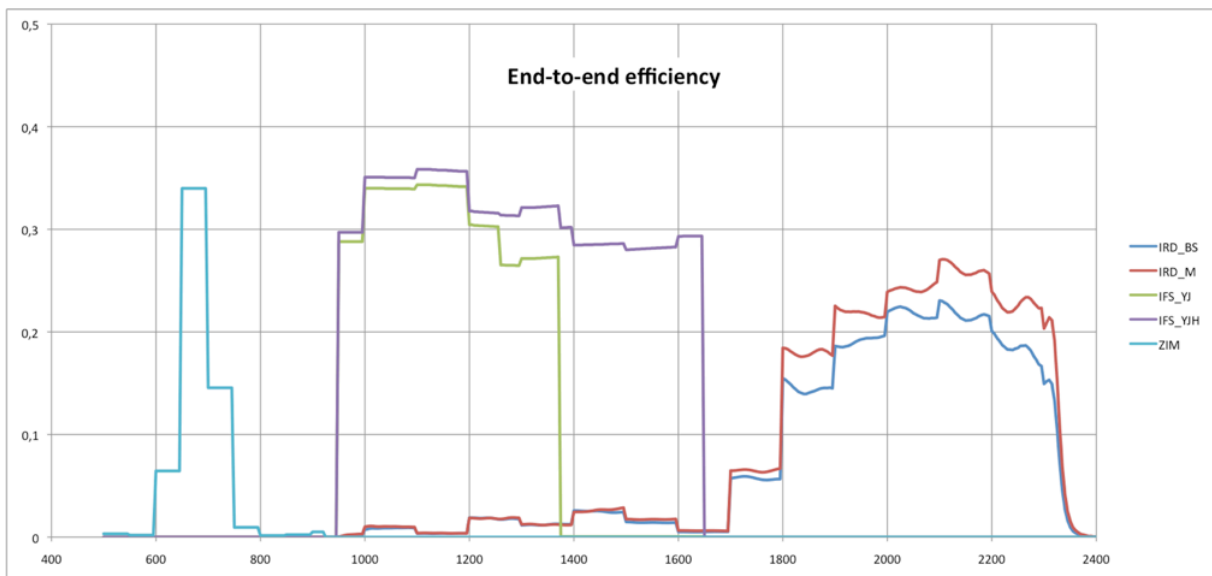


Figure 25: Transmission (as above) with different beamsplitters. In visible: separation between WFS and ZIMPOL uses a dichroic sending more light to ZIMPOL but in R band only; in NIR: the IFS/IRDIS dichroic ‘K’ feeds IFS with the its full Y-H range, with lower efficiency for IRDIS in K band only.

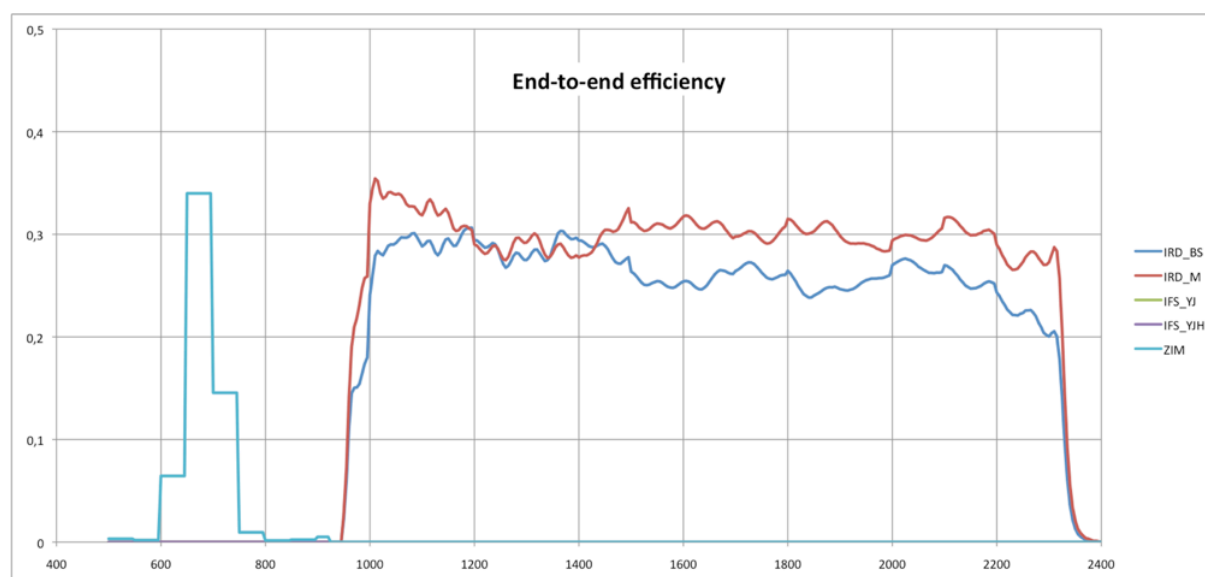


Figure 26: Transmission (as above) in IRDIS alone configuration where all the NIR light is sent to IRDIS.

A3. Neutral densities

Since neutral densities prevent most photons from reaching the detector, their use in science templates should be avoided when possible. Instead, a coronagraph should be considered when trying to prevent saturation. If accurate photometry or astrometry of the primary target is desired, Star center and Flux observations should be considered.

The transmission curves of the VIS and NIR neutral density filters are available here :

<https://www.eso.org/sci/facilities/paranal/instruments/sphere/inst/filters.html>

A3.1 CPI

The transmissions as a function of wavelength of the neutral density filter of CPI are displayed in Figure 27. These ND filters are common to IRDIS and IFS.

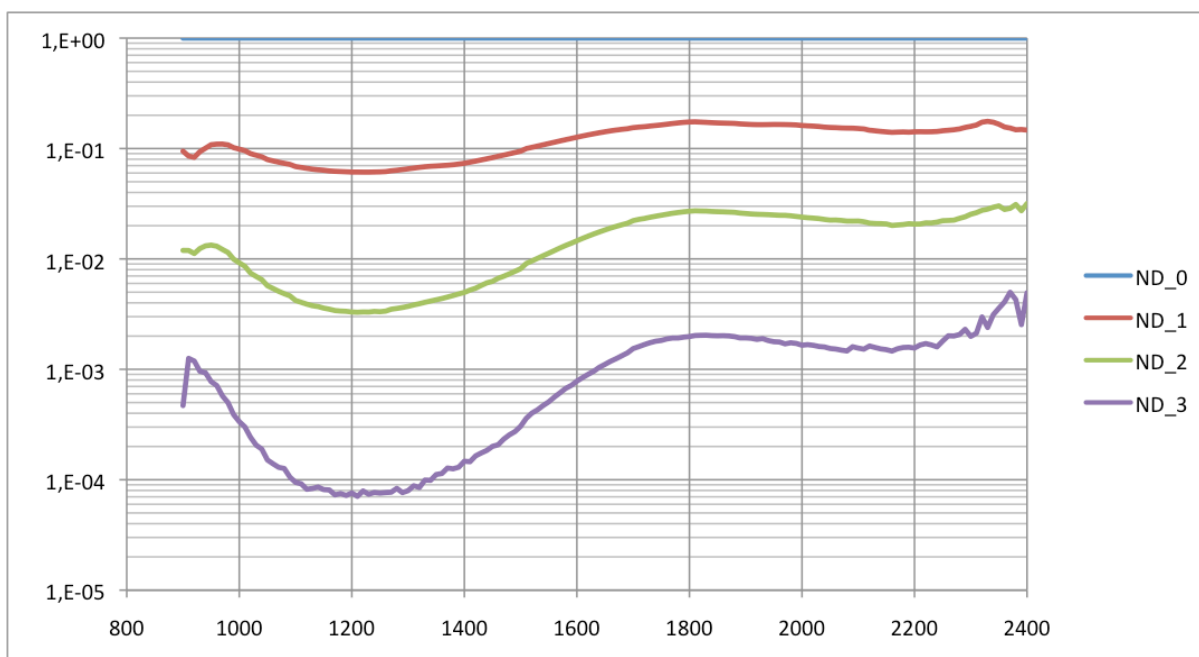


Figure 27: Transmission CPI NIR densities as a function of wavelength (nm).

A3.2 IFS

A filter wheel is mounted within IFS. These filters allow appropriate exposure levels for the IFS internal flat-field lamp. The wheel hosts three neutral density filters (ND1, ND2, ND3). The filters are identical to those in the CPI. They are inclined with respect to the optical axis, to avoid ghosts. This causes a small shift of the optical path.

A3.3 IRDIS

When observing with IRDIS-H in parallel to IFS, it might be useful to reduce the flux seen by IRDIS without affecting IFS data. This can be achieved by using the filter BBF-ND-H (consisting of H + a neutral density filter) instead of BBF-H.

A3.4 ZIMPOL

The transmission as a function of wavelength of the neutral density filters ND1, ND2 and ND4 mounted in filter wheel FW0 are shown in Figure 28.

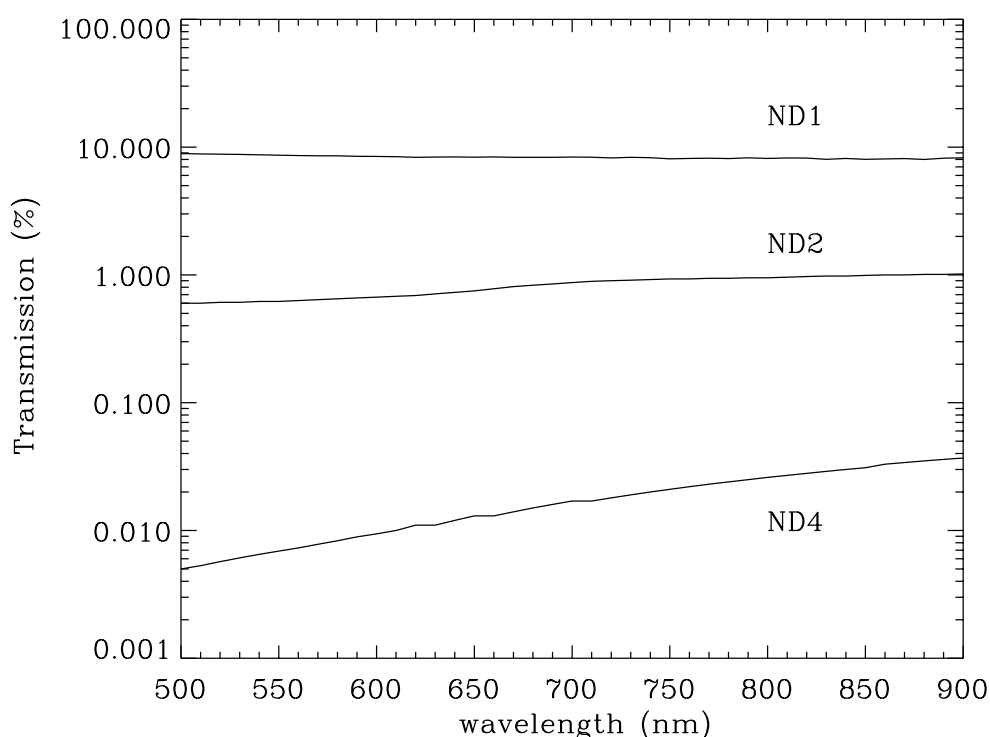


Figure 28: Spectral transmission of the ZIMPOL neutral density filters ND1, ND2 and ND3 (as provided by the manufacturer).

A4. IRDIS beam-splitter

The IRDIS internal beam-splitter separates the flux between the left and the right detector halves. The left (right) half is illuminated by light that is reflected (transmitted) by the splitter. The beam-splitter introduces flux differences between the two detector halves of less than 10% while slightly larger differences are observed for polarized light.

A5. IRDIS filters

IRDIS requires four types of filters: wideband filters (WBF), broadband filters (BBF), narrowband filters covering specific atomic or molecular lines (NBF), and dual band filters used pair wise for dual-band imaging (DBF). WBF, BBF, and NBF are referred to as common filters because they are located in a filter wheel situated in front of the beam separation optics. The DBFs are organized in pairs, located after the beam separation optics. Figure 29, Figure 30 and Figure 31 illustrate the various IRDIS filter transmissions.

Filter available as a function of observing mode:

- **CI can use any filter (except DBF).**
- **DPI can use any of the BBF and NBF.**
- **DBI can use only the DBF.**

The transmission curves of all IRDIS filters are available here :

<https://www.eso.org/sci/facilities/paranal/instruments/sphere/inst/filters.html>

DBF are used in conjunction with BBF (acting as blocking filters). In templates, the user is not asked for setting individual wheels but only pre-defined relevant combinations, as presented in Table 45.

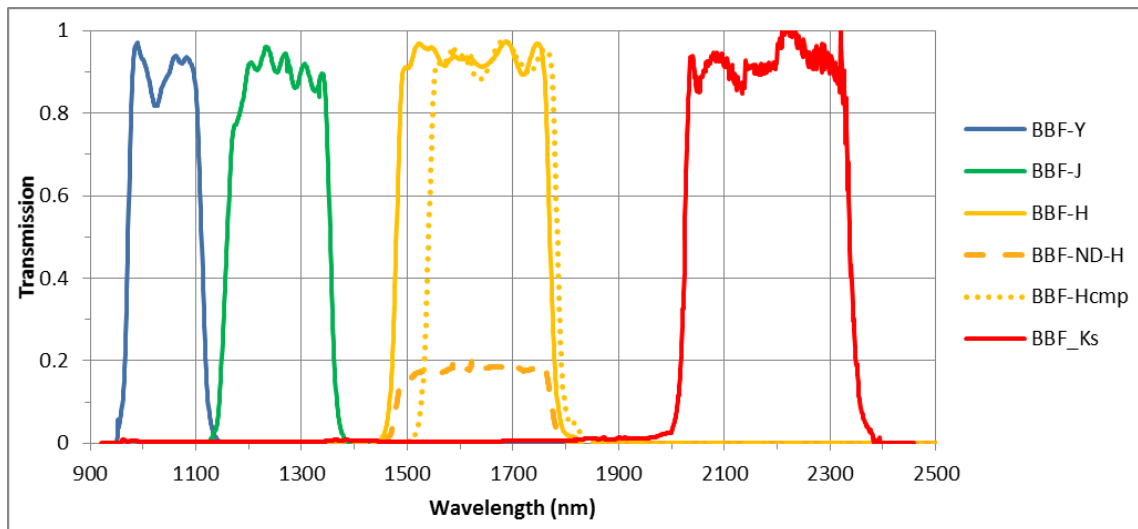


Figure 29: IRDIS BB filters.

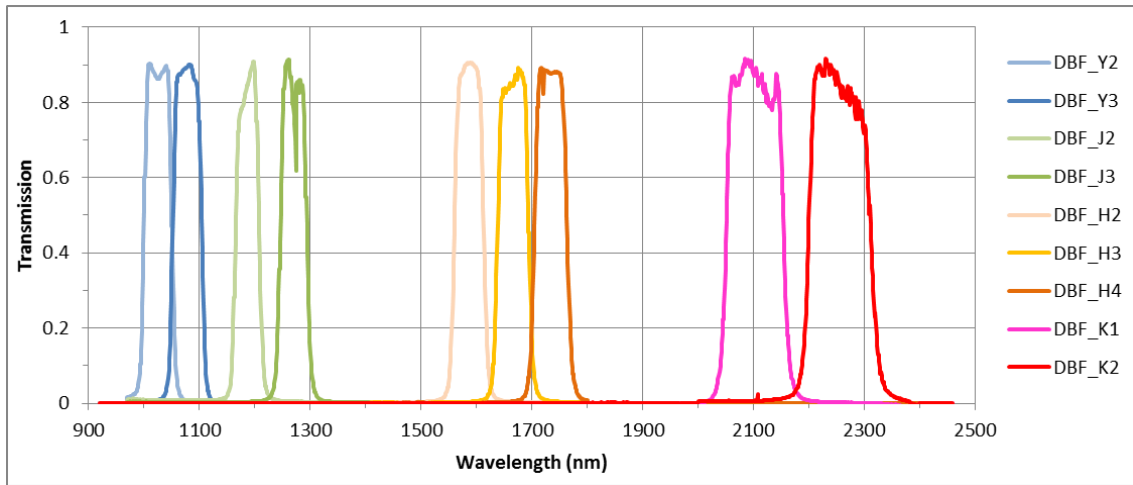


Figure 30: IRDIS DB filters.

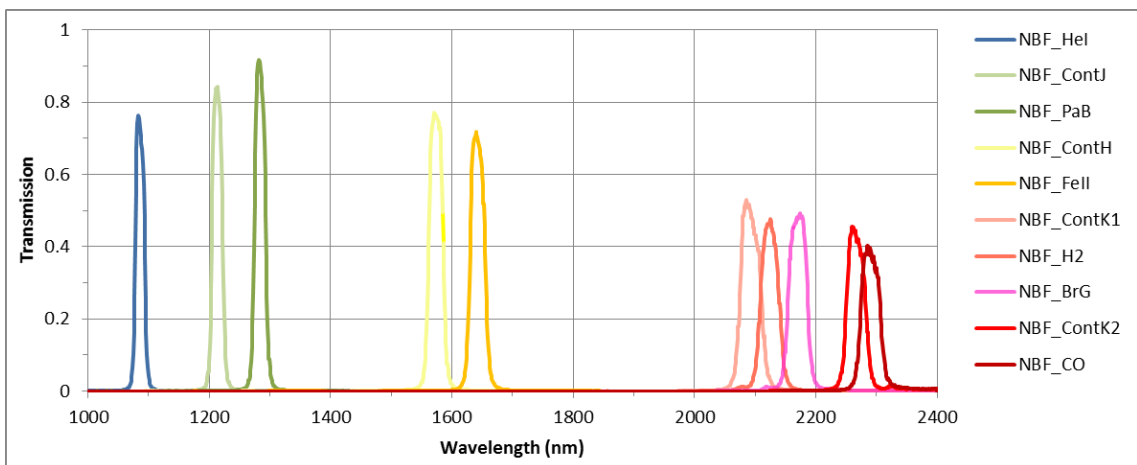


Figure 31: IRDIS NB filters.

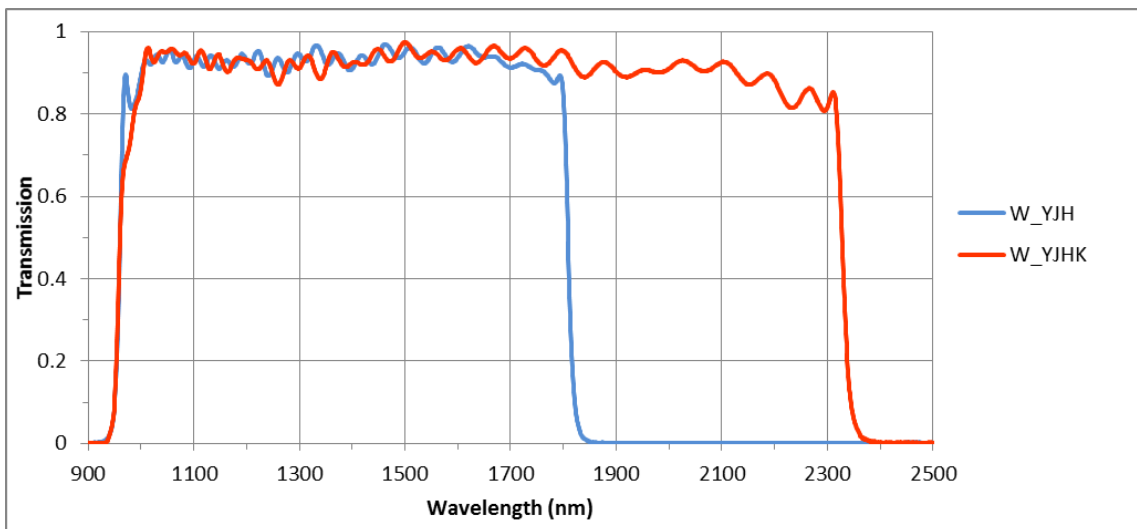


Figure 32: IRDIS wideband filter.

Table 44: IRDIS relevant filter combinations.

| Name | Mode | λ_c (nm) | $\Delta\lambda$ | IRFW1 | IRFW2 | Modes |
|-----------------|-------------------------|------------------|-----------------|----------|-------|---------|
| DBI | | | | | | |
| DB_Y23 | <i>DBI, Y2-Y3</i> | 1025.8 - 1080.2 | 44.8 - 45.5 | B_Y | D_Y23 | DBI, CI |
| DB_J23 | <i>DBI, J2-J3</i> | 1189.5 - 1269.8 | 47.6 - 50.8 | B_J | D_J23 | DBI, CI |
| DB_H23 | <i>DBI, H2-H3</i> | 1588.8 - 1667.1 | 53.1 - 55.6 | B_H | D_H23 | DBI, CI |
| DB_H32 | <i>DBI, H3-H2</i> | 1589.0 - 1665.3 | 53.1 - 55.6 | B_H | D_H32 | DBI, CI |
| DB_H34 | <i>DBI, H3-H4</i> | 1665.0 - 1736.4 | 55.6 - 57.7 | B_Hcmp2 | D_H34 | DBI, CI |
| DB_K12 | <i>DBI, K1-K2</i> | 2102.5 - 2255 | 102 - 109 | B_Ks | D_K12 | DBI, CI |
| DBI + ND filter | | | | | | |
| DB_NDH23 | <i>Including ND 0.5</i> | | | B_ND-H | D_H23 | DBI, CI |
| DB_NDH32 | <i>Including ND 0.6</i> | | | B_ND-H | D_H32 | DBI, CI |
| Broadband | | | | | | |
| BB_Y | <i>Full Y band</i> | 1042.5 | 139 | B_Y | CLEAR | DPI, CI |
| BB_J | <i>Full J band</i> | 1257.5 | 197 | B_J | CLEAR | DPI, CI |
| BB_H | <i>Full H band</i> | 1625.5 | 291 | B_H | CLEAR | DPI, CI |
| BB_Ks | <i>Full Ks band</i> | 2181.3 | 313.5 | B_Ks | CLEAR | DPI, CI |
| Narrowband | | | | | | |
| NB_HeI | <i>HeI (1083nm)</i> | 1092.3 | 17.1 | N_HeI | CLEAR | DBI, CI |
| NB_ContJ | <i>ContJ (1211nm)</i> | 1215.7 | 18.3 | N_ContJ | CLEAR | DBI, CI |
| NB_PaB | <i>PaB (1282nm)</i> | 1281.3 | 20.9 | N_PaB | CLEAR | DBI, CI |
| NB_ContH | <i>ContH (1574nm)</i> | 1557.8 | 24.5 | N_CntH | CLEAR | DBI, CI |
| NB_FeII | <i>FeII (1644nm)</i> | 1645.5 | 26.1 | N_FeII | CLEAR | DBI, CI |
| NB_ContK1 | <i>ContK1 (2098nm)</i> | 2102.7 | 33.0 | N_CntK1 | CLEAR | DBI, CI |
| NB_H2 | <i>H2 (2122nm)</i> | 2128.2 | 32.4 | N_H2 | CLEAR | DBI, CI |
| NB_BrG | <i>BrG (2167nm)</i> | 2162.9 | 37.4 | N_BrG | CLEAR | DBI, CI |
| NB_CO | <i>CO (2294nm)</i> | 2287.5 | 35.1 | N_CO | CLEAR | DBI, CI |
| NB_ContK2 | <i>ContK2 (2267nm)</i> | 2270.5 | 34.0 | N_ContK2 | CLEAR | DBI, CI |
| Spectroscopy | | | | | | |

| | | | | | | |
|------|--------------|---------------|-------------|---------|-------|-----|
| S_LR | <i>YJHKs</i> | <i>1644</i> | <i>1370</i> | W_YJHKs | CLEAR | LSS |
| S_MR | <i>YJH</i> | <i>1384.5</i> | <i>851</i> | W_YJH | CLEAR | LSS |

A6. NIR Coronagraphs

NIR coronagraphs include classical Lyot coronagraphs (CLC) and apodized Lyot coronagraphs (ALC). The available coronagraph combinations for particular wavelengths and optical elements are summarized in Table 45. The value N_NS_CLEAR indicates that no coronagraph will be used. Since only ALC coronagraphs are offered in service mode, when “Coron” is chosen on the Exposure Time Calculators (ETCs), the choice of coronagraph and returned performances are implicitly the ones corresponding to ALCs.

Table 45: List of NIR coronagraph combinations with filters and slit. The most common combinations are highlighted in green.

| Instrument mode | Wavelength/ Filter | Service mode | Visitor mode | |
|------------------------------|---|-----------------------------|----------------------------|-------------------------------------|
| | | Recommended* Coronagraph | Small IWA** Coronagraph | Large IWA Coronagraph |
| IRDIFS or IRDIS alone | IFS-YJ, DB_H23, DB_H34, DB_ND23, DB_NDH23, BB_H | N_ALC_YJH_S (IWA~0''.15) | N_ALC_YJ_S (IWA~0''.08) | N_ALC_YJH_L (IWA~0''.2) |
| IRDIFS-EXT | IFS-YJH, DB_K12, BB_Ks | N_ALC_YJH_S (IWA~0''.15) | N_ALC_YJ_S (IWA~0''.08) | N_CLC_SW_L (IWA~0''.35) |
| IRDIS alone | DB_Y23, BB_Y, NB_Hel | N_ALC_YJH_S (IWA~0''.15) | N_ALC_YJ_S (IWA~0''.08) | N_ALC_YJH_L (IWA~0''.2) |
| IRDIS alone | DB_J23, BB_J, NB_CntJ, NB_PaB | N_ALC_YJH_S (IWA~0''.15) | N_ALC_YJ_S (IWA~0''.08) | N_ALC_YJH_L (IWA~0''.2) |
| IRDIS alone | BB_H, NB_CntH, NB_FeII | N_ALC_YJH_S (IWA~0''.15) | N_ALC_YJ_S (IWA~0''.08) | N_ALC_YJH_L (IWA~0''.2) |
| IRDIS alone | DB_K12, BB_Ks | N_ALC_Ks (IWA~0''.2) | N/A | N_CLC_LW_L (IWA~0''.35) |
| IRDIS alone | NB_CntK1, NB_BrG, NB_CntK2, NB_H2, NB_CO | N_ALC_Ks (IWA~0''.2) | N/A | N_CLC_LW_L (IWA~0''.35) |
| IRDIS LSS | N_S_LR_WL, N_S_MR_WL | Not offered in service mode | N/A | N_S_LR_WL, N_S_MR_WL (IWA~0''.2) |

**Three special coronagraphs (only available in visitor mode, for expert users) are not included in the table. For shorter wavelengths, ALC configurations are optimized depending on band and focal mask: ALC_Y, ALC_YJ_S, ALC_YJ_L.*

A6.1 ALC coronagraphs

The optimal transmission profile of the apodizer depends on the size (in λ/D) of the focal mask. Practically, a given focal mask has a given size in microns, not in units of λ/D . This means that, when observing in broadband filters, a given apodizer and focal mask combination is optimal only at a particular wavelength. The performance of the coronagraph decreases rapidly at longer wavelengths but slowly at shorter wavelengths. The ALC combinations include

- 2 apodizers, APO1 and APO2, optimized for 4 and 5.2 (λ/D) focal masks,
- 3 focal masks, ALC1, ALC2, ALC3, with diameters of 145, 185 and 240 (mas).

The ALC Lyot stop has good transmission (92%) with a large outer radius (96% of VLT pupil). The transmission and resolution are limited by the entrance apodizer. Optimal approved combinations of apodizer-mask-Lyot stop have been preselected, and cannot be changed for now. These combinations are described in Table 46.

Table 46: Definition of the coronagraph combination

| Coronagraph combination name | Applicable band | Apodizer | Lyot Mask and diameter in mas |
|------------------------------|-----------------|----------|-------------------------------|
| N_ALC_YJH_S | YJH | APO1 | ALC2 (185mas) |
| N_ALC_YJH_L | YJH | APO2 | ALC3 (240mas) |
| N_ALC_YJ_S | YJ | APO1 | ALC1 (145mas) |
| N_ALS_YJ_L | YJ | APO2 | ALC2 (185mas) |
| N_ALC_Ks | YJHks | APO1 | ALC3 (240mas) |

A7. IFS dispersive components

There are two alternative dispersive elements in IFS. Both are Amici prisms designed either for the Y-J or the Y-H band. The prisms are associated with filters that define the pass-band of each spectrum, avoiding overlap of consecutive spectra along the dispersion direction. Prism parameters are listed in Table 47.

Table 47: IFS prisms parameters.

| Parameter | Y-J | Y-H |
|--------------------------|------|------|
| Spectral length (pixels) | 35.4 | 35.3 |

| | | |
|---|--------------|--------------|
| Wavelength Range (μm) | 0.96-1.34 μm | 0.97-1.66 μm |
| Average dispersion (nm/pixel) | 10.52 | 19.15 |
| Average Spectral resolution (per FWHM) | 55.1 | 34.5 |

A8. IRDIS dispersive components

A8.1 LSS

LSS requires a long slit located in the coronagraphic focal plane and a dispersive component (prism or grism) that is located in the IRDIS pupil plane. The corresponding focal plane and pupil plane combinations for LSS are listed in. Naming conventions for named LR_N_L to MR_W_S are:

- LR for low resolution and MR for medium resolution,
- N for narrow (90 mas) and W for wide (120 mas) slit width, both larger than the PSF,
- L for large (400 mas) and S for small (200 mas) size of the central blocking mask.

A8.2 Prism

LRS mode uses a double prism designed for zero deviation close to the center of the spectral range and close to linear dispersion function. The wavelength λ to pixel y relation for the prism is fit by:

$$\lambda = \lambda_0 + c_1 * (y - y_0) / 100 + c_2 * ((y - y_0) / 100)^2 + c_3 * ((y - y_0) / 100)^3 + c_4 * ((y - y_0) / 100)^4$$

The laser line is at $\lambda_0 = 1545.07$ nm and its position determines y_0 . Fit parameters are: $c_1 = -9.1293$ for channel M or $c_1 = -9.12795$ for channel BS; c_2 , c_3 and c_4 are equal for both channels. The relative orientation of the double prisms introduces a higher variance in λ_0 and c_1 than for the grism.

A8.3 Grism

The pixel–wavelength relation is linear for the grism. Fitting parameter $c_1 = -1.13878 \pm 0.00022$ (nm/pixel) is related to the focal length of the camera mirror. As the two mirrors are slightly different, this term is slightly different for the two channels. In the fit, y_0 corresponds to a constant offset and varies with slit position. The two parameters, y_0 and λ_0 , are determined as above.

A9. Visible Coronagraphs

The coronagraphs in the visible are all classical Lyot coronagraphs (CLC). The selection of a coronagraph includes setting of different devices: the focal mask and the pupil stop. The CLC focal masks, which have various diameters, are suspended or deposited on substrates (with no suspending wire), and include a field stop (either full ZIMPOL FoV or restricted to inner 1'' FoV for window mode). Relevant combinations are listed in. Naming conventions are:

- CLC, NC: for the type of coronagraph (Classical Lyot Coronagraph or no coronagraph).
- S, M, L, XL: for the size of the focal mask from small to very large (93, 155, 310 and 1240 mas, respectively).
- WF: for the wide field stop.

Table 48: List of visible coronagraph combinations. Recommended configurations are highlighted in green.

| Mode | Filter | Recommended* Coronagraph | Medium/large/ extra large IWA Coronagraph |
|-----------|---|-----------------------------|---|
| ZIMPOL_P1 | RI, R_PRIM, I_PRIM, V, N_R, N_I, KI, TiO_717, CH4_727, Cnt748, Cnt820, CntHa, N_Ha, B_Ha | V_CLC_M_WF | V_CLC_S_WF/ V_CLC_L_WF/ V_CLC_XL_WF |
| ZIMPOL_P2 | RI, R_PRIM, I_PRIM, V, N_R, N_I, KI, TiO_717, CH4_727, Cnt748, Cnt820, CntHa, N_Ha, B_Ha | V_CLC_M_WF | V_CLC_S_WF/ V_CLC_L_WF/ V_CLC_XL_WF |
| ZIMPOL_I | RI, R_PRIM, I_PRIM, V, V_S, V_L, N_R, 730_NB, N_I, I_L, KI, TiO_717, CH4_727, Cnt748, Cnt820, HeI, OI_630, CntHa, B_Ha, N_Ha, Ha_NB | V_CLC_M_WF | V_CLC_S_WF/ V_CLC_L_WF/ V_CLC_XL_WF |

*Not in the table is the *V_CLC_MT_WF* mask (155 mas), which includes a grid of dots that is useful for calibration purposes and/or accurate astrometric reference.

The selection depends on the required halo rejection, none-saturation capability and IWA:

- No coronagraph (V_NC_WF or V_NC_NF): Should be used when the science goal concerns the target itself or its immediate environment at the resolution limit. The N_NC_NF option uses a field stop of 1" (useful for – not yet offered- windowed read-out modes), whereas the full field-of-view is accessible with the V_NV_WF option. Saturation effects are limited thanks to the high CCD pixel-well and by the short DIT possible especially in window mode. Neutral density filters can be inserted unless observing with filters mounted on the FW0. If saturation occurs, the charge leakage is quite limited close to the saturated peak and over the columns. Observations performed so far indicate that artefacts introduced by saturations are very small.
- CLC with increasing mask diameter between 93 and 1240 (mas).
- Special case of V_CLC_MT_WF: this on-substrate 155 mas mask also includes a grid of dots that is useful for calibration purposes and/or accurate astrometric reference.

A10. ZIMPOL filters

ZIMPOL has three filter wheels, FW0 located in front of the polarization modulator and beam splitter, FW1 located in arm 1 of ZIMPOL and FW2 located in arm 2 of ZIMPOL. FW0 contains besides filters for imaging also polarization calibration components and neutral density filters. Recommendations are:

Filters located in FW0 can be used for imaging and they provide the same band-pass in both arms. FW0 cannot be combined with neutral density filters, as they are located in

the same wheel. It is not recommended that the FW0 filter be used for polarimetric measurements because they may introduce polarimetric effects that are difficult to calibrate. The combination of FW0 filters with FW1 or FW2 filters is not supported.

Filters located in FW1 and FW2 can be used for imaging, differential imaging and polarization. Different filters can be used in FW1 and FW2, but one needs to be aware that the detector operation (e.g. exposure time) is identical in both arms. The combination of a narrowband filter with a broadband filter may therefore cause an underexposed image in one arm and an overexposed image in the other arm.

The list of relevant combinations, and their names are listed in Table 49. Note that if the dichroic beam splitter is used between ZIMPOL and WFS then only a small wavelength range in the R-band can be observed. This reduces the useful filters to those highlighted in green in Table 49.

The transmission curves of all ZIMPOL filters are available here :

www.eso.org/sci/facilities/paranal/instruments/sphere/inst/filters.html

Table 49: Measured band-pass of ZIMPOL filters. We list wavelengths (nm), where the transmission is 50% of its maximum, the 50% width and its central wavelength.

| Filter | λ_{\min} | λ_{\max} | FWHM | λ_0 |
|---------|------------------|------------------|-------|-------------|
| RI | 590.1 | 880.6 | 290.5 | 735.4 |
| R_PRIM | 552 | 700.6 | 148.6 | 626.3 |
| I_PRIM | 713.3 | 866 | 152.7 | 789.7 |
| V | 513.7 | 594.3 | 80.6 | 554 |
| V_S | 513 | 550.2 | 37.2 | 531.6 |
| V_L | 560.9 | 602 | 41.1 | 581.5 |
| N_R | 617.5 | 674.2 | 56.7 | 645.9 |
| 730_NB | 705.5 | 760.4 | 54.9 | 733 |
| N_I | 776.5 | 857 | 80.5 | 816.8 |
| I_L | 842.4 | 898.8 | 56.4 | 870.6 |
| KI | 759.6 | 780.8 | 21.2 | 770.2 |
| TiO_717 | 706.9 | 726.6 | 19.7 | 716.8 |
| CH4_727 | 720 | 740.5 | 20.5 | 730.3 |
| Cnt748 | 737.1 | 757.7 | 20.6 | 747.4 |
| Cnt820 | 807.4 | 827.2 | 19.8 | 817.3 |
| HeI | 585.3 | 590.7 | 5.4 | 588 |
| OI_630 | 626.8 | 632.2 | 5.4 | 629.5 |
| CntHa | 642.8 | 646.9 | 4.1 | 644.9 |
| B_Ha | 652.9 | 658.4 | 5.5 | 655.6 |
| N_Ha | 655.85 | 656.82 | 0.97 | 656.34 |
| Ha_NB | 656.04 | 657.02 | 0.98 | 656.49 |

NOTE: The filters highlighted in green are compatible with the dichroic beamsplitter.

A11. Polarimetric calibration components

ZIMPOL is optimized for the measurement of linear polarization. Here we present a short summary of the critical polarimetric calibration components, the reader is invited to read Bazzon et al. 2012 (SPIE 8446, 93B) for further details about the polarimetric concept.

The most important components for the polarimetric calibration are the linear polarizer and HWPZ. Less important are the quarter-wave plate and the circular polarizer. Note that:

- **The achromatic (dichroic glass) polarizer is made of structured absorptive nanoparticles. It provides a contrast $<10^{-3}$ between 600-900 nm and 10^{-2} between 500-600 nm.**
- **Circular polarization is measured with an achromatic quarter-wave plate made out of MgF_2 and quartz. The retardance error is less than $\pm 6\%$ between 500-900 nm.**
- **The circular polarizer is a combination of a linear polarizer with the fast axis at 45° ($\pm 0.5^\circ$) followed by a quarter-wave plate with the fast axis at 0° . Both components are of the same. Since the quarter-wave plate is not perfectly achromatic the circular polarizer has a small leakage of linear polarization of several %.**

The reference orientation for the polarimetric alignment is given by the polarizing beam-splitter of ZIMPOL. The transmitted beam (CCD 1) has a linear polarization parallel to the ZIMPOL bench and the reflected beam (CCD 2) an orientation perpendicular

A12. Waffle spots

When a coronagraph is used with Irdis or Zimpol, the position of the star behind the coronagraph can be known by applying a waffle pattern to the DM. This is critical because most post-processing techniques rely on the accurate registration of the star. The pattern creates four replicas of the PSF, called satellite spots, at a separation of about $14 \lambda/D$. The orientation of this pattern can be chosen, between an x shape (position angle of the spots of 45° , 135° , 225° and 315° as shown in Figure 33) or a + shape (position angle of 0° , 90° , 180° and 270°). These spots can be used to find the star center by intersecting the line joining opposite spots, as illustrated in Figure 33. Non coronagraphic observations of a star with the waffle pattern on were obtained to calibrate the accuracy of this technique as illustrated in Figure 34. The star center as estimated from the intersection of the two lines joining opposite satellite spots and from a direct 2d fit on the PSF core agrees within better than 2.5mas

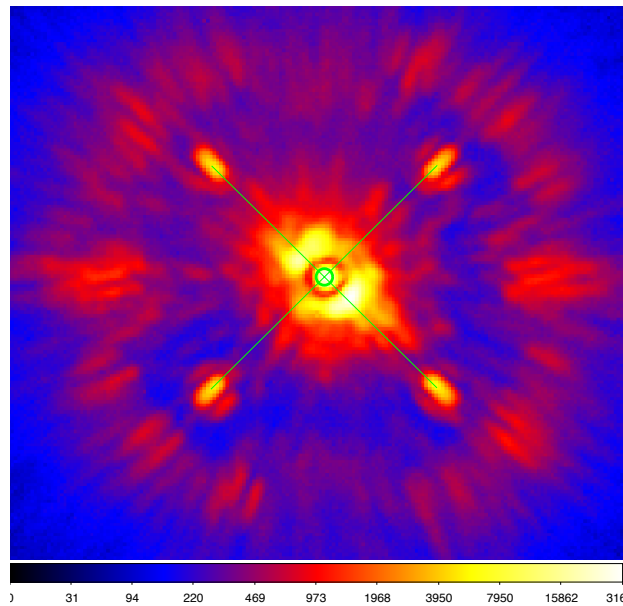


Figure 33. Irdis image in broad-band H, with the N_ALC_YJH coronagraph, with the waffle pattern applied to the DM, creating four satellite spots. These spots are elongated with broad-band filters and point source with narrow-band filters. The green lines start and end points were computed by fitting a 2D Gaussian on each spot, they intersect on the star center, indicated by a green thick circle.

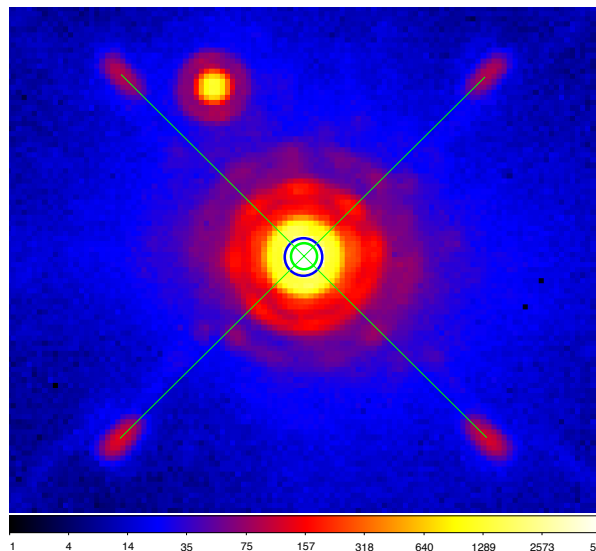


Figure 34 Non coronagraphic image of a star (happening to have a binary companion) in broad-band H with Irdis, after applying a waffle pattern to the DM for calibration purposes. The green thick circle indicates the intersection of the green lines, while the blue thick circle indicates the star position (Gaussian fit). Both agree within 2.5mas.

